THE KINETICS OF ZINC REMOVAL FROM COBALT ELECTROLYTES BY ION EXCHANGE

by

Nathan SWAMI S.

A THESIS SUBMITTED IN PARTIAL FULFILLMENT OF
THE REQUIREMENTS FOR THE DEGREE OF
MASTER OF APPLIED SCIENCE

in

THE FACULTY OF GRADUATE STUDIES
Department of Metals and Materials Engineering

We accept this thesis as conforming
to the required standard

THE UNIVERSITY OF BRITISH COLUMBIA

October 1993

In presenting this thesis in partial fulfilment of the requirements for an advanced degree at the University of British Columbia, I agree that the Library shall make it freely available for reference and study. I further agree that permission for extensive copying of this thesis for scholarly purposes may be granted by the head of my department or by his or her representatives. It is understood that copying or publication of this thesis for financial gain shall not be allowed without my written permission.

Department of Metals & Materials Engg.

The University of British Columbia
Vancouver, Canada

Date 10 Dec. 1993

ABSTRACT

The removal of trace zinc concentrations from the INCO (Port Colborne) cobalt advance electrolyte by solvent impregnated ion exchange, was studied in column and batch tests. The solvent impregnated resins containing the extractants D2EHPA, Cyanex 272 and Cyanex 302, were compared in terms of zinc loading and selectivity.

D2EHPA impregnated OC 1026 resin demonstrated superior zinc loading and selectivity characteristics, but retained objectionably high amounts of cobalt, which were lost in the zinc elution process. Cobalt loading, was found to be closely related to the electrolyte pH drop across the column and could be reduced by a resin pre-treatment with the advance electrolyte at a pH of 3 or by an increase in the feed electrolyte pH to 5, along with operation at a temperature of 40°C and a flow rate of 10 BV/hr.; all of which act to diminish the pH drop.

The kinetics of zinc loading on each of the resins was found to be comparable, and the rate controlling mechanism in batch tests was found to be particle diffusion in the first fifteen minutes, while film diffusion became rate controlling at later time intervals. Pre-treatment enhanced the diffusion coefficient inside the resin phase by nearly an order of magnitude, improved exchange kinetics by allowing a lower pH reduction during the loading process, and improved Co^{2+}/Zn^{2+} exchange in a matrix of the cobalt complex.

An analysis of the breakthrough curves for the resins was done to determine the mass transfer coefficients inside the column, and a range of other parameters useful in the design of ion exchange columns. The rate controlling regime in the column was a mixture of the particle and film diffusion steps, with the former being the dominant control mechanism at the operating flow rate.

Further work is needed in the X-ray microprobe analysis of resin samples from the top, middle and bottom portions of the columns, and of samples from batch tests, to aid in understanding the mechanism of ion exchange. The use of zinc selective electrodes in batch tests could also be undertaken to obtain a more accurate estimate of the diffusion and mass transfer coefficients.

Table of Contents

List of Tables

Table of Figures

List of Symbols

a = Mass transfer area (m^2).

a_i = Activity of species *i*.

c = Concentration of the species (g/L).

c_o = Feed concentration of the species (g/L).

D = Diffusion coefficient of the species (m^2/s).

DC = Distribution constant.

D_{bs} = Degree of bed saturation.

D_q = Energy splitting parameter.

e = Bed voidage (dimensionless).

F = Faraday constant (Coloumb/equivalent).

f = Fugacity of the species.

h_z = Height of an individual zone (m)

H = Height of the resin bed (cm).

H_{tof} = Height of the transfer zone (m).

H_{us} = Height of the unused bed (cm).

J = Flux of the diffusing species (g/m^2 s).

k_m = Mass transfer coefficient in the aqueous film (m/s).

k_1, k_2 = Rate constants of forward and reverse reaction (m/s).

k_L =Liquid phase mass transfer coefficient obtained from Carberry's correlation (m/s).

N = Molar flux of the species (mol/m^2s).

r_o = Radius of the resin particle (m).

Re = Reynold's number (dimensionless).

$\overline{RB}_{eq}$ = Equilibrium concentration of the extracted species in the resin (g/L)

R = Concentration of fixed ionic group (g/L).

Sh = Sherwood number (dimensionless).

Sc = Schmidt number (dimensionless).

t = Time elapsed (seconds).

T = Temperature (°C).

U_s = Superficial fluid velocity through the column (m/s).

U_z = Velocity of mass transfer zone through the bed (m/s).

X = Fraction extracted.

z = Valency of the ion.

Subscripts:

A = Ion diffusing from the resin phase to the aqueous phase.

B = Ion diffusing from the aqueous phase to the resin phase.

Superscripts:

overbar = Resin phase parameter.

* = Resin/solution interface.

b = Bulk solution parameter.

Greek Symbols

α = Separation coefficient (dimensionless).

β = Shape factor of breakthrough curve (dimensionless).

δ = Aqueous phase film thickness (m).

ε = Fractional pore volume of the ion exchanger.

θ = Time elapsed (hrs.).

θ_o = Breakthrough time (hrs.).

θ_m = Mean breakthrough time (hrs.).

θ_s = Bed saturation time (hrs.).

ρ_B = Solid phase bulk density of the resin (kg/m^3).

ρ_L = Density of the liquid phase (kg/m^3).

η = Viscosity of the liquid phase (kg/m s).

λ = Equivalent conductance ($mho/eq.m^2$).

Φ = Electric potential gradient (Volt/m).

Acknowledgements

I would like to take this opportunity to thank a few people who have helped me write this thesis, by lending me timely academic and emotional support.

I thank my research supervisor Prof. David Dreisinger for the trust he placed in my abilities, when he chose me to come to the Univ. of British Columbia to work with him on my Master's. I thank him for his patience and understanding, especially during the early stages of my research work, and for the encouragement he provided throughout my work. I thank Prof. W.C.Coopers for his insightful discussions on electrochemistry which have influenced my understanding and approach to hydrometallurgy. Thanks are also extended to INCO Ltd. for their financial support to my work.

My colleagues have been instrumental in enhancing my understanding of Metals and Materials Engg.. I thank them for working with me as a team and providing me with an environment where I could discuss my problems, and avert many a "dead end". I thank Ish, Brenna, Ben and Paul for the help they provided me with, in the initial set-up of my experimental apparatus. I thank Mike and Ben for always being around in the lab and not making me feel that I was the only one working so hard. I thank Mukunthan, Vinay, Bernardo, Victoire, Anita, Charlie and Harold for the lively discussions on topics ranging from Material Science to spiritualism.

1 CHAPTER ONE - INTRODUCTION

1.1 Ion Exchange Purification

Ion exchange is an important unit process in many metal purification operations, and has a wide variety of applications in the fields of analytical chemistry, biotechnology, catalysis, decontamination and separation technology. Its application is of special importance in the purification of electrolytes and waste streams, by the removal of impurities present in extremely low concentrations. Ion exchange has undergone a great deal of technological advancement since the 1950's, from the development of newer types of selective resins and novel contacting techniques, to intensive studies on the thermodynamics and kinetics of the process to understand the exchange equilibria and mechanisms. In recent years, the resurgence of interest in ion exchange has been in the direction of technological development based on newer theoretical understanding of the process, applied to its under-utilized potential in the recovery of valuable materials from natural resources and waste, and to the prevention or correction of damage to the environment. One step in this direction was the introduction of a selective extractant in the resin matrix, rather than the functional group, to extract the impurity, which greatly enhanced the efficiency and selectivity and led to the development of *solvent impregnated resins* for some specific separation processes. The subject of this thesis is the study of a class of such solvent impregnated resins, for their application to the INCO zinc removal process for cobalt electrolytes, using standard methods to study the kinetics and interpret the process mechanisms.

1.2 Zinc Removal from Cobalt Electrolytes

The removal of zinc impurities from cobalt electrolytes is of the utmost importance in the extractive metallurgy of cobalt, as zinc is a deleterious impurity in cobalt electrowinning. Solvent impregnate technology pioneered by the Bayer Chemical Company, offered the resin OC 1026, an ion exchange resin impregnated with di-2-ethyl-hexyl phosphoric acid (D2EHPA) extractant, which is currently being used at the INCO cobalt refinery at Port Colborne. This resin, however,

shows poor zinc selectivity, and a fair amount of cobalt is retained on the resin at the zinc breakthrough point. This cobalt is lost in the zinc elution process. It has been suggested that phosphinic acids or sulphur substituted phosphinic acids could offer better zinc selectivity. Hence working in collaboration with the University of British Columbia, the Bayer Chemical Company synthesized special resins impregnated with the Cyanamid extractants Cyanex 272 and Cyanex 302. The chemical structure of these extractants is compared to that of D2EHPA in the following figure:

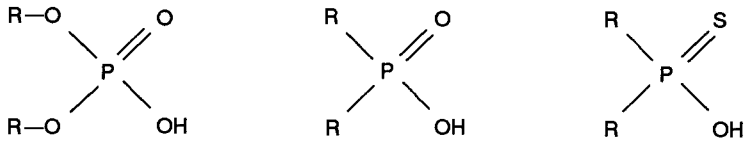

For D2EHPA; R = 2 ethyl hexyl group
For Cyanex 272 and Cyanex 302; R = 2,2,4 trimethyl pentyl group

Figure 1.1 : Organophosphorous extractants used in OC 1026, Cyanex 272 & Cyanex 302

The main objective of this work was to compare the performance of these solvent impregnated resins in terms of zinc loading, cobalt/zinc selectivity and metal exchange kinetics, and to suggest improvements to the INCO zinc removal process. It is hoped that knowledge gained from this investigation will make some useful contributions to the understanding and process developments at the INCO cobalt refinery, and in other processes for the removal of zinc from electrolytes or waste streams.

2 LITERATURE REVIEW

2.1 Ion Exchange Process

Ion exchange is a chemical process in which ions are exchanged by a solid ion exchanger and an aqueous solution as follows:

$$Cation\quad Exchange: \quad \overline{R_mA} + mB^+ \longleftrightarrow m\overline{RB} + mA^+ \qquad .....(2.1)$$

$$Anion\quad Exchange: \quad \overline{R_mA} + mB^- \longleftrightarrow m\overline{RB} + mA^- \qquad .....(2.2)$$

where RA is the solid ion exchanger which is usually an organic polymer (the bar represents the organic phase) and is called a cationic or an anionic exchanger depending on whether it exchanges cations or anions respectively. A and B are called *counterions*, R is the *fixed ion* and m is the valence ratio.

2.2 History and Technological Development of Ion Exchange

Ion exchange has an illustrious history dating back to pre-historic times when Moses softened the bitter waters of Mara to make them potable for his flock in the desert [1]. Aristotle observed that the salt content of water is diminished upon percolation through certain sands [2]. More recently in 1850, ion exchange was studied in a systematic manner by two British soil scientists Thompson and Way [3,4]. With progressing industrialization, the focus, around the turn of the century, shifted to the application of ion exchange to plant-scale water softening, first with natural and later with synthetic ion exchangers [5]. The chance discovery that a shattered phonograph record exhibits ion exchange properties, by English scientists Adams and Holmes [6] led to the invention of ion exchange resins. In World War II, ion exchange contributed significantly to the Manhattan Project by providing solutions to the challenge of separating rare earth elements and other fission products [7-9]. Other important advances after the war include the advent of more stable and reproducible ion exchange resins based on polystyrene [10], the development of strong-base anion exchangers (with quaternary ammonium groups) [11], commercial development of effective inorganic ion

exchangers in the form of *synthetic zeolites* and *molecular sieves* [12] and the development of *macroporous* ion exchange resins. Later developments include novel ion exchange contact methods, and the development of *chelating* and *solvent impregnated* ion exchange resins. Today, a wide range of improved organic and inorganic ion exchangers with a great variety of properties is available for laboratory and plant-scale applications ranging from chemical analyses to preparative separations, from catalysis to organic synthesis, from biomedical uses to decontamination and detoxification.

2.3 Present Applications

Ion exchange has been instrumental in the development of our science and technology, and its thrust and emphasis have continuously evolved to keep up with the changing outlook and needs of the time. Ion exchange processes are actively utilized in the following applications:

(1) Dialysis apparatus for biomedical engineering

(2) Enhanced oil recovery processes

(3) Chemical analyses as in chromatography

(4) Manufacture of gasoline additives to provide an effective no-knock performance

(5) Chemical separations of rare earths, transition metal cations and optical isomers

(6) Decontamination of water used in cooling systems of nuclear reactors and other industrial plants

(7) Recovery of uranium and thorium from dilute leach liquors

2.4 Chemistry of Ion Exchange

Ion exchange resins are solid, water insoluble, high molecular mass polyelectrolytes, which consist of a hydrophobic polymer resin matrix (prepared by emulsion co-polymerization), to which specific functional groups are attached. The ion exchanger must preserve its electro-neutrality at

all times, and this is accomplished by balancing the resin's fixed ions with counterions. The counterions can be exchanged for a stochiometrically equivalent quantity of other ions of the same sign when the ion exchanger is in contact with an electrolyte solution.

2.4.1 The resin matrix

In ion exchange the resin substrate is usually an organic polymer which is produced in bead form (0.5 - 2 mm diameter). One common type of resin is the polystyrene-divinylbenzene matrix, crosslinked to provide structural strength as shown below:

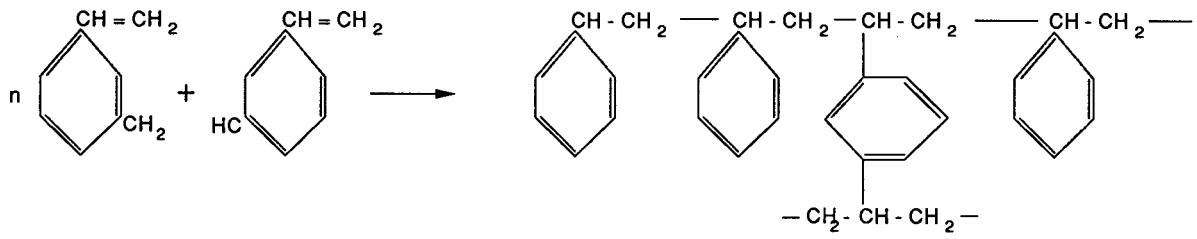

Figure 2.1 (a) : Preparation of a crosslinked resin polymer matrix

Gel type resins (*microporous*) result when only styrene and divinylbenzene are used in the synthesis, while if an inert material such as toluene is added during polymerization and evaporated after bead formation, then a *macroporous* bead results. Macroporosity tends to enhance kinetics (refer Fig. 2.1(b) for a comparison of the structures).

Important physical properties such as swelling, mechanical strength, abrasion resistance, rate of exchange and exchange capacity, which impact the use of ion exchange resins, depend to some extent on the degree of crosslinking. *Swelling* is caused by the adsorption of water into the resin structure, which hydrates the functional groups and lowers the exchange capacity, and is considerably increased by a lower degree of crosslinking. A resin with a low degree of crosslinking will also break or abrade more easily under induced *mechanical* or *osmotic* stresses.

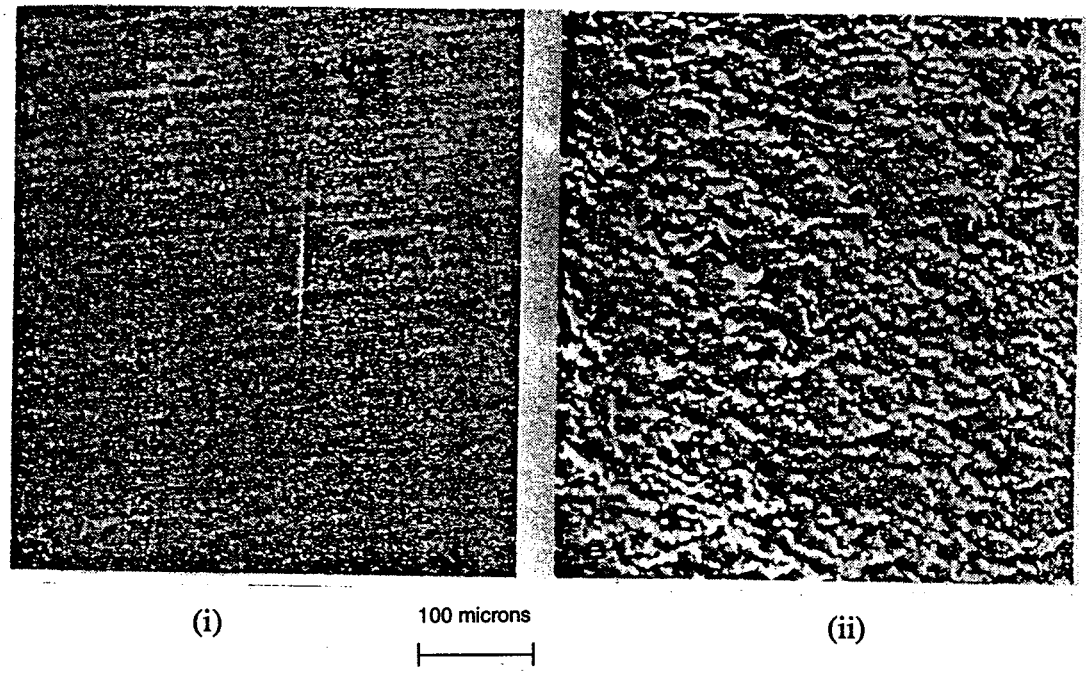

Figure 2.1 (b) : Surface characteristics of ion exchange resins [15].
(i) Microporous resin.
(ii) Macroporous resin.

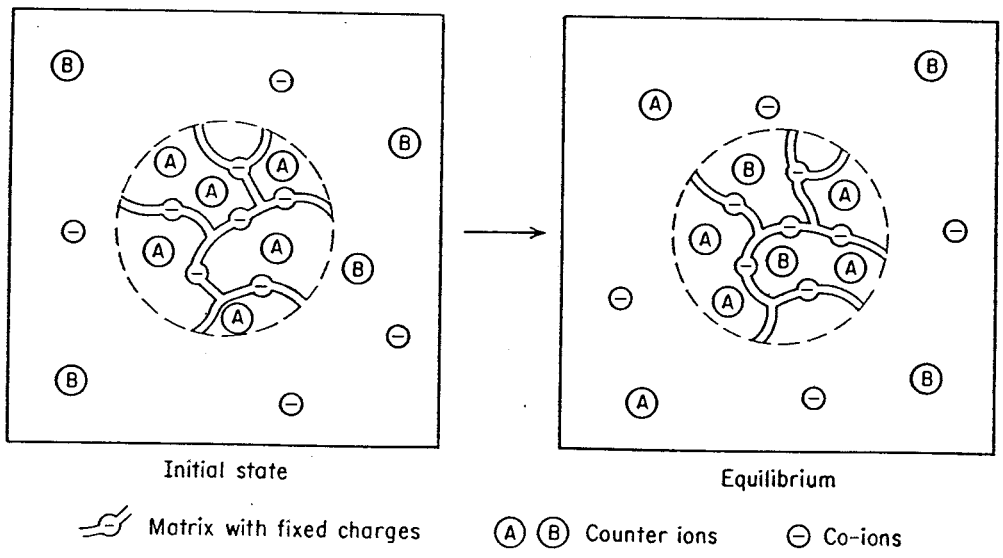

Figure 2.2 : The ion exchange process [15].

In contrast, higher *rates of exchange* are achieved with a low degree of crosslinking. As a trade-off of these factors, the amount of crosslinking for polystyrene-divinylbenzene resins is usually in the range of 4-8% divinylbenzene (DVB).

2.4.2 Functional groups

The nature of ion exchange resins is determined by the functional groups attached to the resin matrix. Ion exchange resins may be classified as follows based on the functional groups:

Table 2.1 : Classification of ion exchange resins based on functional groups.

Nature	Functional group	Range	Applications	Capacity meq/g	Commercial resins
Strong acid	$-SO_3H$	pH < 2	Water softening	5	Lewatit S100, Amberlite IR-200
Weak acid	$=PO_2H$	pH > 4	Rare earth processing	10	Amberlite IFC-84 Duolite CC3
Strong base	$-NR_3X$	0 - 14	Uranium processing	4	Zerolit MPF Lewatit MP200
Weak base	$-NH_2$, $-NR_2$, $-NHR$	0 - 10	Uranium processing	5	Zerolite MPH Lewatit MP62
Chelating resin	Picolylamine $-N(CH_2C_5NH_4)_2$	-	Cu & Ni removal	1.5	XFS 4195

2.4.2.1 Strong and weak acid ion exchangers

Cation exchange can be carried out using sulphonic acid type exchangers. These resins have the functional groups $-SO_3H$, and are called strong acid ion exchangers. They can extract cations at low pH but are relatively unselective. Weak acid ion exchangers have functional groups of the $-CO_2H$ and $=PO_2H$ type, and can extract cations at moderate pH values (pH > 4) only, but are somewhat more selective. The pH limitation of weak acid ion exchangers is due to stability of the protonated weak acid group at high acidities.

2.4.2.2 Strong and weak base ion exchangers

Weak base resins are those with the functional groups $-NR_2$, -NHR and $-NH_2$, and must be protonated to exchange ions. The useful pH range is therefore approximately 0-10. Strong base resins have the functional group $-NR_3X$ and extract anions efficiently over the entire pH range.

2.4.3 Aqueous chemistry of metal ions

The reactivity of metal ions in solution may be related to the following:

(1) electronic configuration of the ion

(2) ionic radii of metal ion

(3) position on the *hard-soft acid base* (HSAB) scale

Ions with electrons in *s* and *p* orbitals (alkali and alkaline earth) show a limited degree of variety in their chemical reactivity, whereas, transition, lanthanide and actinide metal ions with partially filled *d* and *f* orbitals, have a more complex behavior. *Hard bases* are usually small in ionic radii with localized charges, whereas the *soft bases* are large in size with diffuse charges and high polarizabilities (see Table 2.2). A rule of thumb is that soft acids tend to interact preferentially with soft bases, and conversely, hard acids with hard bases. Hard bases tend to form complexes with the following order of stabilities:

Class A (hard bases): $F^- > Cl^- > Br^- > I^-$

$O >> S > Se > Te$

$N >> P > As > Sb > Bi$

Class B (soft bases): H^-, R^-, C_2H_4, C_6H_6, CN^-, RNC, CO

SCN^-, R_3P, RS^-, $S_2O_3^{2-}$

Table 2.2 : Classification of Lewis acids [19].

Hard	Soft
H^+, Li^+, Na^+, K^+	Cu^+, Tl^+, Hg^+
Be^{2+}, Mg^{2+}, Ca^{2+}, Sr^{2+}, Mn^{2+}	Pd^{2+},Cd^{2+},Pt^{2+},Hg^{2+},CH_3Hg^+,$Co(CN)_5^{2-}$
Al^{3+}, Sc^{3+}, Ga^{3+}, In^{3+}, La^{3+}	Tl^{3+},$Tl(CH_3)_3$,BH_3,$Ga(CH_3)_3$,$GaCl_3$
N^{3+}, Gd^{3+}, Lu^{3+}	RS^+, RSe^+, RTe^+
Cr^{3+}, Co^{3+}, Fe^{3+}, As^{3+}, Ce^{3+}	I^+, Br^+, HO^+, RO^+
Si^{4+}, Ti^{4+}, Zr^{4+}, Th^{4+}, Pu^{4+}	I_2, Br_2, ICN
UO_2^{2+},$(CH_3)_2Sn^{2+}$,VO^{2+},MoO^{3+}	Tri-nitrobenzene
$BeMe_2$, BF_3, $B(OR)_3$	Chloranil, quinones
$Al(CH_3)_3$, $AlCl_3$, AlH_3	Tetra-cyano-ethylene
RPO_2^+, $ROPO_2^+$	O, Cl, Br, I, N
RSO_2^+, $ROSO_2^+$, SO_3	M^0 (metal atoms)
I^{7+}, I^{5+}, Cl^{7+}, Cr^{6+}	Bulk metals
RCO^+, CO_2, NC_+	CH_2, carbenes
HX (hydrogen bonding molecules)	

With Class B (soft bases) metal ions, this order is reversed. Quantitative data for stability constants of metallic ions and organic or inorganic ligands is given in reference [13]. An examination of the electronic structure of metal ions helps to screen them into *alkali alike ions* (AAI) and *transition metal alike ions* (TMAI). In the former group steric considerations are predominant, while electronic considerations are predominant in the latter [14]. The formation of a metal complex from a solvated metal ion and a ligand may involve a simple ion pairing mechanism, where the *d* subshell electrons of the transition metal are paired by a simple substitution of the solvent molecule by the ligand, or a chelating mechanism, where more than one solvent molecule is substituted at a time, and hence the metal is attached to the ligand at more than one point. The complexation behavior of the AAI group may be best described in terms of the *host-guest complexation*, where the complementary behavior between the ion (guest) and the ligand (host) is required for the complexation process. For this to occur, an important condition is the complementary sizes of ionic radii and ligand cavity. Fig. 2.3 shows the Periodic Table in a steric perspective, pointing out the large differences in ionic radii of alkaline cations.

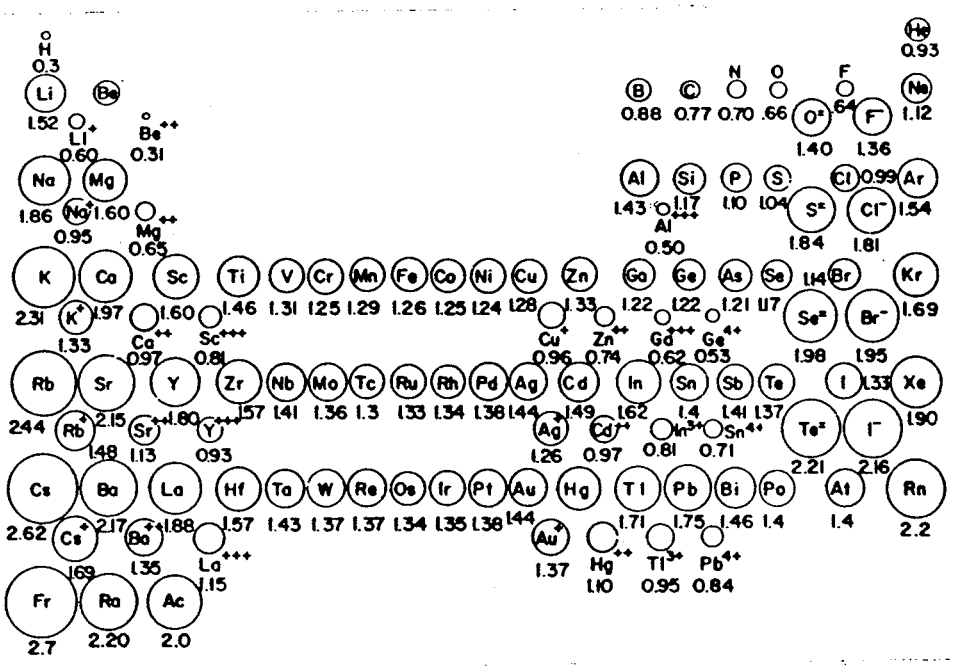

Figure 2.3 : The periodic table in steric perspective (atomic and ionic radii in angstrom units) [14]

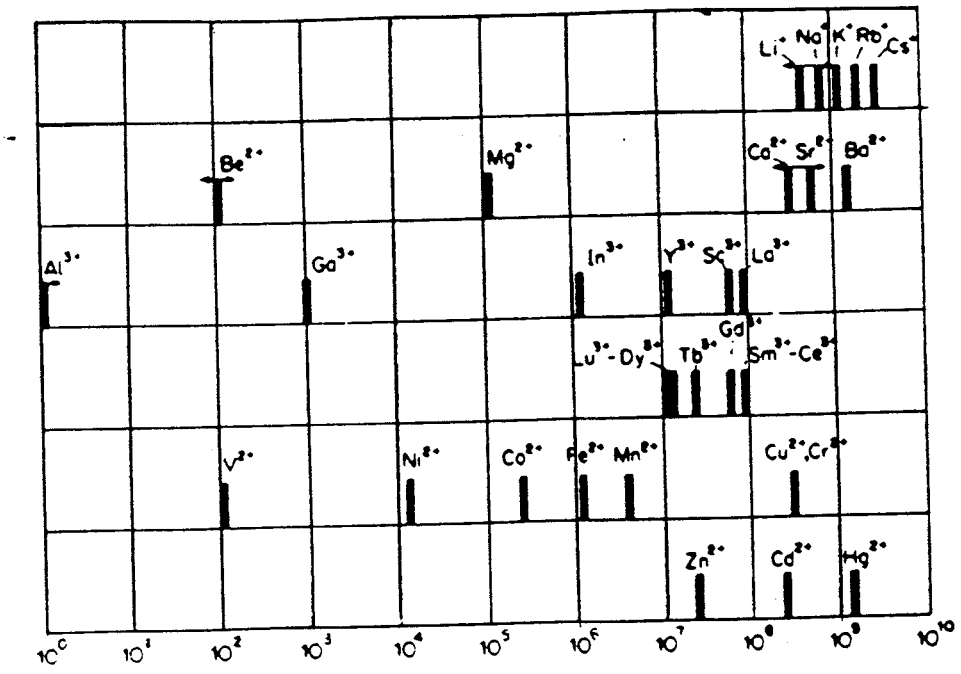

Figure 2.4 : Characteristic rate constants (sec^{-1}) for substitution of inner sphere H_2O of various aquo ions [14]

Figure 2.4 shows the rate constants for substitution of inner sphere H_2O of various aquo-ions. Ions to the right of the diagram, are termed labile, because of faster exchange kinetics than those on the left. Figure 2.5 shows the different kinds of co-ordinate bonds possible for a co-polymer.

In the TMAI group, electronic configuration, complex structure and stereochemistry are important. Crystal field splittings of the *d*-orbitals of an ion in tetrahedral, octahedral, tetragonal and square planar complexes are shown in Fig. 2.6. The energy difference between the degenerate *d* levels of the cation and the stabilized *d*-orbitals of the complex is indicative of the thermodynamic stability of the complex. Crystal field stabilization energies for d^n complexes (n designates the number of electrons in the d-orbital) of common octahedral and square planar configurations, and for both weak and strong field ligands are shown in Table 2.3. It may be observed from the table that d^0 and d^{10} ions (also d^5 ions at weak field ligands) are not stabilized by complex formation, while d^7 and d^8 ions benefit from complex formation of both octahedral and square planar configurations, particularly with strong field ligands.

2.4.4 Guidelines for ligand selection

For a given separation task it may be necessary to go through the following steps to develop a schematic approach to process development:

(1) A study is made of the inorganic chemistry of the target metal ion under the defined working conditions.

(2) The predominant interactions between the metallic ion and ligands are determined.

(3) A separation strategy is selected for the given ion based on the *host-guest interaction*, *chelate formation* or *ion-pairing* mechanisms.

(4) The effect of the various separation strategies on other counter-ions and co-ions needs to be considered.

(5) Finally, the strategies for successful elution need to be considered.

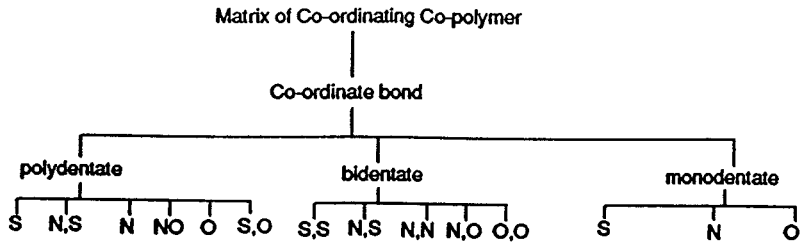

Figure 2.5 : Co-ordinating copolymers - donor atoms in one ligand [19]

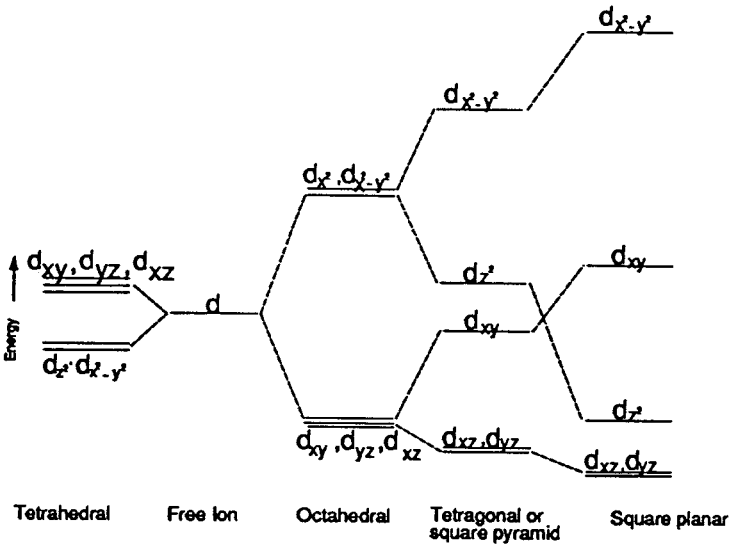

Figure 2.6 : Crystal field splittings of the d-orbitals of a central ion in regular complexes of various structures [14]

Table 2.3 : Crystal field stabilization energy of d^n complexes [14]

System	Example	Octahedral		Square Planar	
		Weak field	Strong field	Weak field	Strong field
d^0	Ca^{2+}, Sc^{3+}	0 Dq	0 Dq	0 Dq	0 Dq
d^1	Ti^{3+}, U^{4+}	4	4	5, 14	5, 14
d^2	Ti^{2+}, V^{3+}	8	8	10, 28	10, 28
d^3	V^{2+}, Cr^{3+}	12	12	14, 56	14, 56
d^4	Cr^{2+}, Mn^{3+}	6	16	12, 28	19, 70
d^5	Mn^{2+}, Fe^{3+}, Os^{3+}	0	20	0	24, 84
d^6	Fe^{2+}, Co^{3+}, Ir^{3+}	4	24	5, 14	29, 12
d^7	Co^{2+}, Ni^{3+}, Rh^{2+}	8	18	10, 28	26, 84
d^8	Ni^{2+}, Pd^{2+}, Pt^{2+}	12	12	14, 56	24, 56
d^9	Cu^{2+}, Ag^{2+}	6	6	12, 28	12, 28
d^{10}	Cu^+, Zn^{2+}, Cd^{2+}, Ag^+, Hg^{2+}, Ga^{3+}	0	0	0	0

2.5 Ion Exchange Technology

The theory and practice of ion exchange are well documented [15-18], and only the essential definitions and principles are elucidated here.

An ion exchange reaction may be expressed in general as follows:

$$mA + \overline{R_mB} \longleftrightarrow m\overline{RA} + B \qquad \text{.....(2.3)}$$

The thermodynamic equilibrium constant of the above reaction can be defined as :

$$K_A^B = \left(\frac{\overline{a}_A}{a_A}\right)^m \left(\frac{a_B}{\overline{a}_B}\right) \qquad \text{.....(2.4)}$$

where the a_i is the activity of the ion i.

Replacing the activities by concentrations we get :

$$K_B^A = \left(\frac{[\overline{A}]}{[A]}\right)^m \left(\frac{[B]}{[\overline{B}]}\right) \qquad \text{.....(2.5)}$$

K^A_B is known in ion exchange technology as the *selectivity coefficient.*

The extent of exchange in the process is defined by the distribution coefficient for the ion A; D_A:

$$D_A = \frac{milliequivalents\ \ of\ \ ion\ \ A\ \ per\ \ gm.\ \ of\ \ exchanger}{milliequivalents\ \ of\ \ ion\ \ A\ \ per\ \ ml\ \ of\ \ solution} \qquad \text{.....(2.6)}$$

When a number of counter-ions are being exchanged by the resin matrix, the ease with which the ion exchange process can separate one of the ions from the rest is expressed as the *separation coefficient* of ion A over ion C:

$$\alpha_C^A = \frac{D_A}{D_C} \qquad \text{.....(2.7)}$$

The *exchange capacity* is the number of ionogenic groups per specified weight of the resin. It is usually expressed in milli-equivalents per gram (meq./g) of dry resin or equivalents per litre (eq./L) of the wet settled resin. The following factors lead to a high exchange capacity [19] :

(1) Little or no cross-linking.

(2) Flexible crosslinks (alkyl rather than aryl crosslinks).

(3) Maximum number of active functional groups on the co-polymer.

(4) Maximum number of active donor atoms per active functional group eg. chelating rather than monodentate.

(5) High metal to ligand affinity.

(6) Strong metal-ligand bonds.

(7) Low co-ordination number of the metal.

When an ion exchanger is brought into contact with an aqueous solution, a considerable amount of water may enter the resin phase and cause swelling of the resin. Swelling is opposed by the elastic force in the matrix and attains an equilibrium value. Swelling hydrates functional groups and reduces capacity. Excessive swelling in ion exchange units can cause bed movement and lead to undesirable channeling.

Selectivity is the preference of a resin for any particular ion among many present in an aqueous solution and depends on both the resin and the counterion for strong and weak cation (acid) exchangers as follows [19] :

(1) Selectivity increases with the charge on the cation (Th(IV) > La(III) > Ca(II) > Na(I))

(2) Selectivity increases with decreasing hydrated radius of the cation.

(3) Selectivity increases with increasing polarizing power (related to the effective nuclear charge so that an ion with a high charge and a small radius like Al^{3+} has a high polarizing power).

(4) Selectivity is decreased by association and complexation in the aqueous phase as these decrease the activity of the free counterions available for exchange.

2.6 Kinetics of Ion Exchange

Initial theories on the kinetics of ion exchange were based on the speculative consideration of the process as a chemical reaction of a kinetic order corresponding to its stoichiometric coefficients. Much later in the 1950's the process was understood to be essentially a statistical redistribution of ions by diffusion, with a rate limited by mass transfer resistances in either the particle or the external fluid [21]. The next advance was made in the 1950's with the realization that ions, as carriers of electric charges, are subject to the electrical field that their own diffusion generates, thus obeying Nernst-Planck equations more closely than Fick's laws [15]. Shortcomings in the application of the Nernst-Planck equations arose due to variations in the swelling conditions and the relaxation behaviors of resin networks, which resulted in changes in particle size and ionic mobility, and the diffusion coefficient becomes a function of time as well as concentration [31]. A more fundamental problem arose later when the *individual diffusion coefficient* premise, present in the Nernst-Planck equations, did not satisfy experimental conditions, but an array of interaction coefficients as in Stefan-Maxwell equations provide more promising answers [43]. This led to the development of ion exchange kinetic models based on the *thermodynamics of irreversible processes* [46]. This section surveys the work done so far in these fields, leading up to the models used in the formulation of rate laws in ion exchange kinetics.

In general, in most kinetic studies of ion exchange processes, information on the following points is vital to process understanding and design [20] :

(1) The mechanism of the ion exchange process

(2) The rate determining step of the process

(3) The rate laws obeyed by the process

2.6.1 Mechanism of ion exchange

An ion exchange process is represented by :

$$\overline{R_mB} + mA \quad \longleftrightarrow \quad m\overline{RA} + B \qquad \text{.....(2.8)}$$

and could involve the following steps:

(1) Diffusion of ions A through the film surrounding the particle to the resin surface - film diffusion.

(2) Diffusion of ions A through the resin to the exchange sites - particle diffusion.

(3) Chemical exchange of ions A and B at the sites of functional groups of the exchanger.

(4) Diffusion of the exchanged ions B through the particle to the surface of the resin.

(5) Diffusion of the exchanged ions B through the liquid film surrounding the particle into the bulk solution.

However, the principle of electroneutrality requires that steps (1) and (5) occur simultaneously at equal rates and analogously steps (2) and (4) must occur at equal rates in opposite directions. As a result, the number of rate determining steps is reduced to the following three:

- film diffusion
- particle diffusion
- chemical reaction

The diffusion and loading inside the resin particle may proceed through three possible mechanisms as shown in Fig. 2.7, along with the associated concentration gradients [20]. Apart from the more common *gradient diffusion* mechanism based on Fick's theory, two other possible mechanisms expected to occur are the homogeneous mechanism (or progressive conversion) where the concentration gradient in the resin is homogeneous as discussed by Wen [22] and Levenspeil [23], and the shell progressive mechanism (or unreacted core model), developed by Yagi and Kunii [24].

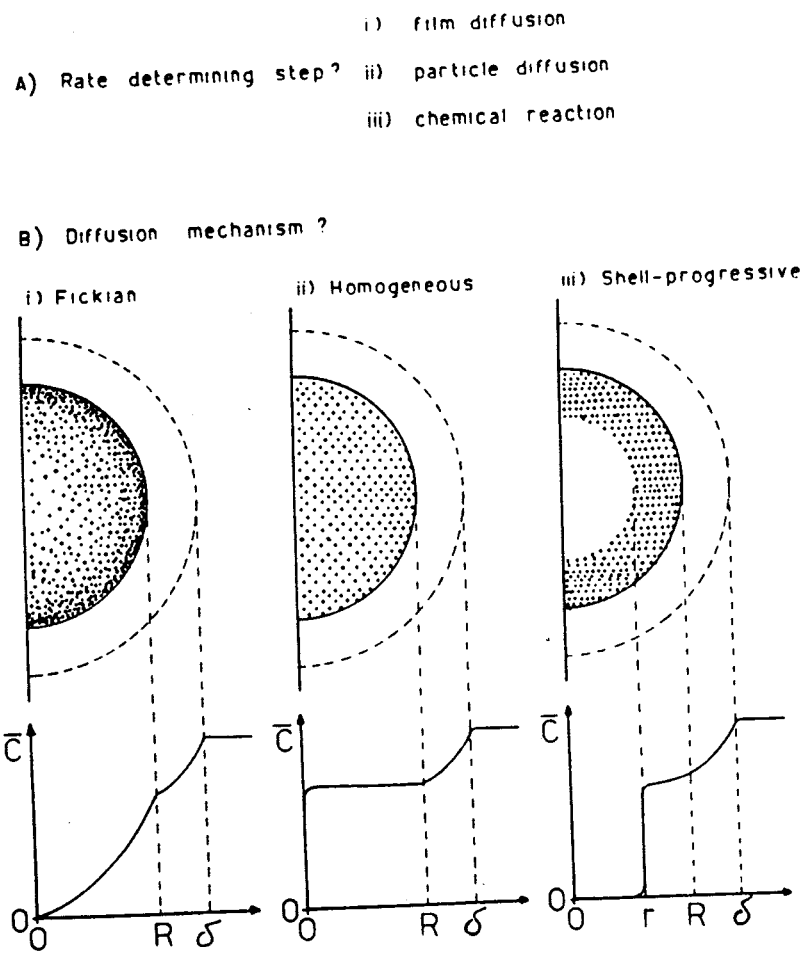

Figure 2.7 : Fundamental questions in kinetic investigations [20]

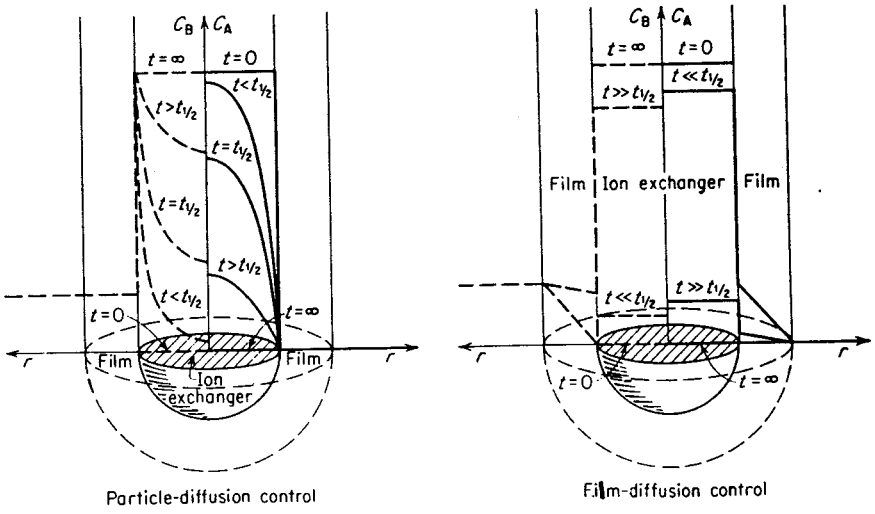

Figure 2.8 : Rate determining steps [15]

2.6.2 Rate determining step

Ion exchange processes are commonly controlled by the diffusion of counter-ions in the adherent film or in the resin matrix, rather than by the chemical exchange reaction. The rate controlling step often depends primarily upon the concentration of the external solution, and as a general rule, the film diffusion step is slow with solutions of the order of 0.01 N or less, while particle diffusion may become controlling with solutions of the order of 0.1 N or more [21] (Fig. 2.8). Helfferich [15] developed the following criteria for predicting the rate determining step, by comparison of the half times of particle and film diffusion:

$$\textit{Particle Diffusion Control} \;:\; \frac{\overline{RD}\delta}{CDr_o}(5+2\alpha_{A/B}) \;\ll\; 1 \qquad .....(2.9)$$

$$\textit{Film Diffusion Control} \;:\; \frac{\overline{RD}\delta}{CDr_o}(5+2\alpha_{A/B}) \;\gg\; 1 \qquad .....(2.10)$$

where R = concentration of fixed ionic group (equivalents)

C = concentration of counter-ions in the aqueous solution(equivalents)

D = diffusion coefficient in solution (overbar symbol for the resin phase) (m^2/s)

δ = film thickness (m)

r_o= radius of the resin bead (m)

$\alpha_{A/B}$ = separation factor (dimensionless)

The quantities R, C, r_o and $\alpha_{A/B}$ are usually known or may be determined based on the properties of the resin [15]. The values of the diffusion coefficient in the aqueous and resin phases are determined as harmonic means of the individual diffusion coefficients of counter-ions A and B as follows [91]:

$$\overline{D}_{AB} = \frac{\overline{D}_A\overline{D}_B(z_A+z_B)}{z_A\overline{D}_A+z_B\overline{D}_B} \qquad .....(2.11)$$

$$D_{AB} = \frac{D_AD_B(z_A+z_B)}{z_AD_A+z_BD_B} \qquad .....(2.12)$$

where z_i = electrochemical valence of species *i*.

In the case that $\overline{D}$ values are not available, it can be assumed that $D/\overline{D}$ = 10 or other estimates may be obtained from Wheeler [25] :

$$\overline{D}_i = \frac{D_i \varepsilon}{2} \qquad \text{.....(2.13)}$$

or Mackie [26] :

$$\overline{D}_i = \frac{D_i \varepsilon^2}{(2-\varepsilon)^2} \qquad \text{.....(2.14)}$$

where ε = fractional pore volume of the ion exchanger

The film thickness δ is obtained through the Sherwood number as follows:

$$Sh = \frac{2r_o}{\delta} = \frac{2k_m r_o}{D} \qquad \text{.....(2.15)}$$

where Sh = Sherwood number

k_m = mass transfer coefficient in the film

The Sherwood number is a function of the Reynolds (Re) and Schmidt (Sc) numbers [88]:

$$Sh = 0.37(Re)^{0.6}(Sc)^{0.33} \quad for \quad 20 < Re < 150000 \qquad \text{.....(2.16)}$$

$$Sh = 2 + 0.37(Re)^{0.6}(Sc)^{0.33} \quad for \quad Re < 20 \qquad \text{.....(2.17)}$$

Depending on the hydrodynamic conditions, the film thickness is usually in the order of 10^{-2} - 10^{-1} mm. Further distinction can be made on the rate determining step based on experimental data as follows:

Table 2.4 : Dependence of ion exchange rate on experimental conditions [15].

Factor	Rate of PDC	Rate of FDC
Counter-ion mobility :		
In particle	$\propto \overline{D}$	No effect
In aqueous film	No effect	$\propto \overline{D}$
Co-ion mobility	No effect	No effect
Particle size	$\propto 1/r_o^2$	$\propto 1/r_o$
Capacity of resin	No effect	$\propto 1/X$
Degree of crosslinking	Decreases with increase in crosslinking	No effect
Concentration of solution	No effect	$\propto C$
Temperature	Increases 4-8% per °C	Increases 3-5% per °C
Rate of agitation or flow	No effect	Increases with agitation rate

Note : PDC = Particle Diffusion Control
FDC = Film Diffusion Control

2.6.3 Rate laws of ion exchange

The rate of ion exchange is a complicated function of physico-chemical and hydrodynamic parameters. All these parameters except the diffusion coefficient of the ions in the liquid film and in the resin particle are known or readily obtainable. One method of conducting kinetic studies involves trying to fit the experimental rate data to various available rate equations from literature and computing diffusion coefficients from this analysis. This, however, creates the danger of choosing a rate law which gives the best fit of experimental data, obtained under specific conditions, but which does not necessarily reflect the actual ion exchange process. An alternative but more complex approach is based upon the fundamental physico-chemical processes occurring during the course of ion exchange. The necessary tools and equations for carrying out both approaches are outlined in the following sections.

2.6.3.1 Ion exchange systems not involving chemical reactions

Kinetic analyses of this kind were initially worked out by Boyd and co-workers [21,27,28]. In very dilute solutions, if the mobility of the counter-ions is equal, the diffusion flux of species *i* may be adequately described by Fick's first law:

$$Film\ \ Diffusion\ :\ J_i = -D_i\ grad\ c_i \qquad .....(2.18)$$

$$Particle\ \ Diffusion\ :\ \overline{J}_i = -\overline{D}_i\ grad\ \overline{c}_i \qquad .....(2.19)$$

where J_i = flux of diffusing species *i* ($kg/m^2\ s$)

D_i = diffusion coefficient of species *i* (m^2/s)

c_i = concentration of species *i* (kg/m^3)

and overbar species represent the resin phase.

(A) Particle Diffusion Control

The time dependence of the concentration is related to the material balance by Fick's second law:

$$\frac{\delta \overline{c}_i}{\delta t} = -div\overline{J}_i \qquad .....(2.20)$$

Combining equation (2.19) and (2.20) for spherical particles:

$$\frac{\delta \overline{c}_i}{\delta t} = \overline{D}_i\left(\frac{\delta^2 c_i}{\delta r^2} + \frac{2}{r}\frac{\delta c_i}{\delta r}\right) \qquad .....(2.21)$$

This equation may be solved for this and various other diffusion geometries [31] given the initial and boundary conditions. For a linear driving force relation, this was approximated by Glueckauf and Coates as follows [29] :

$$\frac{\overline{dc}_i}{dt} = \frac{\overline{D}_i k}{r_o^2}(\overline{c}_i^* - \overline{c}_i) \qquad .....(2.22)$$

where $\overline{c_i}$ =average concentration of the resin phase in equilibrium with the external solution

k = empirical constant

r_o = radius of the resin

A closer approximation of equation (2.21) is obtained by the quadratic relationship of Vermeulin [30] :

$$\frac{\overline{dc_i}}{dt} = \frac{\overline{D}_i \pi^2}{r_o^2} \frac{\overline{c}_i - \overline{c}_i^2}{2c_i} \qquad .....(2.23)$$

where c_i is the mole fraction rather than concentration of species *i*.

(B) Film Diffusion Control

From the material balance condition and the requirement of equilibrium at the particle film interface, the following equation was obtained by Boyd [21] :

$$\frac{dc_i}{dt} = \frac{3cD}{r_o \overline{c}} \frac{(c_i^b - c_i^*)}{\delta} \qquad .....(2.24)$$

where c_i^* = concentration of species *i* at the particle-film interface(kg/m^3)

c_i^b = concentration of species *i* in the bulk solution(kg/m^3)

c = total counterion concentration in solution (and in the resin phase for the overbar term) (kg/m^3)

2.6.3.2 Ion exchange accompanied by chemical reactions

Even though most ion exchange processes are diffusion controlled as argued by Boyd [21], through a mathematical coincidence, a quantitative description of ion exchange as a reversible second order reaction proved much more tractable than the diffusion rate laws when applied to calculations of ion exchange columns [32] and so the reaction model was retained

by engineers who formalized this convenience by relating the reaction rate coefficient to the mass transfer coefficient [33,34]. However, recently, more rigorous models of reaction in ion exchange have surfaced once again.

Ion exchange systems involving neutralization, hydrolysis and complex-formation reactions have been analyzed from a theoretical point of view, by Helfferich [35]. For certain types of ion exchange processes occurring in a spherical resin bead, such as for example, the proto-nation of a weak base or weak acid resin or complex formation reactions, Helfferich postulated the likelihood of a sharp moving boundary. The existance of sharp moving boundaries has been demonstrated by Dana and Wheelock [36] who studied elution of copper amine com-plexes from a sulfonic acid exchanger and by Holl and Sontheimer [37] who investigated protonation of a weak acid resin. Both these groups of investigators used resins with a transparent matrix in their studies. This permitted visual observations of sharp moving boundaries in the reacting resin beads.

2.6.3.3 Electric potential gradient and the Nernst-Planck equation

Ions, as carriers of electric charge are subject to electric forces. Their diffusion generates an electrical potential gradient, a *diffusional potential*, whose action on the ions has to be taken into account in their equation of motion. This is done by the Nernst-Planck equation:

$$J_i = -D_i\left(grad c_i + z_i c_i \frac{F}{RT} grad\phi\right) \qquad .....(2.25)$$

Flux *Diffusion* *Electrical* *transference*

where z_i = Valency of the ion

F = Faraday's constant

R = Universal gas constant

Φ = Electric potential gradient

This proposes that an initial minute disparity of diffusion fluxes causes a minute deviation from electroneutrality, immeasurable except through observation of electric potential differences. The electric potential gradient produces electric transference of both ions, in the direction of the diffusion flux of the slower ion, in effect retarding the faster ion and accelerating the slower one as shown below:

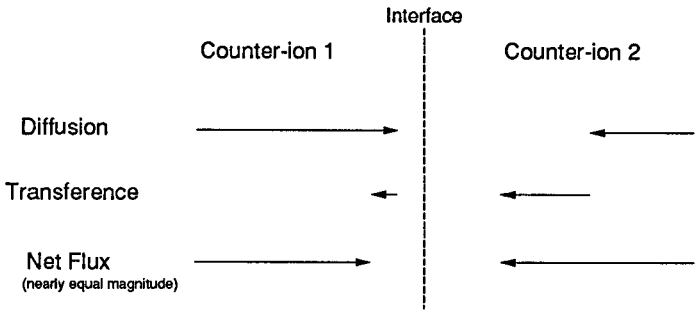

Figure 2.9 : Electric transference acts to equalize the net flux

The electric potential gradient thus is the mechanism which enables the system to maintain a state so close to electroneutrality, that the deviation is negligible in just about all cases of practical interest in ion exchange kinetics [39].

Initial applications of the Nernst-Planck equations integrated for ideal systems, under the constraints of electroneutrality and absence of an electric current, for the geometry of a homogeneous sphere, and under the simplest conceivable initial and boundary conditions were tried by Helfferich [39]. Nernst-Planck equations have been applied to the deviation from electroneutrality at the particle-solution interface and in and around extremely small ion exchanger particles [38]. Another problem requiring a more elaborate treatment is that of ion exchange with macroporous resins, for which the flux equations must be solved for a more complex geometry [39]. Along different lines, application of the Nernst-Planck equations to real systems calls for the inclusion of an additional term accounting for the effect of gradients of activity coefficients :

$$J_i = -D_i\left(grad\,c_i + c_i grad \ln f_i + z_i c_i \frac{F}{RT} grad\,\phi\right) \qquad .....(2.26)$$

and has been carried out for the case of zeolites [40,41]. Still another complication to be accounted for, concerns co-ions which are transferred in the direction of the faster counterion with the solvent being transferred in the opposite direction, and this adds a convective term to the Nernst-Planck equation [42]. It may also be necessary to account for concentration gradients in both the film and particle, with non-linear equilibrium at the particle surface then deserving special attention [43].

2.6.3.4 Systems involving diffusion and reaction

Inspite of the understanding of ion exchange as a statistical redistribution of ions, there are, however, situations in which a *reaction* - i.e. the formation or dissolution of a chemical bond, is undoubtedly involved. Among the reactions that often accompany ion exchange are acid-base neutralization, dissociation of weak electrolytes in solution or weak ionogenic groups in an ion exchanger, complex formation, or combination of these, resulting in an abnormally low apparent interdiffusion coefficient in the ion exchangers. A few examples are listed below:

$$\overline{RSO_3^-} + H^+ + Na^+ + OH^- \rightarrow \overline{RSO_3^-} + Na^+ + H_2O \qquad .....(2.27)$$

$$\overline{RCOO^-} + Na^+ + H^+ + Cl^- \rightarrow \overline{RCOOH} + Na^+ + Cl^- \qquad .....(2.28)$$

$$\overline{RNH_2} + H^+ + Cl^- \rightarrow \overline{RNH_3^+} + Cl^- \qquad .....(2.29)$$

$$\overline{2RSO_3^-} + Ni^+ + 4Na^+ + EDTA^{4-} \rightarrow \overline{2RSO_3^-} + 2Na^+ + 2Na^+ + NiEDTA^{2-} \qquad ..(2.30)$$

The distinguishing feature is that the basic material balance must now account for mass transfer and reaction rate as follows:

$$\frac{\delta c_i}{\delta t} = -div J_i + R_i \qquad .....(2.31)$$

The effect of this on kinetic behavior can be significant. The rate may be decreased by several orders of magnitude, the dependence on variables such as solution concentration is considerably altered, and quite distinct mechanistic features may appear [44]. If the reaction is slow compared to diffusion, then in the limiting case the diffusion is fast enough to level out any concentration gradients within the ion exchanger particle, and hence with the reaction at the fixed site being the sole rate controlling factor, the rate is independent of the resin particle size. Such a situation, however, has never been convincingly demonstrated for ion exchange [38]. The more common case is that of the reaction being faster than diffusion, so that local equilibrium exists at any point. The rate here is controlled by (slow) diffusion which, in turn, is affected by the equilibrium of the (fast) reaction leading to the *progressive shell mechanism.*

2.6.3.5 Progressive shell mechanism

In this case a fast and practically irreversible reaction in the particle eliminates or generates one of the exchanging ions [44] as in neutralization of a weak acid cation exchanger in free acid form by a strong base:

$$\overline{RCOOH} + Na^+ + OH^- \rightarrow \overline{RCOO^-} + Na^+ + H_2O \quad .....(2.32)$$

The base reacts immediately with acid groups as soon as it reaches the unconverted ion exchanger site of *RCOOH*. As a result, conversion to the Na^+ form proceeds with a sharp front from the surface towards the centre of the particle. At any time, an unconverted, shrinking *core* still completely in free-acid form is surrounded by a converted (to the Na^+ form) *shell* and growing in thickness. Such behaviour variously called *progressive shell, shrinking core, unreacted core* or *moving boundary mechanism* was verified by Dana et al [36], and a model for the same is developed in a later section.

2.6.3.6 Further developments in kinetic studies

The inherent premise of the Nernst-Planck approach is that diffusion and transference are additive phenomena, both characterized by a coefficient describing the mobility of the respective ion, and that the fluxes are coupled only through the electric potential gradient. In recent years, several more fundamental approaches to mass transfer in ion exchangers have been taken, with statistical considerations [45], thermodynamics of irreversible processes [46,47] or the Stefan-Maxwell equation [47,48] as the starting point, and a more complex picture emerges in which fluxes are coupled not only through the electric potential gradient, and more than one coefficient per species is required to characterize kinetic behavior.

2.7 Experimental Methods in Ion Exchange Kinetic Studies

Kinetic studies may be carried out on ion exchange processes for a variety of reasons. The applied researcher may desire to know, at a certain stage of development of a new application (usually after equilibrium evaluation), how the kinetic features of the resin compare with its selectivity performance, while a design engineer may carry out these studies to experimentally determine mass transfer coefficients, and other kinetic parameters to design an ion exchange plant or to compare the performance of various resins. This section surveys the various types of apparatus used by researchers, and suggests investigation techniques and experimental conditions relevant to particular ion exchange processes.

2.7.1 Selection of the apparatus for rate studies

The general type of apparatus used for kinetic studies may be broadly divided as *batch systems* (where the concentration of the counter-ions in the external solution changes with time) and *shallow bed techniques* (where the concentration of counter-ions in the external solution remains constant during the experiment). The design engineer, however, finds the traditional laboratory column studies more practical in terms of the relevant design information obtained, and hence the technique is also outlined here.

2.7.1.1 The batch system

Appropriate volumes of the ion exchange resin and solution of known initial composition are mixed and vigorously stirred (1000 - 3000 rpm to minimize mass transfer resistances through the film), while the time variation of a representative property of the system (eg. pH, conductivity, electric potential, concentration of ion or radioactivity etc.) is recorded. The experimental method outlined by Kressman and Kitchener [49] uses a centrifugal stirrer (see Fig. 2.10), which encases the resins. Centrifugal action forces the inner solution to leave the stirrer through the radial holes in the encasing, being instantaneously replaced by fresh solution entering the cage at the bottom. This also allows for the instantaneous separation of the resins and solution by raising the stirrer out of the solution. The method used by Boyd and Saldano [27] contacts an exchanger equilibrated with a radioactive isotope, with a feed solution containing the same counter-ion as the ion exchanger but free of the radio-isotope. Aliquots of solution are withdrawn at various times and analyzed for the radioactive isotope using a scintillation counter. The radioactivity of the solution is proportional to the fractional attainment of equilibrium.

2.7.1.2 Limited bath method [49,50]

A known quantity of resin in A-form is contacted with the solution containing an equivalent quantity of counter-ion B. After the desired period of time the resin is quickly removed from the solution and one of the two phases analyzed. The procedure is repeated at various time intervals, to obtain the necessary relationship of fractional attainment of equilibrium as a function of time.

2.7.1.3 Indicator method [51,52]

This method is applicable to systems involving the transfer of hydrogen ions. It was used for measuring the rate of Na^+ uptake by hydrogen-form sulphonic acid resins. Aqueous solutions containing sodium chloride (larger amount), sodium hydroxide (smaller amount)

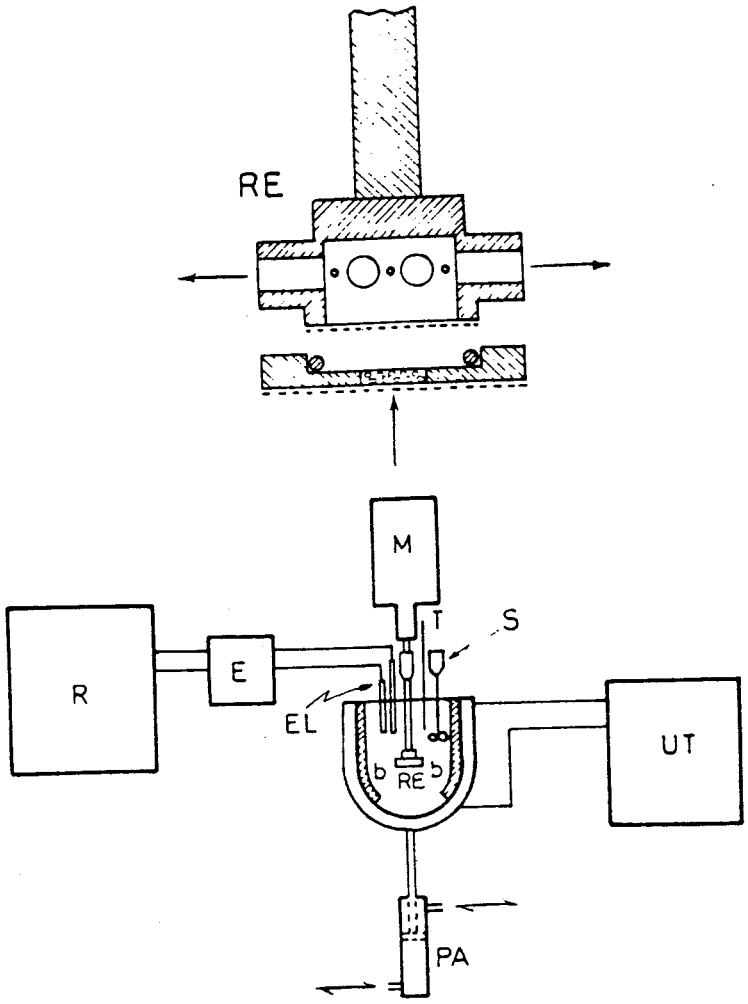

Figure 2.10 : Schematic diagram of the apparatus for the batch Process [49]
RE=centrifugal stirrer, E=potentiometer, R=recorder, M=stirrer, T=thermometer, EL=electrodes, PA=pneumatic piston, UT=ultra-thermostat, B=jacketed vessel, bb=baffles, S=supplementary stirrer

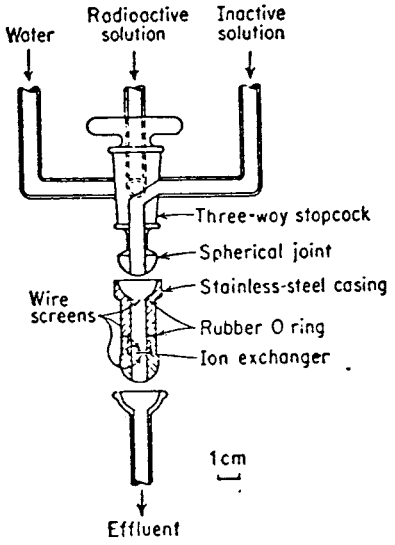

Figure 2.11 : Shallow bed apparatus for ion exchange kinetics [21]

and bromocresol green indicator were contacted with a sulphonic acid resin. On the equivalent basis, the quantity of resin was always greater than that of the sodium hydroxide but less than that of the sodium chloride. The time at which the indicator changed color (i.e. when all NaOH was consumed by the liberated hydrogen ions) was recorded. A series of experiments was performed at constant phase ratio and Na^+ concentration in the aqueous phase, but with variable concentration of the sodium hydroxide in the feed solution. If the sodium chloride is added in a large excess, the concentration of Na^+ in the aqueous phase is virtually constant and this simplifies the mathematical treatment of the data.

2.7.1.4 Shallow bed technique

In this method a thin layer of ion exchanger beads is placed in a micro-column and a known solution is forced to enter the layer as in Fig. 2.11. The variation of some representative parameter is determined with time to give a description of the kinetic behaviour of the system [21]. The main advantage of this technique over the batch technique is that if the solution flow is high enough, the exchange occurs under *infinite solution volume* (ISV) conditions - i.e. negligible concentration of the ion released by the resin to the solution throughout the process; a situation that greatly simplifies the calculations (the same ISV condition may be realized for the batch technique by using an *equivalent ratio* - solution to resin of greater than 100). This technique results in a plot of exchange flux as a function of time. This is converted to fraction of ion extracted (X) by graphical integration of the flux function.

2.7.1.5 Photographic method [36,37]

This method is applicable to ion exchange systems involving sharp moving boundaries. In order to observe the position of an unreacted core as a function of time, the resin matrix must be transparent. A monolayer of resin beads, initially in the A-form, is contacted in a column with a solution of the counter-ion B. The monolayer of the resin is photographed

using a microscope at different time intervals. This function curve gives the position of an unreacted core as a function of time, which can easily be converted to fraction extracted as a function of time.

2.7.1.6 Cone model method [53]

A cone with a large ratio of the height to the base diameter is filled with an ion exchanger in the A-form. The lower section of the cone is assembled from rings approximately 1 mm thick. The base of the cone is covered with a porous filter. The assembled cone cell is then placed into an agitated vessel containing a solution of the counter-ion B. After a certain period of time the cone is removed from the vessel and the resin is sliced into thin layers along the rings. The resin from the individual layers is analyzed to provide a curve showing the uptake of the counter-ion B as a function of the cone height. A number of such experiments are performed for different contact times.

2.7.1.7 Laboratory column

Column studies provide more practical data of interest for the design engineer like resin exchange capacity, breakthrough capacity, exhaustion time etc. (Fig. 2.12), which compare well with those obtainable in industrial columns, if experimental conditions are similar (i.e. the use of real solutions, similar flow rates etc.). Crucial parameters [54] are column bed depth (usually about 60 cm or more to permit the full development of the exchange zone within the column) and diameter (at least 40 times the average resin diameter to minimize wall effects (a column diameter of 1.2 cm or more with commercial resins).Effluent aliquots are withdrawn at various known time intervals to obtain the *breakthrough curve*, which is extremely useful for practical purposes such as over-all and dynamic resin exchange capacities, comparison of different resins for a similar industrial application, evaluation of service time, throughput etc.. Further, breakthrough curves may also be used to determine the type of equilibrium by determining the pattern of the curve as the bed depth is increased [15], or to discriminate

between particle and film diffusion kinetics by determining the variation of the midpoint slope of the curve with feed flow rate, which would be independent of the feed rate for particle diffusion, but would be dependent on the square root of feed spatial velocity for film diffusion controlled kinetics [55]. The following compares the features of the experimental techniques:

Table 2.5 : Comparison of experimental techniques for kinetic studies [20].

	Batch system	Shallow bed system	Laboratory column
Outputs	Extraction (X) vs t	Flux vs. t	Breakthrough curve
Advantages	-minimum film resistance -direct diffusion coeff. calculations -choice of analytical parameters -FSV and ISV possible	-ISV easy -direct diffusion coeff. calculations	-practical design information -choices of analytical parameters
Disadvantages	-indirect design information -ISV is difficult	-indirect design information -radioactive measurement generally necessary -high liquid ressistance	-FSV rather than ISV -indirect calculation of diffusion coeff. -high liquid resistance

Note : FSV = Finite Solution Volume; ISV = Infinite Solution Volume

2.7.2 Monitoring techniques and operating conditions

The selection of monitoring techniques and operating conditions is a crucial factor in carrying out kinetic tests with the objective of determining the diffusion coefficients, from a well defined theoretical background. In the kinetic investigation, an electrochemical property such as pH or conductivity may be followed continuously and reproducibly when H^+ or OH^- ions are exchanged by other, less conductive species. Potentiometric measurements may be usefully performed when selective electrodes for one of the species exchanged are available. By means of reference

curves, these properties are easily related to the actual concentration of the species exchanged so that the fractional attainment of equilibrium can be obtained. When the difference between the electric properties of the exchanging counter-ions is small, or when the extent of exchange is limited (such as in *differential exchanges*, where only 10-20 % of resin conversion takes place in an experiment) or more generally, whenever the ISV condition is to be applied, the use of a radioactive species appears extremely useful with precise and affordable measurements being possible.

The techniques mentioned so far are indirect techniques. Direct monitoring techniques such as autoradiography and X-ray microprobe analysis may also be used. Autoradiography, which requires the use of at least one radioactive species, consists of thin sections of resin particle, loaded with appropriate amounts of the isotope, being contacted in the dark with special films sensitive to isotopic radiation. The magnified picture of the section at different values of fraction converted (X) permits visible verification of the mechanism of isotope distribution inside the resin particle (Fig. 2.13) [56,57]. X-ray microprobe analysis does not require the use of isotopes, as the energy of the electron beam of the instrument may be adjusted so as to reveal selectively almost any element present in the section of the resin bead, and follow its distribution in the resin phase (eg. Fig. 2.14). Another direct investigation technique devised by Hoell [58] uses the variation of the refractive index of methacrylic resins when converted from the H^+ form to the metal-alkali form.

The dependence of exchange kinetics on experimental conditions such as stirring rate, temperature, resin particle diameter etc., is determined by whether the operating mechanism is particle diffusion controlled (PDC) or film diffusion controlled (FDC). In order to ensure infinite solution volume (ISV) conditions, it is necessary to have the equivalents of counter-ions in solution of at least one hundred times that in the resin. In general low values of solution concentration, stirring speed, resin particle diameter, ion diffusion coefficient in solution and a high resin exchange capacity facilitate the film diffusion controlled mechanism.

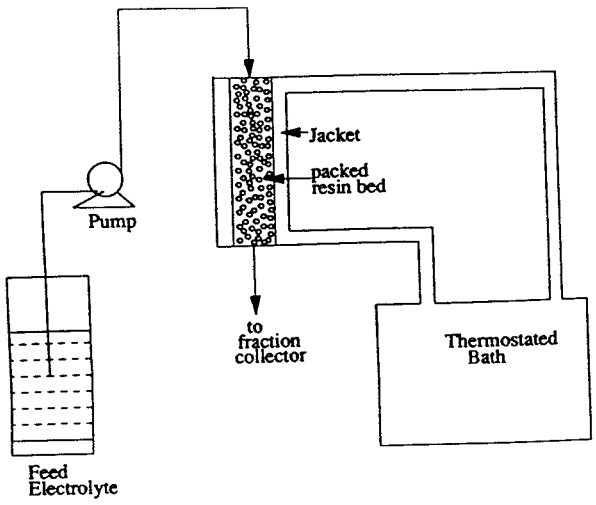

Figure 2.12 : The laboratory column

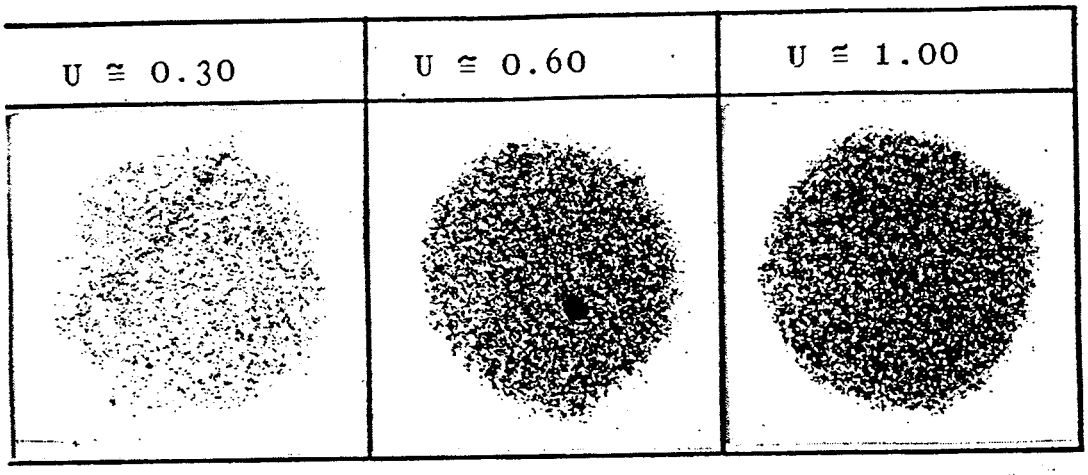

Figure 2.13 : A typical autodiagram (U=fraction extracted) [57]

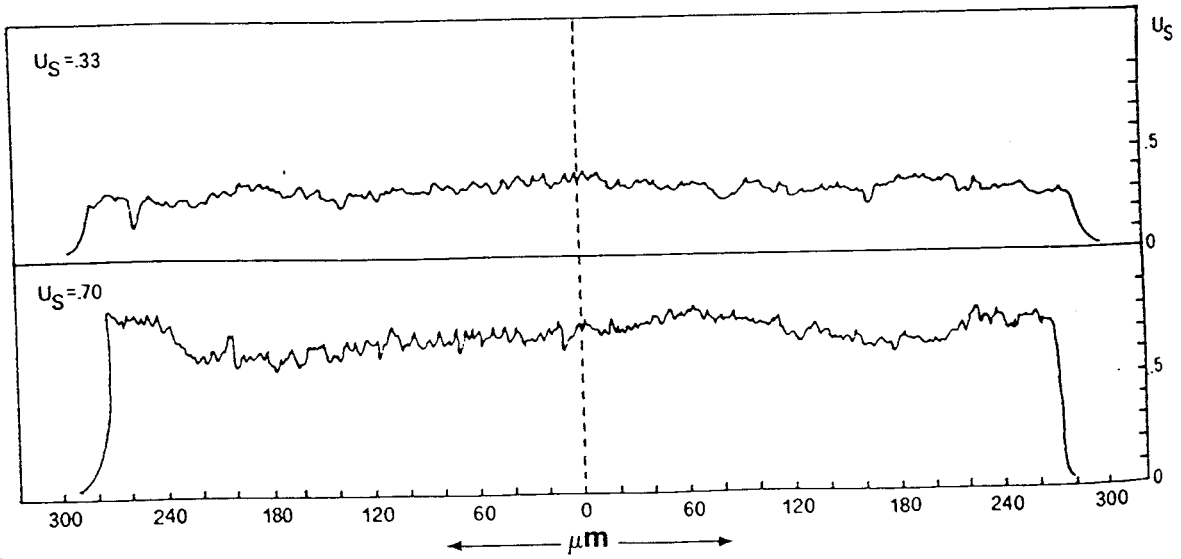

Figure 2.14 : A typical X-ray microprobe analysis at 33% and 70% extraction [20]

2.8 Solvent Impregnated Resins

Ion exchange is today viewed as one unit process amongst several separation methods, and is closely related to solvent extraction and membrane separation processes. Solvent extraction offers better selectivity, larger mass output, lower reagent costs, but greater operating costs and considerable risks. Membrane separation processes offer the highest dynamic output efficiencies, excellent safety features, though the reagent costs are high and the selectivity is not as good. Ion exchange performs well in concentrating metals from very dilute solutions with fairly good selectivities, whereas for the similar operation, solvent extraction would pose the problem of high reagent losses, even though the selectivity would be better. There are, however, problems with ion exchange, such as hydrophobicity of the resin, insufficient mobility of the resin bound ligand, and much weaker complexation constants in the resin phase, which reduce extraction efficiency considerably in very dilute solutions. This led to the development of special *solvent impregnated resins*, which combine the selectivity and specificity of conventional liquid extractants, with the advantages of a discrete polymer support material, thus tailor-making adsorbents for a specific separation process. These resins may be prepared by physical impregnation of the reagent onto a polymeric or other porous support without chemical bonding of any sort. Alternatively, co-polymerization of a monomer (eg. styrene) - crosslinking agent (divinylbenzene) in the presence of a reagent (eg. tri-n-butyl phosphate or di-2-ethylhexyl phosphoric acid) will produce a polymer encapsulated product. Typical of these products are the Levextrel resins developed by Bayer [59]. An exhaustive review of extraction with solvent impregnated resins has been published by Warshawsky [60]. The principal difficulty in the use of these materials is the slow diffusion of the reagent out of the polymer matrix.

2.9 Cobalt Purification

2.9.1 Introduction

Sulphide ores mined by INCO Limited from the Sudbury basin, contain copper, nickel and small quantities of cobalt, as well as trace precious metals. During benefication, cobalt distribution to various streams is similar to nickel. Recovery of the metals is carried out in multi-stage milling, smelting and refining processes. After smelting, nickel is selectively extracted by carbonyl refining and the cobalt remains in the carbonylation residue. This residue is processed in a specialized hydrometallurgical plant [61] (the CRED plant at Copper Cliff, Ontario) to produce precious metal residues, copper cathodes, and a nickel-cobalt carbonate intermediate product, containing about 20 % cobalt. This nickel-cobalt carbonate is shipped to the refinery at Port Colborne, Ontario, where the cobalt is separated to cobaltic hydroxide in the *Cobalt Hydrate Plant* and refined to metallic cobalt in the *Electro-Cobalt Plant* (refer Fig. 2.16 & 2.17 for the process flowsheets).

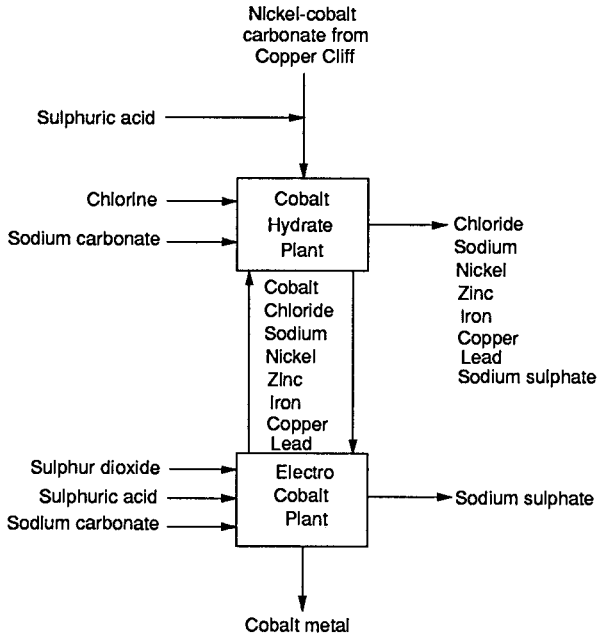

Figure 2.15 : Cobalt purification at Port Colborne

2.9.2 Cobalt Hydrate Plant

The slurry of nickel-cobalt carbonate is leached in a batch process, in which pre-reduced spent electrolyte is mixed with sufficient nickel-cobalt carbonate, to replenish the spent electrolyte strength from 45 g/L to 95 g/L cobalt. Copper removal takes place initially by cementation and zinc removal by Bayer Lewatit OC 1026 resin, which is the focus of this study. Nickel removal is then accomplished by the addition of chlorine and soda ash, which oxidises the cobalt(II) to the cobalt(III) state, and raises the pH to about 5.0, bringing about the hydrolytic precipitation of cobaltic hydroxide. This upgraded cobaltic hydrate is now sent to the Electro-Cobalt Plant.

2.9.3 Electro-Cobalt Plant

The cobaltic hydrate purification circuit forms an integral part of the process because of the two-way transfer of some of the cobalt and impurities between the hydrate circuit and the refining process (Fig. 2.15). The slurry of cobaltic hydrate is aerated to remove the Cl_2 from the previous process and is then filtered and washed. Barium carbonate and sulphur dioxide are then added with NaOH. Barium carbonate is added to co-precipitate lead and the leach liquor copper, while sulphur dioxide reduces the cobaltic hydroxide to the cobaltous form. At the endpoint of this step, a small amount of cobaltic hydrate is added to scavenge any excess sulphur dioxide and to oxidize the ferrous iron. The solids are returned to the cobalt hydrate plant for cobalt recovery and rejection of impurities. Practically all the zinc and nickel, and a minor amount of copper remaining in the solution are polished down to required concentration levels by a series of ion exchange systems. Copper is removed using DOW XF 4195 resin in a single column. Nickel is also removed by DOW XF 4195 resin with four columns in series. All ion exchange columns operate downflow in the flooded mode. The electrowinning process relies on several novel developments and process conditions [63], which allow for electrowinning with a very high cobalt depletion from the all sulphate electrolyte, using bagged and hooded lead anodes of special design and assembly. The

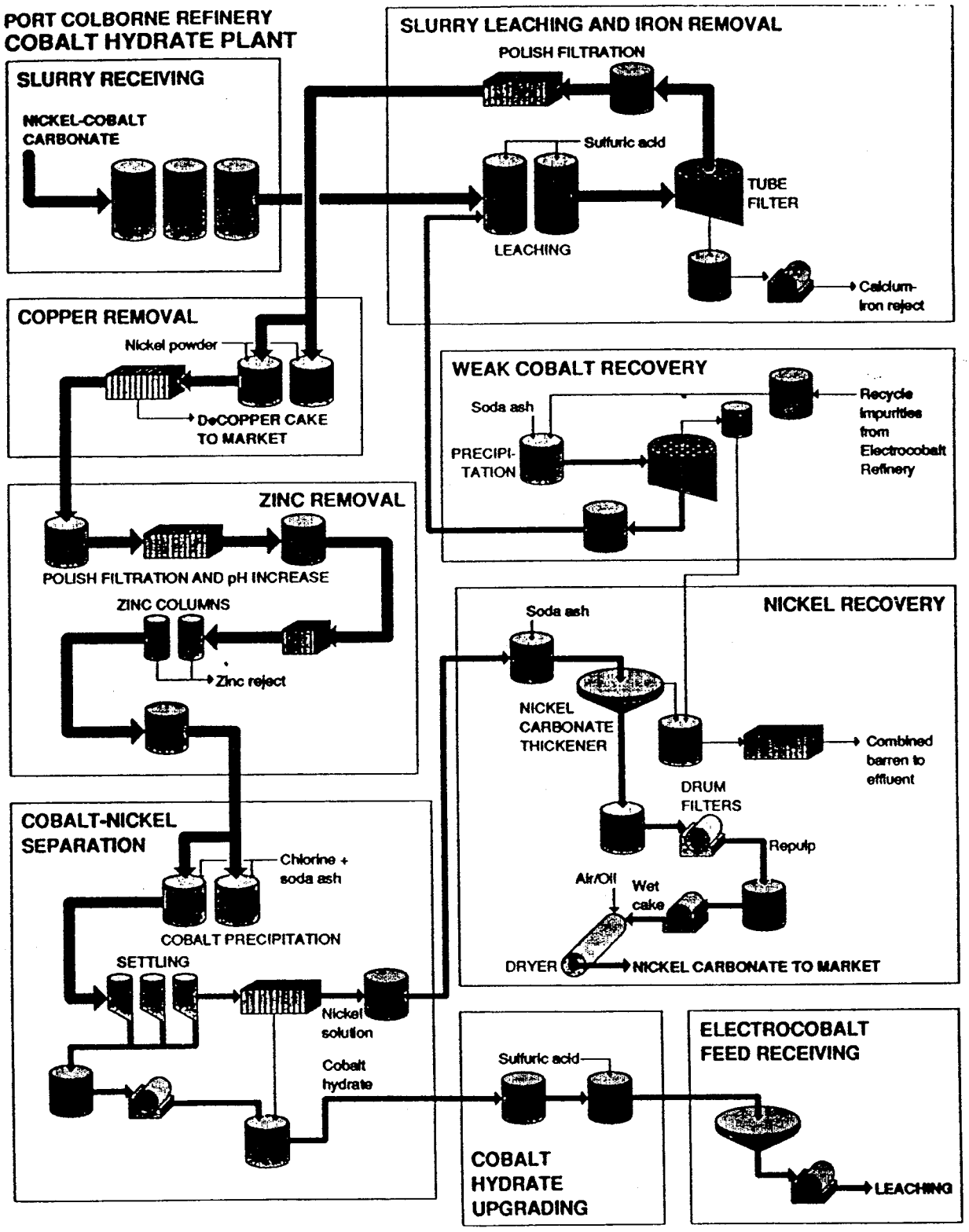

Figure 2.16 : The Cobalt Hydrate Plant [62]

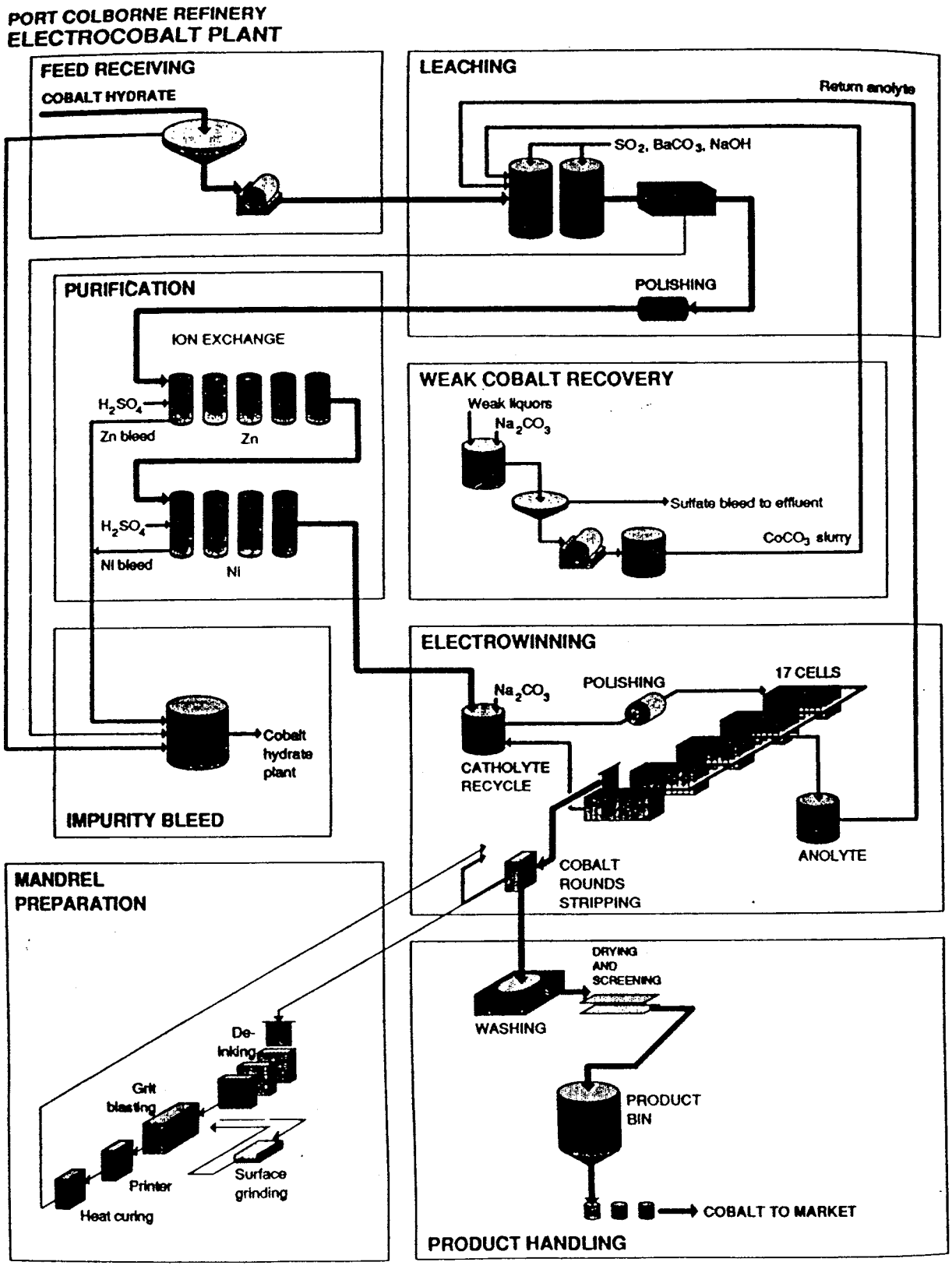

Figure 2.17 : The Electro-Cobalt Plant [62]

electrolytic tankhouse atmosphere is made cobalt and acid-free, and high purity cobalt rounds are produced on 304 stainless steel mandrels. Plating conditions are summarized in the following table:

Table 2.6 : Plating conditions for cobalt electrowinning.

Parameter	Value
Current density (based on total cathode area)	200 A/m^2
Temperature	60 °C
Catholyte pH	3.5
Cell voltage	4.0 V
Current efficiency	92 %
Plating time	5 days

The one inch diameter rounds are washed and harvested through an automated system. After drying, the rounds are processed on a continuous basis through a hydrogen degassing system followed by storage and barrelling for sale in 250 kg. drums. The following table presents a typical analyses of process streams at various stages.

Table 2.7 : Analyses of process streams at various stages of the flowsheet.

Concentration at Stage (g/L)	Cu	Ni	Fe	Zn	Pb	Ca	Co
Feed Stock Slurry, g/L	8	45	0.8	0.03	0.00005	2	45
After dissolution & Fe removal(g/L)	6	35	<0.003	0.02	0.00005	0.6	35
After initial Cu & Zn removal(g/L)	0.005	35	<0.003	0.001	0.00005	0.5	35
Redissolution and Co/Ni separation	0.0001	1	<0.003	0.001	0.00002	0.5	95
Feed to Electrowinning, g/L	0.0002	0.2	<0.003	0.0002	0.00002	0.5	90
Electrocobalt, ppm	1	500	3	5	5	3	99.94%

2.10 Extractants for Zinc

The primary recovery of zinc from leach liquors through solvent extraction or ion exchange processes is presently limited to only a few plants. These processes are however used widely for

the removal of zinc impurities from various electrolytes and waste streams. The following sections deal with the extractants used for zinc recovery or removal, and survey their chemistry, extraction equilibria and industrial applications.

2.10.1 Di (2-ethylhexyl) phosphoric acid

Di (2-ethylhexyl) phosphoric acid (hereafter referred to as D2EHPA in the text and as HL in equations) is an alkylphosphoric acid which has become widely used in solvent extraction practice, as in the separation and recovery of uranium, cobalt/nickel and rare earths. It has adequate kinetics, moderate separation capability, low aqueous solubility, and is chemically stable [66]. Its wide availability and low cost make it popular, compared to other reagents.

2.10.1.1 Chemistry

The chemical formula of D2EHPA is as follows:

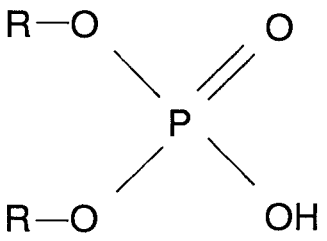

R = 2 ethyl hexyl group

Figure 2.18 : Sketch of the D2EHPA extractant (pK = 1.2)

It is a weak acid, and is relatively insoluble in water. The reaction between a metal cation and the D2EHPA dimer may be expressed by the following generalized equation:

$$M^{m+} + n\overline{(HL)_2} \longleftrightarrow \overline{ML_m(HL)_{2n-m}} + mH^+ \qquad \ldots(2.33)$$

where M represents the metal being extracted, HL is the extractant (D2EHPA), m is the valence of the metal cation, n represents the number of dimerized extractant molecules participating in the reaction. The D2EHPA molecule usually exists as a dimer in nonpolar media (i.e. in most aromatic and aliphatic solvents) and is monomeric in highly polar media (i.e. alcohols, carboxylic acids and water). The D2EHPA dimer consists of two D2EHPA monomers, joined by hydrogen bonds between adjacent *P=O* and *P-OH* groups, as shown below:

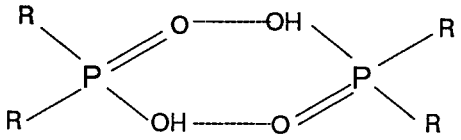

Figure 2.19 : The D2EHPA dimer

The dimerization reaction is:

$$2\overline{HL} \longleftrightarrow (\overline{HL})_2 \quad ; \quad K_2 = \frac{[(\overline{HL})_2]}{[\overline{HL}]^2} \qquad .....(2.34)$$

Komosawa [70] reported $K_2 = 3.1 \times 10^4\ m^3/kmol$ in heptane, and concluded that the dimerization was strong.

D2EHPA exhibits significant interfacial activity, and Komosawa [70] studied the distribution of the monomeric extractant to the aqueous phase:

$$\overline{HL} \longleftrightarrow HL \quad ; \quad K_d = \frac{[HL]}{[\overline{HL}]} \qquad .....(2.35)$$

and determined that $K_d = 1.6 \times 10^4$ for D2EHPA in heptane. The actual total amount of extractant reporting to the aqueous phase is also affected by the acid dissociation constant K_a which was reported [70] as $10^{1.51}$. Table 2.8 summarizes the equilibrium concentration of extractant calculated to be present in the aqueous phase for the overall equilibrium:

$$(\overline{HL})_2 \longleftrightarrow 2\overline{HL} \longleftrightarrow 2HL \longleftrightarrow 2H^+ + 2L^- \quad .....(2.36)$$

Table 2.8 : Calculated equilibrium aqueous phase extractant concentrations. $[(HL)_2]$=0.1 kmol/m^3, K_2=3.1 x 10^4 m^3/kmol, K_d=1.6 x 10^4, K_a=10$^{1.51}$

pH	[L$^-$] (kmol/m^3)	[HL] (kmol/m^3)	[HL] + [L$^-$] (kmol/m^3)
1.0	1.1 x 10^{-7}	3.55 x 10^{-7}	4.65 x 10^{-7}
2.0	1.1 x 10^{-6}	3.55 x 10^{-7}	1.46 x 10^{-6}
3.0	1.1 x 10^{-5}	3.55 x 10^{-7}	1.14 x 10^{-5}
4.0	1.1 x 10^{-4}	3.55 x 10^{-7}	1.10 x 10^{-4}
5.0	1.1 x 10^{-3}	3.55 x 10^{-7}	1.10 x 10^{-3}

2.10.1.2 The Zn-D2EHPA system

The extraction chemistry of zinc with D2EHPA has been studied by numerous workers [67-69]. Ajawin [67] reported the overall equilibrium as:

$$Zn^{2+} + 1.5(HL)_2 \longleftrightarrow ZnL_2HL + 2H^+ \quad .....(2.37)$$

At low metal loadings the equilibrium is reported as [68]:

$$Zn^{2+} + 2(HL)_2 \longleftrightarrow ZnL_2(HL)_2 + 2H^+ \quad .....(2.38)$$

Sastre and Muhammed [69] in a computer model treatment of the extraction equilibrium, showed that both the ZnL_2HL and $ZnL_2(HL)_2$ complexes are possible under variable loading conditions. The cobalt and nickel equilibria are as follows [70]:

$$Co^{2+} + 2(HL)_2 \longleftrightarrow CoL_2(HL)_2 + 2H^+ \quad .....(2.39)$$

$$Ni^{2+} + 3(HL)_2 \longleftrightarrow NiL_2 . 2(HL)_2 + 2H^+ \quad .....(2.40)$$

Table 2.9 summarizes the extraction constants (K_{ex}) reported (units are $kmol^{0.5}\ m^{-1.5}$ for the Zn-complex and $m^3\ kmol^{-1}$ for the Ni-complex):

Table 2.9 : Extraction constants for various metal complexes.

Metal ion	Aqueous phase	Diluent	K_{ex}	Reference
Zn (as ZnL_2HL)	$(Na,H)ClO_4$	kerosene	4.9×10^{-2}	[69]
Zn (as $ZnL_2(HL)_2$)	$(Na,H)ClO_4$	kerosene	7.6×10^{-2}	[69]
Co	$(Na,H)NO_3$	heptane	4.0×10^{-5}	[70]
Ni	$(Na,H)NO_3$	heptane	4.5×10^{-8}	[70]

Ritcey et al. [67] studied the D2EHPA system and concluded that the extraction order was as follows (Fig. 2.20):

$Fe^{3+} > Zn^{2+} > Cu^{2+} > Co^{2+} > Ni^{2+} > Mn^{2+} > Mg^{2+} > Ca^{2+}$

2.10.1.3 Applications

The Zincex process [72,73] uses two solvent extraction circuits to recover zinc from pyrite cinder leach solutions. An amine extractant is used in the first circuit to produce a purified zinc chloride solution. D2EHPA is then used in the second circuit to extract zinc. The zinc is then stripped with spent sulphuric acid electrolyte and recovered in a conventional electro-winning plant. Even after passing through the first circuit, some iron remains in the purified solution, which is removed by bleeding some of the D2EHPA and treating it with strong HCl.

The METSEP process [74,75] was developed to recover zinc and iron from galvanizing pickling solutions. Zinc is removed using an ion exchange column. The column is then eluted with HCl and the zinc is extracted with D2EHPA. Zinc is stripped using sulphuric acid, and then electrowon. The Valberg process [73,75] is used to extract zinc from rayon manufacturing waste waters. A plant in Sweden uses D2EHPA in kerosene in a two-step counter-current process to reduce the zinc concentration from 0.2 g/L to less than 2 ppm. Sulphuric acid is used to strip the zinc from the organic solution. The resulting 80 g/L zinc solution is recycled back to the rayon spinning bath.

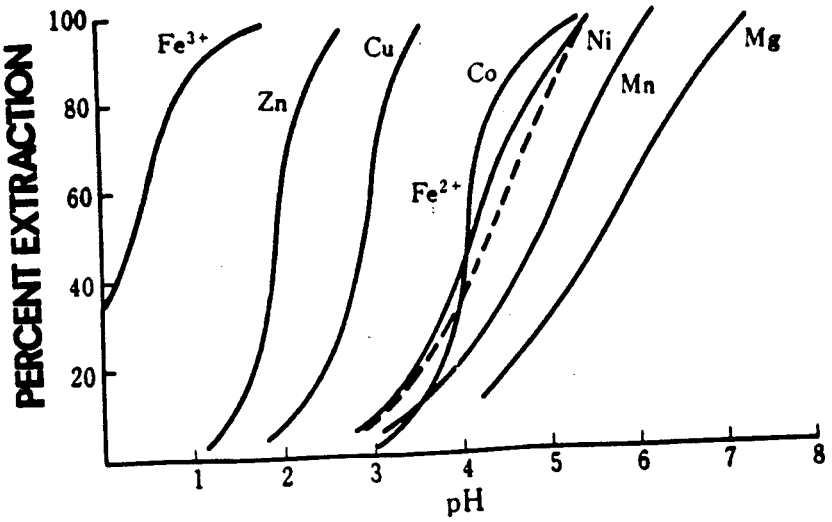

Figure 2.20 : Extraction order of various metals by D2EHPA [67]

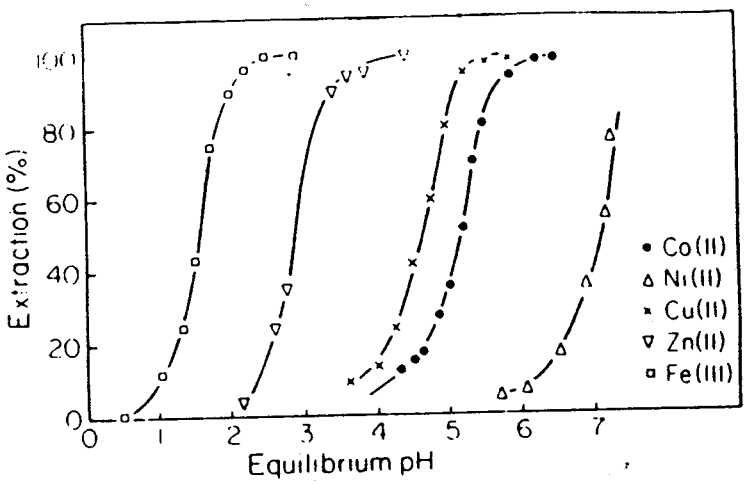

Figure 2.21 : Extraction order of various metals by Cyanex 272 [78]

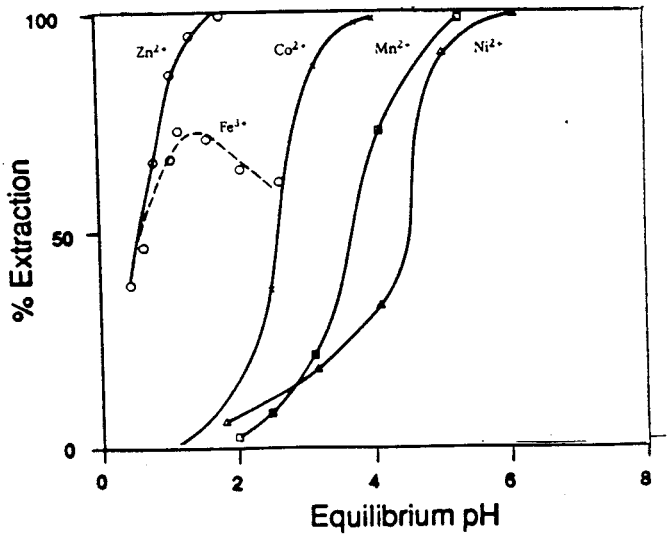

Figure 2.22 : Extraction order of various metals by Cyanex 302 [79]

2.10.2 Cyanex 272 - The phosphinic group

The American Cyanamid Company in 1982, introduced Cyanex 272 analyzing 85% Bis (2,4,4-trimethylpentyl) phosphinic acid, which has the following chemical structure:

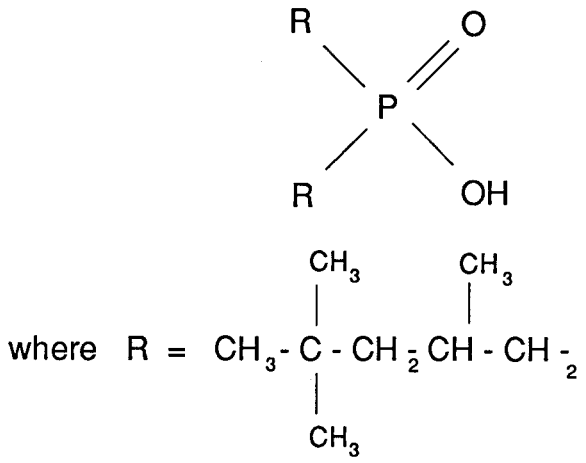

Figure 2.23 : Sketch of the Cyanex 272 extractant (pK = 6.37)

Rickleton et al. [76] studied this reagent for the separation of cobalt and nickel, and determined the extraction order as in Figure 2.21, with the added ability to reject calcium. At low metal loadings, the extraction reactions form a tetrahedral Co-complex and an octahedral Ni-complex as follows:

$$Co^{2+} + 2\overline{(HL)_2} \longleftrightarrow \overline{Co(HL_2)_2} + 2H^+ \quad .....(2.37)$$

$$Ni^{2+} + 3\overline{(HL)_2} \longleftrightarrow \overline{Ni(HL_2)_2(HL)_2} + 2H^+ \quad .....(2.38)$$

Cyanex 272 extracts other transition metals - cadmium, copper and zinc from nitrate solutions as follows [77]:

$$M^{2+} + (p+2)\overline{HL} \longleftrightarrow \overline{ML_2(HL)_p} + 2H^+ \quad .....(2.39)$$

The extracted zinc complexes in sulphate solutions are $\overline{ZnL_2(HL)}$ and $\overline{ZnL_2(HL)_2}$, with the predominant species depending on pH and extractant concentration.

2.10.3 Cyanex 302 - The thio-phosphinic group

Cyanex 302, also an American Cyanamid product, analyzes 84% Bis (2,4,4-trimethylpentyl) monothiophosphinic acid and has the following chemical structure:

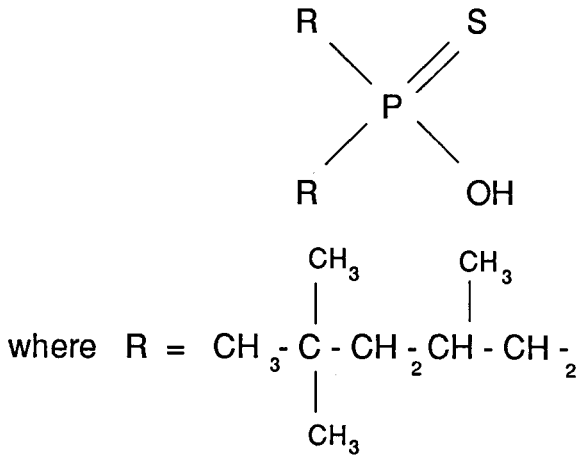

Figure 2.24 : Sketch of the Cyanex 302 extractant (pK = 5.63)

Its extraction order is shown in Fig. 2.22 [79] and has the advantage of being able to extract zinc at lower pH values. An added feature is that from a pH of 1.0 onwards, it extracts zinc in preference to Fe(III). In Figure 2.25, the zinc extraction performance of the three reagents is compared, while Figure 2.26 compares the cobalt extraction. It is seen that Cyanex 302 performs better than D2EHPA which performs better than Cyanex 272 in terms of zinc extraction. The cobalt extraction of Cyanex 302 and D2EHPA is comparable in the pH range 3.5 to 4.5, implying that Cyanex 302 could be considered to possibly replace D2EHPA based on Co/Zn selectivity.

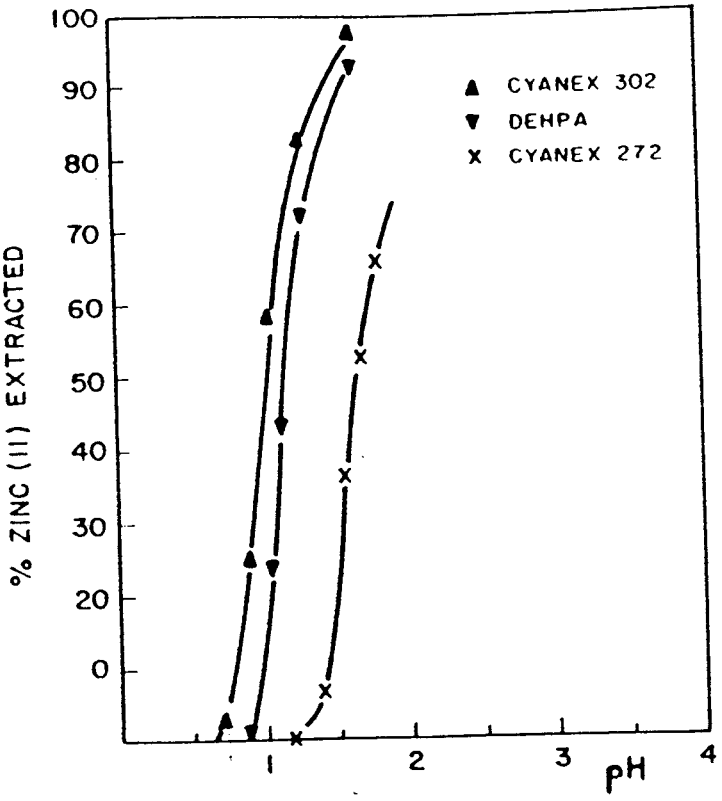

Figure 2.25 : Comparison of zinc extraction by various organophosphorous derivatives. Organic phase: 20% extractants in kerosene, aq. 1g/L zinc; A/O=1 [79]

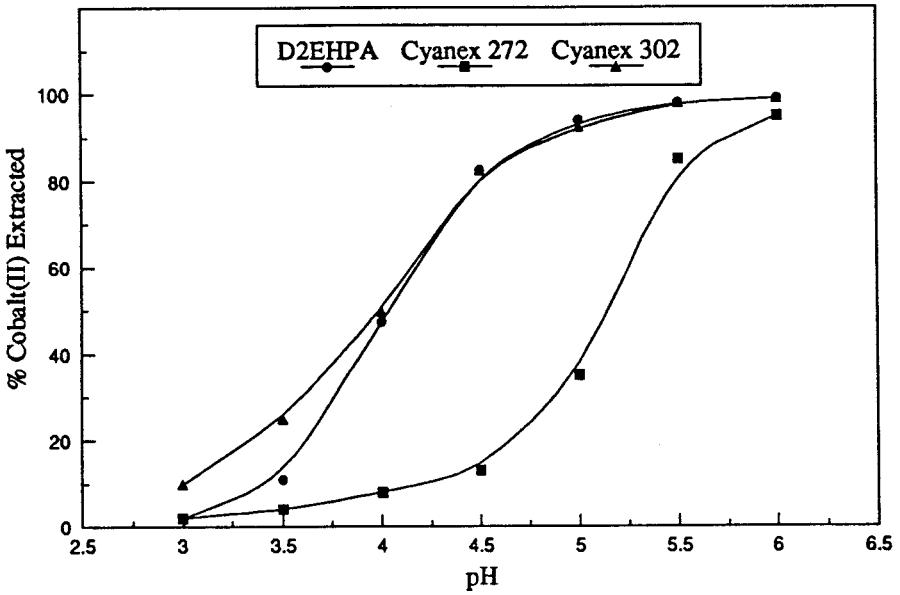

Figure 2.26 : Comparison of Cobalt extraction of the resins (Obtained from data in [67], [78] and [79], considered under similar conditions). Organic phase: 0.1 M extractant, aq. phase: 1 x 10-3 M.

2.11 Scope and Objectives of this Work

From the review of the literature presented in the preceding sections, it seems that the reagents Cyanex 272 and Cyanex 302 perform a comparable zinc extraction to that of D2EHPA. Further, according to the Hard-Soft Acid-Base concept [14,78] (in Section 2.4.3), the complexation of a soft Lewis acid, such as Zn(II), Co(II), Cu(II) or Ni(II), with a soft Lewis base should occur with high selectivity. The donor atoms of the common Lewis bases have electro-negativities increasing in the order S<Br<N<Cl<O<F. Sulphur substitution of the organophosphorous reagents should therefore prove beneficial to the extraction of these metal ions.

The project was initiated in consultation with INCO Ltd., to compare the resins OC 1026, Cyanex 272 and Cyanex 302 for their performance in the INCO zinc removal process. The research objectives may be summarized as follows:

(1)To compare the performance of the resins in fixed bed column tests, on the basis of their zinc breakthrough points and the cobalt retained on the resins at this point.

(2)To study the effects of resin pre-treatment, electrolyte pre-treatment, temperature, flow rate and loading cycles on zinc breakthrough and selectivity in column tests, and to explain the effects based on mechanisms operating in the column.

(3)To compare the kinetics of zinc extraction from the electrolyte by the resins, in batch tests, and propose a mechanism for the extraction.

The methodology followed was to divide the experimental work into column and batch tests, and results from these tests were fitted to kinetic models, to compare the resin performances and gain an insight into the process mechanism.

3 EXPERIMENTAL

3.1 Resins

The resins used in this work - OC 1026, Cyanex 272 and Cyanex 302, collectively called Levextrel resins, are styrene-divinyl benzene based co-polymers of a predominantly macroporous structure that contain a selective extractant. Representative samples of these resins were obtained from Bayer AG, Ltd.. Two of these resins, Cyanex 272 and Cyanex 302 were synthesized by Bayer AG Ltd., for this work, and hence little information is available about their properties.

3.1.1 Structure of the resins

Figures 3.1 and 3.2 show stereoscan photographs of OC 1026 [92]. Each individual Levextrel bead consists of a large number of microbeads, which are firmly attached to one another. The space between them is filled with the active substance (extractants D2EHPA, Cyanex 302 or Cyanex 272), which is retained by adsorption. The size of the microbeads and the space between them depend on the type and volume of the extractant used, as well as on the degree of crosslinking of the polystyrene beads.

3.1.2 Particle size and distribution

The mean particle diameter of the respective resin fractions, was determined by photographing representative samples and measuring the diameter of each particle, and computing the mean (Table 3.1). The particle size distribution, determined by wet screening of the resin sample is also reported in Table 3.1.

3.1.3 Physical properties

The physical properties of the resins were determined by conventional methods [93] and are summarized in Table 3.1.

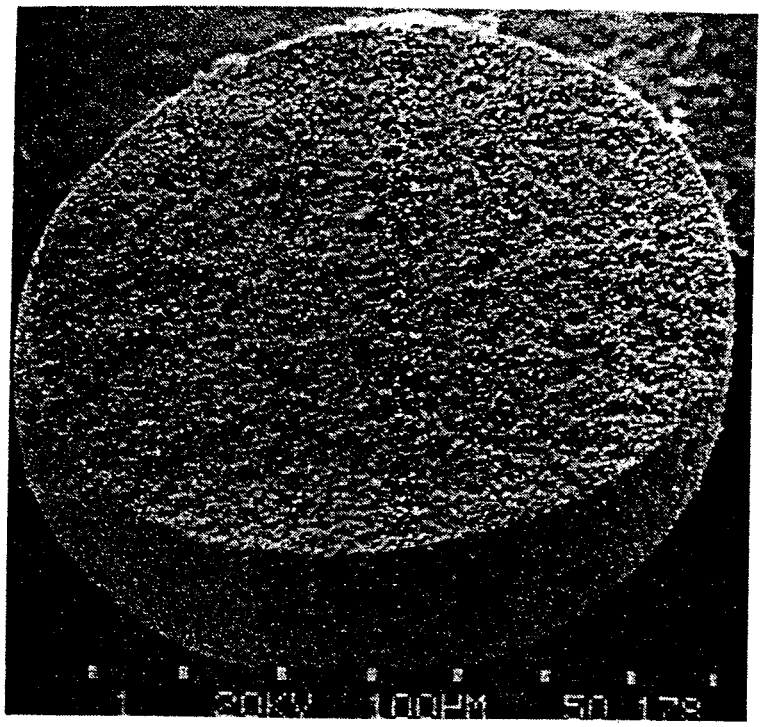

Figure 3.1 : Surface structure of the fractured Levextrel OC 1026 bead [94]

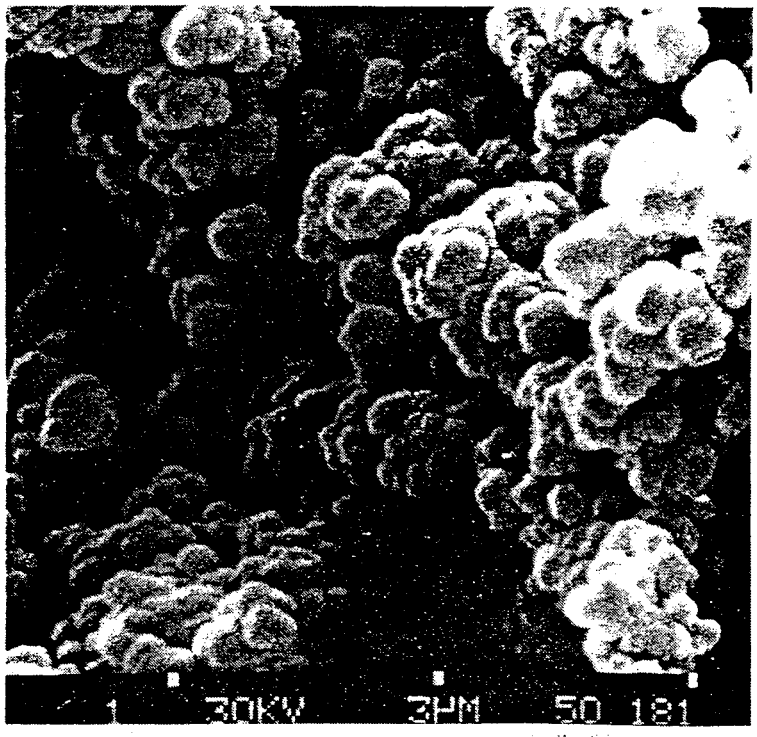

Figure 3.2 : Interior bead structure of the Levextrel OC 1026 bead [94]

Table 3.1 : Properties of the Levextrel resins OC 1026, Cyanex 272 and Cyanex 302.

Resin	Active substance	Capacity (eq/L)	Particle size (μm)	Size range (mm)	Bulk density (g/cc)	true density (g/cc)	Void fraction	Water content by wt.
OC 1026	D2EHPA	0.5	700	0.3 - 1.0	0.5882	0.930	0.4883	0.3%
Cyanex 272	Cyanex 272	0.41	450	0.4 - 0.7	0.4882	1.023	0.5	-
Cyanex 302	Cyanex 302	0.44	510	0.4 - 0.8	0.51	1.100	0.5	-

The bulk density of the resins is rather low and approximately in the range of those of the macroporous weakly basic anion exchangers. The specific gravity is lower than that of normal ion exchange resins and they are hydrophobic. The beads also have a particularly low water content. The active substances are retained in the resin structure by adsorption, rather than chemical bonding, and their losses to aqueous solutions in column operations are negligible, particularly in the acidic range. In the treatment of a 20% cobalt sulphate solution [89], OC 1026 had an average loss of active substance of only 5 mg/L, and about 12 mg/L during the elution of the loaded column, using 10% sulphuric acid. However, a greater loss of active substance is observed in stir tests, especially at high stirring speeds or with magnetic stirrers.

3.2 Reagents

3.2.1 Cobalt advance electrolyte

The cobalt advance electrolyte was obtained from the INCO cobalt refinery at Port Colborne, Ontario. The analysis and properties of the electrolyte are as listed in Table 3.2:

Table 3.2 : Analysis and properties of the cobalt advance electrolyte from INCO Port Colborne.

Co (g/L)	Ni (g/L)	Zn (g/L)	Fe (g/L)	Cu (g/L)	Density kg/m^3	Viscosity kg/ms	pH
45	40	0.012	0.008	0.010	1284 at 25°C	5 x 10^{-3} at 25 °C	3.34

3.2.2 Zinc - free cobalt electrolyte

Zinc - free cobalt electrolyte, was used to pre-treat the resins in the batch tests. It was obtained from the effluent solutions of the column tests, with zinc content of less than 0.5 ppm in the electrolyte.

3.2.3 Cobalt sulphate solution

This was prepared by dissolving the appropriate amount of reagent grade cobalt sulphate ($CoSO_4.7H_2O$), in deionized water and adjusting the pH to the required value.

3.2.4 Zinc sulphate solution

This was prepared by dissolving the appropriate amount of reagent grade zinc sulphate ($ZnSO_4.7H_2O$), in deionized water.

3.2.5 Sodium hydroxide

Sodium hydroxide was used in batch tests, for pH stabilization and maintaining the solution at a particular pH value during pre-loading and loading. It was prepared by dissolving the appropriate amount of NaOH in deionized water, and then standardized against potassium hydrogen phthalate (KHP), with phenophthalein as the indicator.

3.2.6 Sulphuric acid

10% sulphuric acid was used to strip the resins of cobalt and zinc during column elution tests. This was prepared by adding 100 ml of bottle strength sulphuric acid to 900 ml of deionized water in a 1000 ml volumetric.

3.3 Experimental Apparatus

The apparatus for column experiments (Figure 3.3), consisted of a chromatography column, a needle valve to finely adjust the effluent flow rate to equal the influent flow, a Masterflex pump

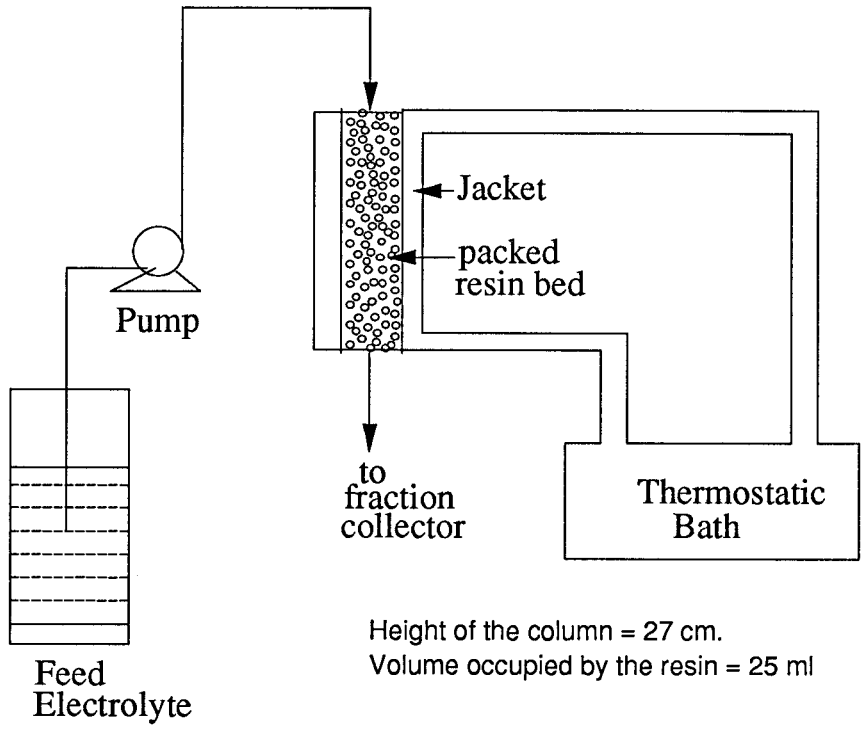

Figure 3.3 : Apparatus for column studies

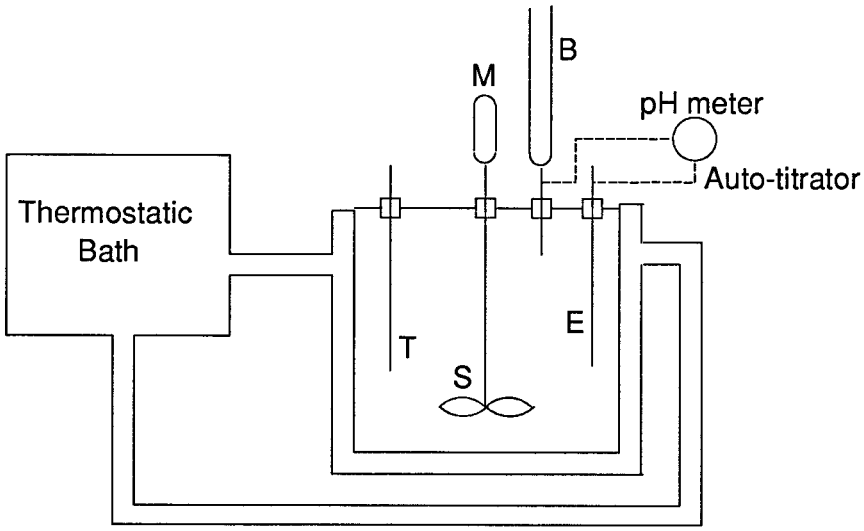

T = Thermocouple
M = Variable Speed Motor
S = Stirrer
B = Auto-burette
E = pH Electrode
Volume of vessel = 500 ml

Figure 3.4 : Apparatus for batch studies

(Cole Parmer model no. 7520-35), attached with a number of variable occlusion cartridges (model no. 7519-60) to deliver multiple pumping at different flow rates, a Cole-Parmer polystat circulator, which maintained a thermostatic bath by circulating water of the particular temperature through the column jacket, and an Eldex Universal Fraction Collector (UFC 3462) to collect volumes of effluent at different time intervals. The chromatography column was 60 cm long and 1.5 cm in diameter, and was glass fritted at the bottom to hold the resins.

Figure 3.4 shows the experimental set-up used for batch tests. The impellor (or stirrer S) was mounted on a lab stand anchored at each end to prevent vibration. The beaker (500 ml capacity) was held thermostatic by the polystat circulator. The pH of the solution was maintained constant using an autoburette B, which is part of an auto-titration system, consisting of a Radiometer PHM 82 pH meter, an ABU80 autoburette and a TTT80 titrator. The volume of the titrant dispersed to maintain constant pH was recorded. A lid with holes for the stirrer, pH probe, thermocouple and titrant addition was used to seal the beaker and prevent any evaporation during the experiment.

3.4 Experimental Procedure

3.4.1 Column tests

The ion exchange resins used in this work were used as recieved, without rinsing with deionized water (to prevent any extractant loss). The column was filled with 25 ml of the respective resin, keeping a low water level initially, so that the resin was not totally covered with water, as the resins tend to float due to the hydrophobic nature of the bead surface. Water washing (upflow) was used to remove all the air bubbles, and achieve a compact bed of 25 ml of resin. As the beads tend to float, the water was first drained out completely, and then a block of glass wool was inserted from the top of the column on the bed, to maintain the compact bed and prevent any flotation of the beads during column operation. The bed was then filled with water to just a few centimeters above the bed level.

The resin column was then attached to the externally mounted water jackets, and the polystat circulator was set at the respective temperature and started. The Masterflex pump was then calibrated to deliver the particular flow rate for its variable occlusion cartridges. The pH meter was then calibrated using buffers at pH of 1 and 7, at the operating temperature of the experiment, and the pH of about 100 ml of the cobalt advance electrolyte was then adjusted to 3, for use during pre-treatment. The fraction collector was set so as to collect column effluent samples every 30 minutes.

During pre-treatment, the cobalt advance electrolyte with pH adjusted to 3 was pumped through the resin bed at a flow rate of 4.67 BV/hr. (116 ml/hr.). The needle valve at the mouth of the column was finely adjusted, such that the flow out of the column equalled flow in (through the Masterflex pump). The pH of the effluent was measured continuously until it was equal to 2. At this point, the flow to the column was shut off, and the cobalt advance electrolyte was simultaneously pumped into the column at the same flow rate to begin loading. The timer at the fraction collector was started, and effluent samples were collected every 30 minutes in test tubes at the fraction collector. The fraction collector was covered to prevent any evaporation. The pH of the effluent samples was determined, and the samples were then taken in acid washed sample tubes and diluted appropriately to analyze for cobalt, nickel, zinc, copper and iron, using atomic absorption spectrophotometry.

Before elution, the resin bed was first washed with 3 BV (75 ml) of deionized water, collecting samples of 25 ml (every 12 minutes 50 seconds), and then the column was filled to a particular level with 10% sulphuric acid and left standing for two hours. The effluent was called the first strip solution - *S1*. The bed was again washed with 3 BV (75 ml) of deionized water, collecting 25 ml samples, and the stripping was carried out once again by filling the column with 10% sulphuric acid to the same level and analyzed as the second strip solution - *S2*. The bed was washed again with 3 BV (75 ml) of deionized water, and the pre-treatment for the next loading cycle was started.

3.4.2 Batch tests

500 ml of zinc-free INCO cobalt advance electrolyte (obtained from the effluent samples of the column tests, analyzing less than 0.5 ppm zinc), was transferred to the water jacketed beaker shown in Figure 3.4. The polystat circulator was set to the particular temperature, and water at that temperature was circulated to thermostat the beaker. A series of 1 mL syringes, with a mouth of less than 0.03 cm diameter (so that the resin particles could not enter it), were cleaned and arranged for ready use. The pH meter was then calibrated at that particular temperature and then used along with the auto-titrator, to set the pH of the solution to 3 (or any other desired value), by the addition of the NaOH titrant. The lid was then placed on the beaker to seal it and the temperature was maintained for some time. About 1 g of the respective resin was weighed out and added to the beaker. Simultaneously, the autotitrator and the timer were started and the amount of titrant added with time was noted. After about half an hour, the resins reached an equilibrium with the solution, and no further titrant addition was needed to maintain the pH at the particular value. Now an appropriate amount of zinc pipetted from the zinc sulphate solution was added, so as to attain a zinc concentration of 12 mg/L in the beaker with 500 mL of the electrolyte. The timer was reset and started again, and small aliquots of the electrolyte were withdrawn after every minute, for the first ten minutes, and later every five minutes, in the 1 mL syringes and analyzed for zinc.

3.5 Solution Analysis

As mentioned before, the NaOH solution was standardized by using potassium hydrogen phthalate; which was dried for 3-4 hours and then titrated against the unknown NaOH solution. The raffinates of the column tests and samples of the batch tests were analyzed for Co, Ni, Zn, Fe and Cu, after appropriate dilution by atomic absorption spectrophotometry, with matched matrix standards and simultaneous background correction. Results quoted here have a relative precision of better than 2%.

3.6 Reproducibility of the Results

In column loading tests, the reproducibility of the results was excellent, with almost the same breakthrough points (interpreted as zinc effluent concentration of greater than 1 ppm) obtained during trial runs. In elution tests, the reproducibility was good if the elutions were run within an hour after the loading tests, and the volume of the wash water was kept constant during the runs. The reproducibility of batch test results was found to be greatly dependent on the impeller speed, the depth of the impeller head and the particle size of the resin samples. A slight change in any of these parameters resulted in quite different results than those reported. The qualitative trend of the results was, however, similar. In particular, particle size and size distribution played a major role, as the reaction rate is inversely proportional to the square of the particle radius, and hence even a small deviation in particle size between two resin samples, would show a measurable difference in their kinetic performance. Wet screening of the resin samples before their application in the batch tests, could not be accomplished, as this resulted in loss of extractant, and hence the results would not be a true picture of the resin performance. As the exchange process was to some extent mass transfer controlled, small changes in impeller speed had an observable influence on the results. It was not possible to increase impeller speed sufficiently or to use baffles to bypass the mass transfer control region, as this resulted in breakage of the beads and spilling of the solution. Inspite of these constraints, the reproducibility of the results was satisfactory. Even though the absolute numbers varied by about 8%, the underlying mechanisms, determined from the trends in the diffusion and mass transfer coefficients, remained the same as those proposed here.

4 KINETIC MODELS

From a survey of the various rate laws that may be used to describe ion exchange kinetics in Section 2.6.3, the Fickian particle and film diffusion models and the progressive shell (unreacted core) models, were found useful in describing the ion exchange kinetics of the system chosen. These models are briefly described here for purposes of this work. The reader is advised to refer to the literature [15,20,80] for more detailed descriptions. A model is also outlined for kinetic studies on column loading, based on the methods suggested by Doulah and Jafer [83] and Rodrigues and Costa [85].

For the ion exchange equilibrium represented by:

$$\overline{RA} + B \longleftrightarrow \overline{RB} + A \qquad \text{.....(4.1)}$$

the general assumptions for all of the diffusion models are as follows:

(1)The resins are spherical particles of uniform size.

(2)There are no temperature gradients in the resin bead or the aqueous film.

(3)The effective diffusivity in the resin phase and the mass transfer coefficient in the aqueous phase film are constant.

(4)The concentration of the external solution is constant through the process (Infinite solution volume condition).

4.1 Fickian Film Diffusion Model

This model assumes, in addition to the initially mentioned assumptions, that diffusion of ions takes place through a quasi-stationary film (i.e. diffusion across the film is extremely fast when compared to concentration changes at the film boundaries), and the film is treated as planar and one-dimensional (Fig. 4.1). The kinetic analyses in Section 2.6.3.1, equation (2.24) gives:

$$\frac{dc_B}{dt} = \frac{3Dc}{r_o\bar{c}}\frac{(c_B^b - c_B^*)}{\delta} \qquad \text{.....(4.2)}$$

where c^*_B= concentration of B at the resin-solution interface.

c^b_B= concentration of B at the solution bulk.

c = total counterion concentration in the aqueous phase.

$\bar{c}$ = total counterion concentration in the resin phase.

The term $\frac{c}{\bar{c}}$ is evaluated by the ion exchange equilibrium :

$$\frac{c}{\bar{c}} = \frac{[B_b]}{\overline{(RB)}_{eq}} \qquad \text{.....(4.3)}$$

$[B]_b$ = concentration of B in the solution bulk.

$\overline{(RB)}_{eq}$ = concentration of B in the resin at equilibrium.

In the initial state, the concentration of B in the bulk solution is equal to $c^b_{init,B}$, while that at the resin-solution interface is equal to zero:

$$t = 0, \quad r = r_o, \quad c_B = 0 \qquad \text{.....(4.4)}$$

$$t = 0, \quad r > r_o + \delta, \quad c_B = c^b_{init.,B} \qquad \text{.....(4.5)}$$

The boundary condition is defined by the infinite solution volume condition, which states that the bulk solution concentration is maintained at a value defined by the exchange equilibrium, through the entire process:

$$t > 0, \quad r > r_o + \delta, \quad c_B = \left(\frac{c}{\bar{c}}\right) c^b_{init.,B} \qquad \text{.....(4.6)}$$

The equation (4.2) is solved with the equilibrium condition (4.3) and initial conditions (4.4) & (4.5) and boundary condition (4.6) to give (X=fraction extracted):

$$X(t) = 1 - \exp\left[-\left(\frac{3D[B]_b}{r_o\delta\overline{(RB)}_{eq}}\right)t\right] \qquad \text{.....(4.7)}$$

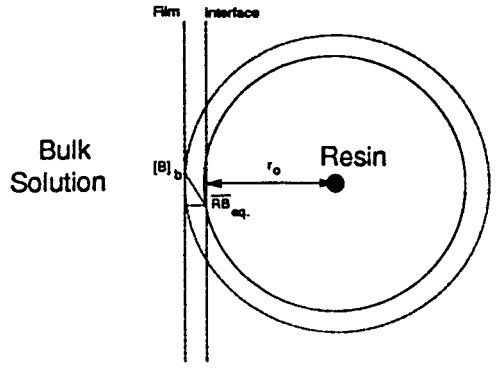

Figure 4.1 : The Film Diffusion Model

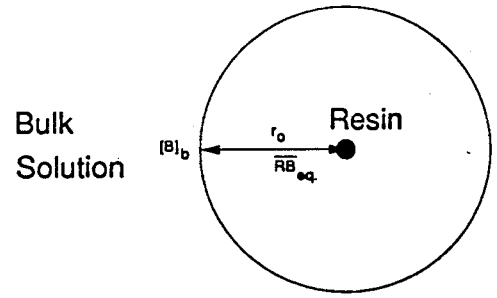

Figure 4.2 : The Particle Diffusion Model

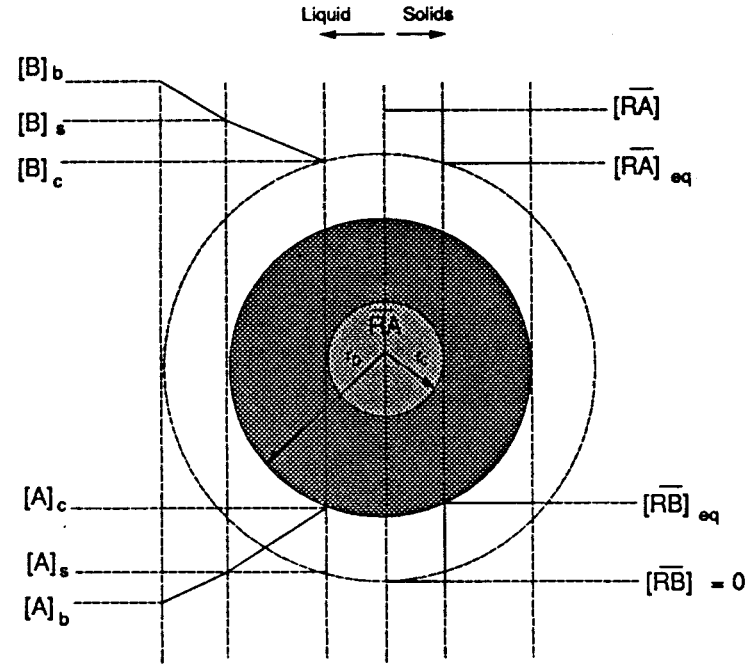

Figure 4.3 : The Unreacted Core Model

4.2 Nernst-Planck Film Diffusion

From Section 2.6.3.3 and references [15,20], the Nernst-Planck criterion for ions of equal mobility may be incorporated into equation (4.7) by including a selectivity parameter α^B_A for the exchange equilibrium in equation (4.1).

$$\alpha_A^B = \frac{\overline{c}_B c_A^*}{\overline{c}_A c_B^*} \qquad .....(4.8)$$

where the superscipt * represents the resin-solution interface. Hence:

$$\ln(1-X) + \left(1-\frac{1}{\alpha_A^B}\right)X = -\left(\frac{3D[B]_b}{r_o \delta \overline{(RB)}_{eq}} \frac{1}{\alpha_A^B}\right)t \qquad .....(4.9)$$

4.3 Fickian Particle Diffusion Model

Diffusion in the resin particle is rate controlling (Fig. 4.2), and hence from Section 2.6.3.1:

$$\frac{\delta c_B}{\delta t} = \overline{D}_B\left(\frac{\delta^2 c_B}{\delta r^2} + \frac{2}{r}\frac{\delta c_B}{\delta r}\right) \qquad .....(4.10)$$

In the simplest initial condition, the concentration of B in the resin phase is zero and that at the resin-aqueous interface is a value of $[B]_b$. Hence:

$$t=0, \quad 0<r<r_o, \quad \overline{c}_B = 0 \qquad .....(4.11)$$

$$t=0, \quad r=r_o, \quad \overline{c}_B = B_b \qquad .....(4.12)$$

The boundary conditions are defined by assuming infinite solution volume conditions, and hence the resin-aqueous interface is at an equilibrium value defined by the exchange equilibrium:

$$t>0, \quad r=r_o, \quad \overline{c}_B = \overline{(RB)}_{eq} \qquad .....(4.13)$$

Equation (4.10) is solved with initial conditions (4.11) and (4.12), and boundary condition (4.13), and along with the Vermeulen's approximation (eq. 2.23) [30] to give:

$$X(t) = \left[1 - \exp\left(-\frac{[B]_b}{\overline{(RB)}_{eq}} \frac{\overline{D}\pi^2}{r_o^2} t\right)\right]^{(1/2)} \qquad .....(4.14)$$

E

4.4 Unreacted Core Model

The theory of the unreacted core shrinking model (Fig. 4.3), has been presented in the literature for irreversible solid-fluid non-catalytic reactions [80-82]. For the equilibrium in equation (4.1), the material balances for the various processes of film diffusion, particle diffusion and chemical reaction may be written as follows:

Film Diffusion:

$$-\frac{1}{4\pi r_o^2}\frac{dN_B}{dt} = \frac{1}{4\pi r_o^2}\frac{dN_{\overline{(RB)}}}{dt} = k_m([B]_b - [B]_s) \qquad .....(4.15)$$

Diffusion through the reacted resin layer:

$$\frac{1}{4\pi r_o^2}\frac{dN_{\overline{(RB)}}}{dt} = \overline{D}_e\left(\frac{d[B]}{dr}\right)_{r=r_o} \qquad .....(4.16)$$

Chemical reaction:

$$\frac{1}{4\pi r_c^2}\frac{dN_{\overline{(RB)}}}{dt} = k_1[\overline{RA}][B]_c - k_2[RB][A]_c \qquad .....(4.17)$$

where dN_i/dt = infinitesimal change in the number of moles of component *i*.

[I] = molar concentration of the I-component.

r_o, r_c = radius of the particle and of the unreacted core respectively.

$\overline{D}_e$ = effective diffusivity in the reacted resin layer.

k_1, k_2 = rate constants of forward and reverse reactions

These equations are solved to give the following rate expression for the fraction extracted (X):

$$\frac{2\overline{D}_e}{r_o k_m}X + 1 + 2(1-X) - 3(1-X)^{2/3} + \frac{3\overline{D}_e}{k_1 r_o[\overline{R}_o]}\left(\frac{1}{(1-X)^{2/3}} - 1\right) = \frac{6\overline{D}_e[B]_b}{r_o^2[\overline{RB}]_{eq}}t \qquad ..(4.18)$$

E

For pure particle diffusion through the reacted layer:

$$1 + 2(1-X) - 3(1-X)^{2/3} = \frac{6\overline{D}_e[B]_b}{r_o^2[\overline{RB}]_{eq}}t \qquad ..(4.19)$$

4.5 Kinetic Modelling of Column Tests

Kinetic data may be obtained from column tests, by the analysis of the breakthrough curves, which have a characteristic slope, time of appearance and mean time, that can be directly related to parameters influencing the performance of ion exchange equipment. The method is based on the following assumptions [83]:

(1)The solute concentration wave in a solid bed of particulate sorbents, moves through the bed length by forming zones of saturated particles, with a uniform solute concentration across the crossection of the bed. Figure 4.4 shows the zone movement, for a typical breakthrough curve.

(2)All zones in a bed are of equal length.

(3)Fluid velocity in an operation is greater than the solid phase concentration phase wave velocity.

(4)The fluid flows through the bed of particulate solids in a plug flow fashion, and longitudinal liquid diffusion is absent.

Following the analysis in references [83-85], the parameters characteristic to a breakthrough curve; β, θ_o and θ_m (defined below) may be related to solute concentration as follows:

$$\left(\frac{c}{c_o}\right) = 1 - \exp\left[-\left(\frac{\theta-\theta_o}{\theta_m}\right)^{\beta}\right] \qquad .....(4.20)$$

where β = shape factor (dimensionless).

θ_o = time of appearance of the breakthrough curve.

θ_m = mean time of the breakthrough curve function.

This may be written as:

$$\log[\ln(1/(1-c/c_o))] = \beta\log(\theta-\theta_o) - \beta\log\theta_m \qquad .....(4.21)$$

Therefore from a log-log plot of $\ln(1/(1-c/c_o))$ vs. $(\theta-\theta_o)$, the slope of the straight line obtained would be β, and the X-axis value of the point at which $c/c_o=0.632$ (Figure 4.6) would be equal to θ_m (as at $c/c_o=0.632$, $\ln(1/(1-c/c_o))=1$ and from (4.21); $\theta-\theta_o=\theta_m$). These characteristic parameters (β, θ_o and θ_m) may be used to determine a range of kinetic parameters.

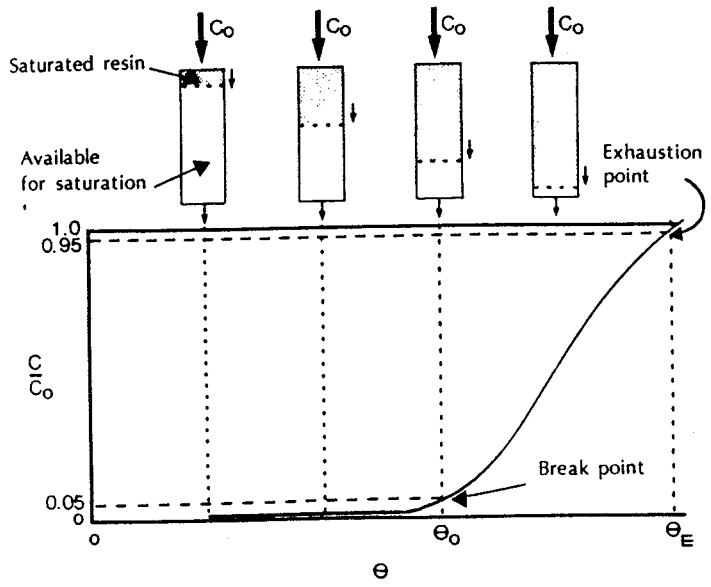

Figure 4.4 : Typical breakthrough curve with the representation of the characteristic parameters and movement of the zones

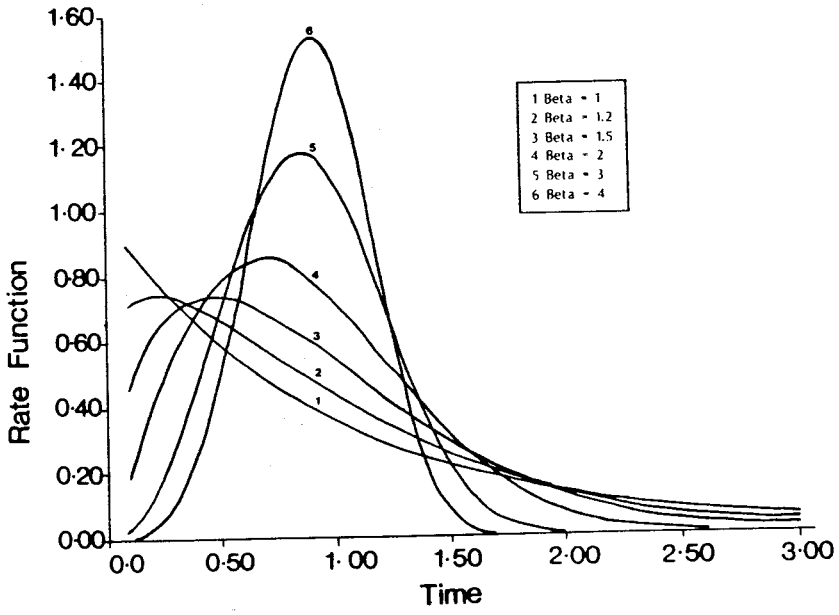

Figure 4.5 : Variation of the rate function $d(C/C_o)/d\theta$ with β

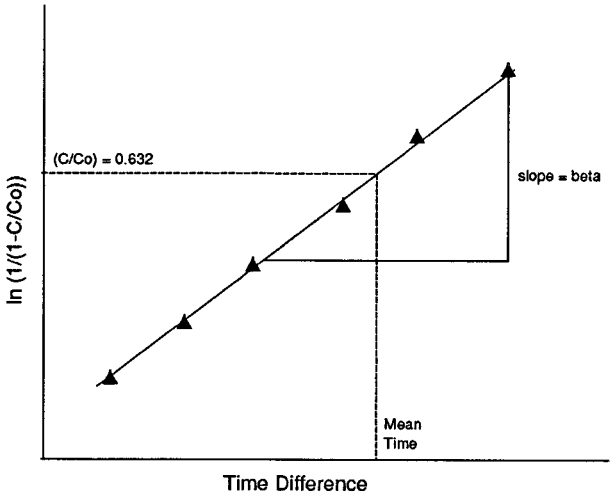

Figure 4.6 : Determination of characteristic parameters from a plot of equation (4.1).

The *overall mass transfer coefficient* in the liquid phase (k_f) is determined by:

$$k_f a = \beta/\theta_m \qquad .....(4.22)$$

where, a= *mass transfer area*, and for spherical particles:

$$a = 1.5e^2/d \qquad .....(4.23)$$

where, e= bed voidage (dimensionless); and d= resin particle diameter.

The *bed saturation time* (θ_s) is given by:

$$\theta_s = \theta_o + \theta_m \qquad .....(4.24)$$

The *number of exchange zones* (N_z) is given by:

$$N_z = (\theta_o + \theta_m)/\theta_m \qquad .....(4.25)$$

The *height of an individual zone* (h_z) is given by: (where H = bed height)

$$h_z = H\theta_m/(\theta_o + \theta_m) \qquad .....(4.26)$$

The velocity with which a mass transfer zone moves in a resin bed (U_z) is determined by:

$$U_z = h_z/\theta_m \qquad .....(4.27)$$

If, U_s = superficial velocity of the fluid (m/s); and ρ_B=solid phase bulk density (kg/m^3), then the *height of a transfer unit* (H_{tof}) is given by:

$$H_{tof} = U_s\theta_m/\beta \qquad .....(4.28)$$

and the *saturation capacity* (q_o) is given by:

$$q_o = U_s c_o(\theta_o + \theta_m)/(H\rho_B) \quad \text{.....(4.29)}$$

The *distribution constant* (*DC*) is given by:

$$DC = q_o/c_o = U_s(\theta_o + \theta_m)/(\rho_B H) \quad \text{.....(4.30)}$$

The *degree of bed saturation* (D_{bs}) at the breakthrough point is:

$$D_{bs} = \theta_o/\theta_s = \theta_o/(\theta_o + \theta_m) \quad \text{.....(4.31)}$$

The *unsaturated fractional bed length* (H_{us}) at the breakthrough point is:

$$H_{us} = H\left(1 - \frac{\theta_o}{\theta_o + \theta_m}\right) \quad \text{.....(4.32)}$$

Equations (4.21) to (4.32) may be used to determine the respective parameters, which are extremely useful in the design of the ion exchange columns. Figure 4.5 shows the variation of the rate function $\frac{d(c/c_o)}{d\theta}$ against time (θ), and it is seen that β determines the shape of the rate curve, which is directly influenced by the mechanism of mass transfer. It was concluded [83] that for values of β less than 1.5, particle diffusion is the rate controlling step; while for values greater than 3, film diffusion is the rate controlling step. The value of the overall mass transfer coefficient, k_f obtained from equation (4.22), may be compared to the value of k_L (liquid phase mass transfer coefficient) obtained from Carberry's correlation [86]:

$$k_L = 1.15\left(\frac{\rho_L d U_s}{\mu_L e}\right)^{-1/2}\left(\frac{\mu_L}{\rho_L D_L}\right)^{-2/3}\left(\frac{U_s}{e}\right) \quad \text{.....(4.33)}$$

where ρ_L = liquid phase density (kg/m^3).

μ_L = liquid phase viscosity (kg/ms).

d = diameter of the resin particle (m).

U_s = superficial velocity of the fluid (m/s).

D_L = liquid phase diffusivity (m^2/s).

e = bed voidage

The liquid phase diffusivity is determined by correlations with the liquid film thickness, δ [15], which is defined empirically for fixed bed columns with spherical resin beads, operating at low flow rates as [87]:

$$\delta = \frac{0.2r_o}{(1+70r_oU_s)} \qquad .....(4.34)$$

Furthermore, breakthrough curves may be used to determine whether the exchange equilibrium is favorable or not, depending on whether the curve remains constant or flattens respectively, with increasing bed depth [15]. Finally, the variation of the mid-point slope of the breakthrough curve with flow rate, would be independent of the feed spatial velocity for particle diffusion control kinetics, while the variation would depend on the square root of the feed spatial velocity for a film diffusion control mechanism [20].

4.6 Minimum Superficial Velocity of Solution in Column Operations

In most column processes, the superficial velocity of the solution should be fixed at a value, at which particle diffusion kinetic control is the dominant mechanism. This is possible at such a value of U_s, at which:

$$k_m \gg \overline{D}/\delta \qquad .....(4.35)$$

From Perry's Chemical Engineering Handbook, 4-th Edition [88], the following relation for mass transfer coefficient is obtained:

$$k_m a_p = \frac{5.45U_s(1-e)}{r_o}\left(\frac{D_L}{2r_oU_s}\right)^{0.51}\left(\frac{D_L\rho_L}{\eta_L}\right)^{0.12} \qquad .....(4.36)$$

This may be rewritten as follows, to obtain the minimum superficial velocity for column operation (U_{min}), for the column to operate in the particle diffusion control regime.

$$U_{\min} = \left[\frac{k_m a_p r_o}{5.45(1-e)}\left(\frac{D_L}{2r_o}\right)^{-0.51}\left(\frac{D_L\rho_L}{\eta_L}\right)^{-0.12}\right]^{2.0408} \qquad ....(4.37)$$

5 RESULTS AND DISCUSSION

This chapter presents the results of the work, and a discussion on the possible mechanisms operating in these processes, and their outcome during industrial applications. Column and batch test results are presented, followed by a general discussion on the exchange process. A greater effort is made to the analyze data obtained from tests on OC 1026, as this was the more efficient resin, and is being used in the INCO zinc removal process at Port Colborne.

5.1 COLUMN TEST RESULTS

5.1.1 Zinc loading on untreated OC 1026

Initial trial runs were carried out by passing INCO electrolyte through a 25 ml bed of untreated OC 1026 at various flow rates and temperatures, and the zinc concentration and pH of the effluent were followed until about 250 bed volumes (BV) of the electrolyte had been passed. During the initial feeding, a bright blue coloration, probably from the Co/HDEHP complex, spread slowly downwards. This coloration, however, disappeared slowly to become a lighter color as the feeding progressed.

Fig. 5.1 shows the results obtained by using untreated OC 1026 at 40°C with a feed flow rate of 5 BV/hr.. The electrolyte pH drops from the initial value of 3.7 at 40°C to a value of about 2, after which it rises rapidly in the first 50 BV, and then at a slower rate, until it reaches a value of about 2.75 after 250 BV of electrolyte have passed. The loading of zinc on the resin seems fairly efficient, as breakthrough (interpreted as a zinc effluent concentration greater than 1 ppm) takes place only after about 210 BV of electrolyte have been passed. Fig. 5.2 shows the results of the test carried out using untreated OC 1026 at 40°C, but with a flow rate of 10 BV/hr.. The profiles seem similar, but the breakthrough takes place a little earlier in this case, after 190 BV. Fig. 5.3 shows the profiles for a test carried out using untreated OC 1026 at 60°C with a flow rate of 4.67 BV/hr.. Zinc breakthrough takes place much later here, after about 320 BV, showing

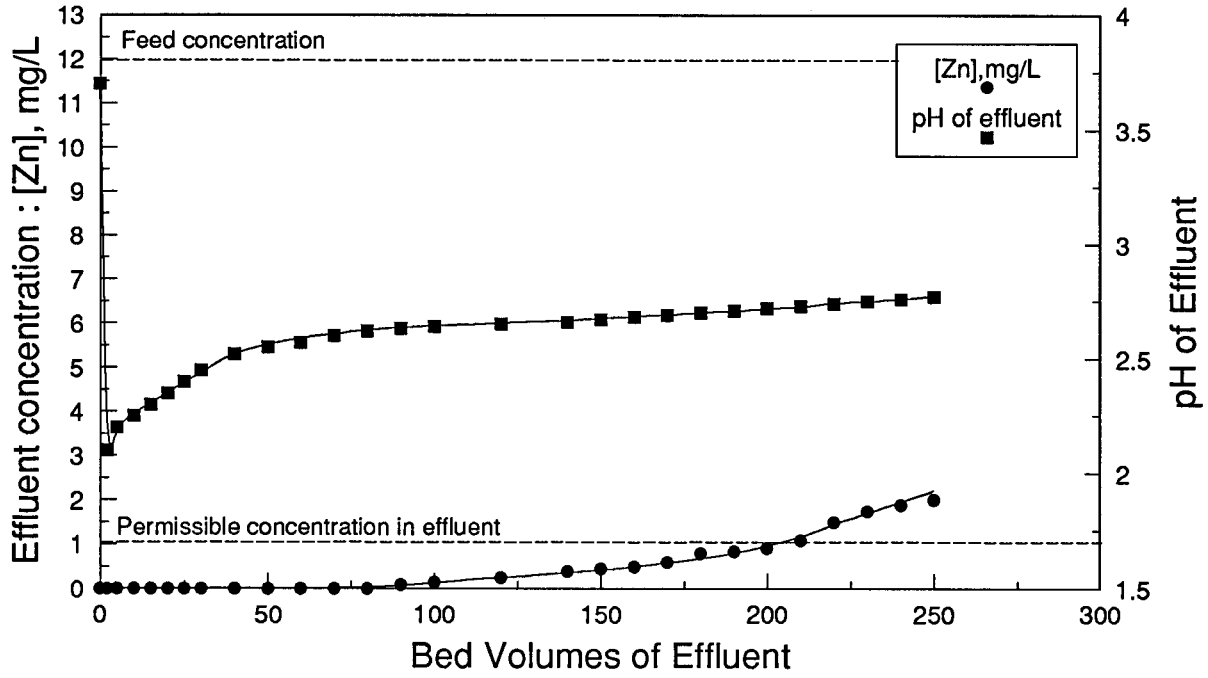

Figure 5.1 : Zinc loading on untreated OC 1026 at 40°C and 5 BV/hr.. INCO electrolyte feed (pH 3.7 at 40°C, [Zn]=12 mg/L), flow rate=5 BV/hr., OC 1026 bed = 25 ml.

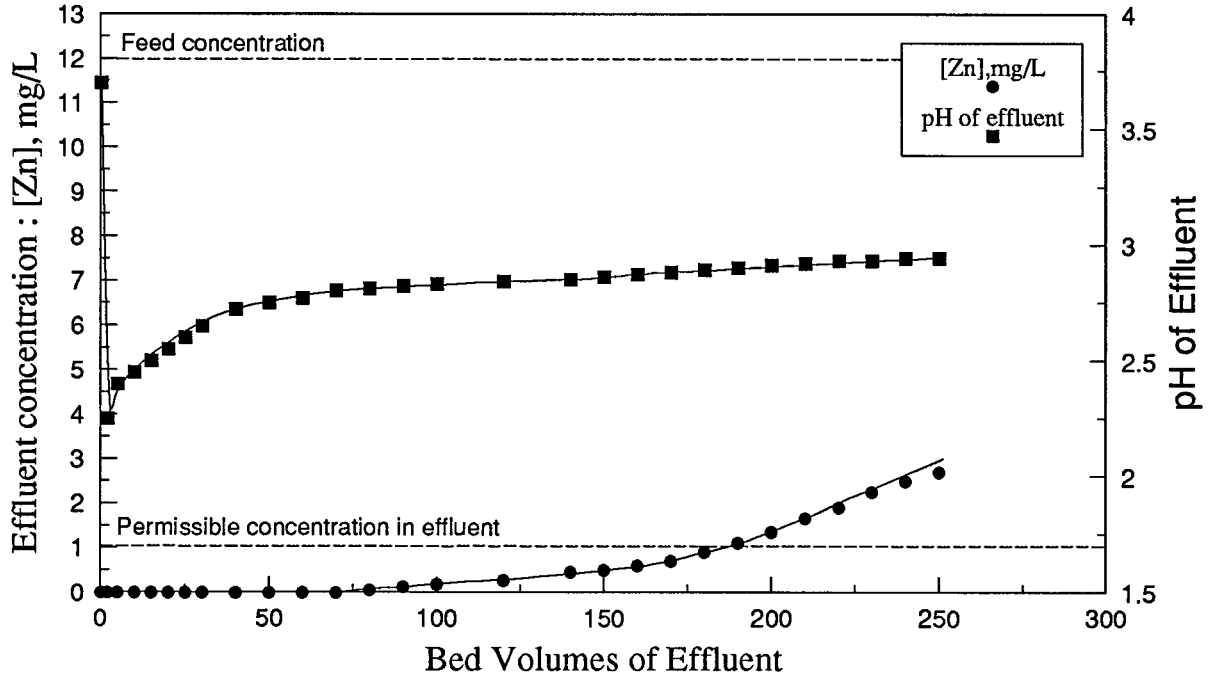

Figure 5.2 : Zinc loading on untreated OC 1026 at 40°C and 10 BV/hr.. INCO electrolyte feed (pH 3.7 at 40°C, [Zn]=12 mg/L), flow rate=10 BV/hr., OC 1026 bed = 25 ml.

that an increase in temperature enhanced zinc loading. The pH of the electrolyte falls from an initial 3.75 to about 1.9 and then rises rapidly in the first 80 BV, and then slowly up to a final value of 2.94 after 500 BV of electrolyte have been passed. The results from the tests are summarized in the following table :

Table 5.1 : Results of Zn-loading on untreated OC 1026 from INCO electrolyte.

Temp.°C	Flow rate (BV/hr.)	Initial pH	pH after 1 BV	pH after 250 BV	pH after 500 BV	Break-through
40	10	3.7	2.25	2.94	-	190 BV
40	5	3.7	2.1	2.77	-	210 BV
60	4.67	3.75	1.9	2.76	2.94	320 BV

Thus it seems from these results that a decrease in flow rate from 10 BV/hr. to 5 BV/hr. marginally enhances zinc loading, while an increase in temperature from 40°C to 60°C shows a significant increase in zinc loading. The loading of zinc and cobalt (or any other divalent metal cation) proceeds through a reaction of the type :

$$M^{2+} + n(HL)_2 \quad \longleftrightarrow \quad ML_2.HL_{2n-2} + 2H^+$$

where M = Zn or Co

Thus the extraction of the metal results in a decrease in pH. A lower pH may thus be interpreted as greater extraction of metal cations by the resin, and hence it may be concluded from these results that the extraction capacity of the resins is higher at a lower flow rate and at a higher temperature. This does not yet tell us anything about the selectivity of the resin under these conditions.

5.1.2 Zinc loading on pre-treated OC 1026

Two kinds of pre-treatment were carried out - one by using INCO electrolyte at pH 3 for preloading, as carried out at the Port Colborne Refinery, and one using $CoSO_4$ at pH 4 to

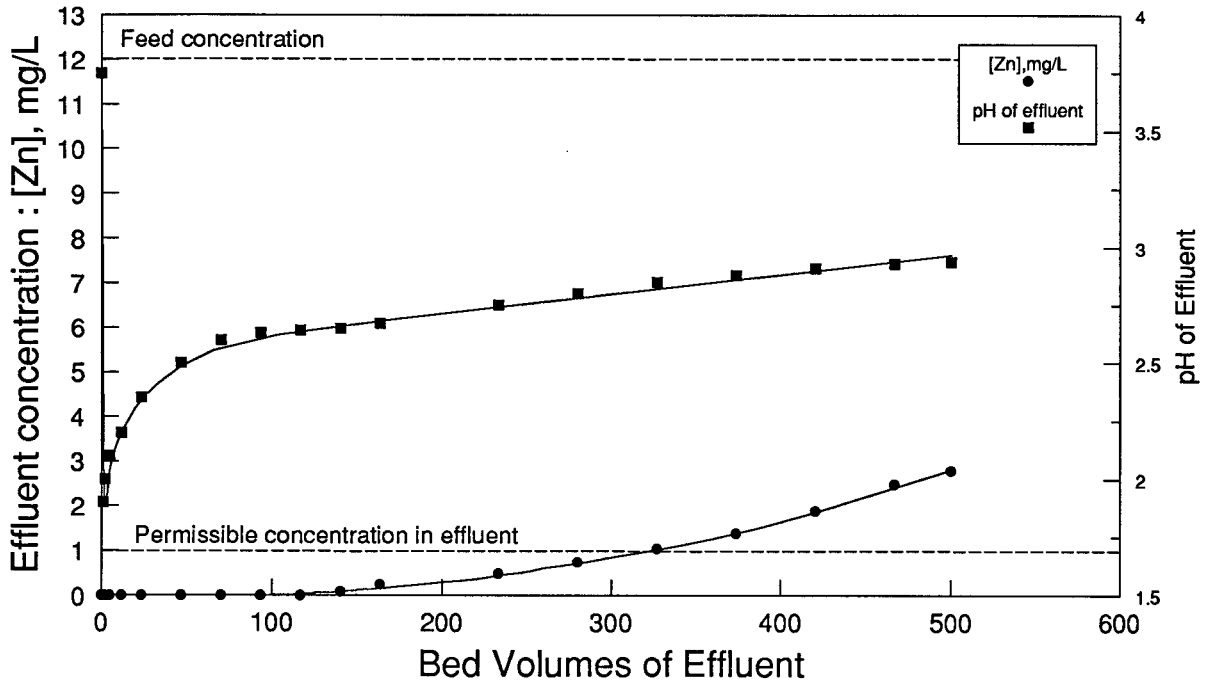

Figure 5.3 : Zinc loading on untreated OC 1026 at 60°C and 4.67 BV/hr.. INCO electrolyte feed (pH 3.75 at 60°C, [Zn]=12 mg/L), flow rate=4.67 BV/hr., OC 1026 bed = 25 ml.

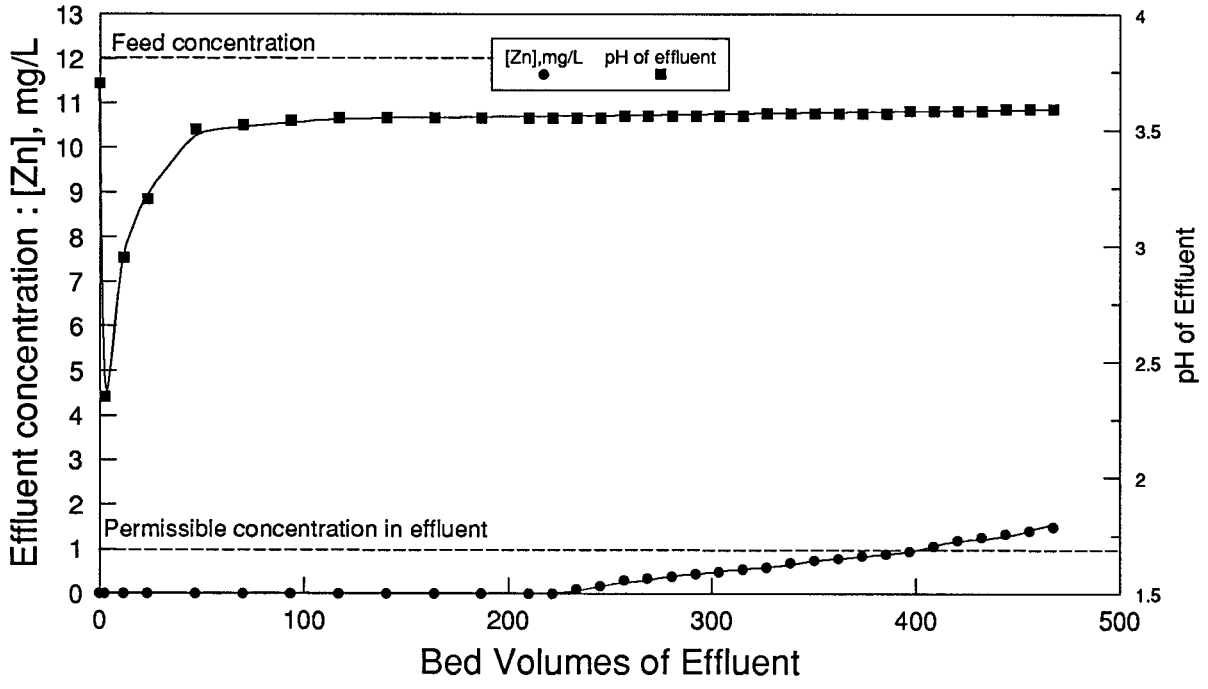

Figure 5.4 : Zinc loading on pre-treated OC 1026 at 60°C. INCO electrolyte feed (pH 3.75 at 60°C, [Zn]=12 mg/L), flow rate=4.67 BV/hr., OC 1026 bed = 25 ml, resin pre-treatment : INCO electrolyte fed at pH 3 until effluent pH 2.

preload cobalt. Preloading INCO electrolyte at pH of 3 (Fig. 5.4), seems to enhance the zinc loading considerably as breakthrough takes place only at about 400 BV, while the fall in the effluent electrolyte pH is smaller; from 3.75 to about 2.35, from which it rises very rapidly to about 3.5 in 50 BV, after which it levels off at about 3.57. Pre-treatment at pH=4 and 25°C (Fig. 5.5) was not very successful in improving zinc loading as breakthrough takes place as early as 90 BV.

5.1.3 Effect of pre-treatment on zinc loading and selectivity

The efficiency of zinc loading is judged by how much later the breakthrough of zinc takes place through the column, while the selectivity of the resin for zinc over cobalt is determined by stripping the loaded resin and computing the amount of cobalt and zinc on the resin. This analysis, however, assumes that all the cobalt and zinc loaded on the resin, is completely stripped off during the elution run. The values of cobalt retained on the resin are those determined using 10% sulphuric acid as the stripping solution (the cobalt in the wash water was not significantly different, and hence not taken into account). Table 5.2 summarizes the results obtained in the study of the effect of pre-treatment on zinc loading.

Table 5.2 : Effect of pre-treatment on zinc loading and the pH profiles.

Treatment	Flow rate	Initial pH	pH after 1BV	pH after 50 BV	pH after 250 BV	pH after 500 BV	Break-through
Untreated	4.67	3.75	1.9	2.5	2.76	2.94	320 BV
Pretreated	4.67	3.75	2.35	3.5	3.56	3.57	408 BV

Fig. 5.6 shows a comparison of the zinc loading and pH profiles for the untreated and pre-treated resins. The concentration of the INCO feed electrolyte is as follows:

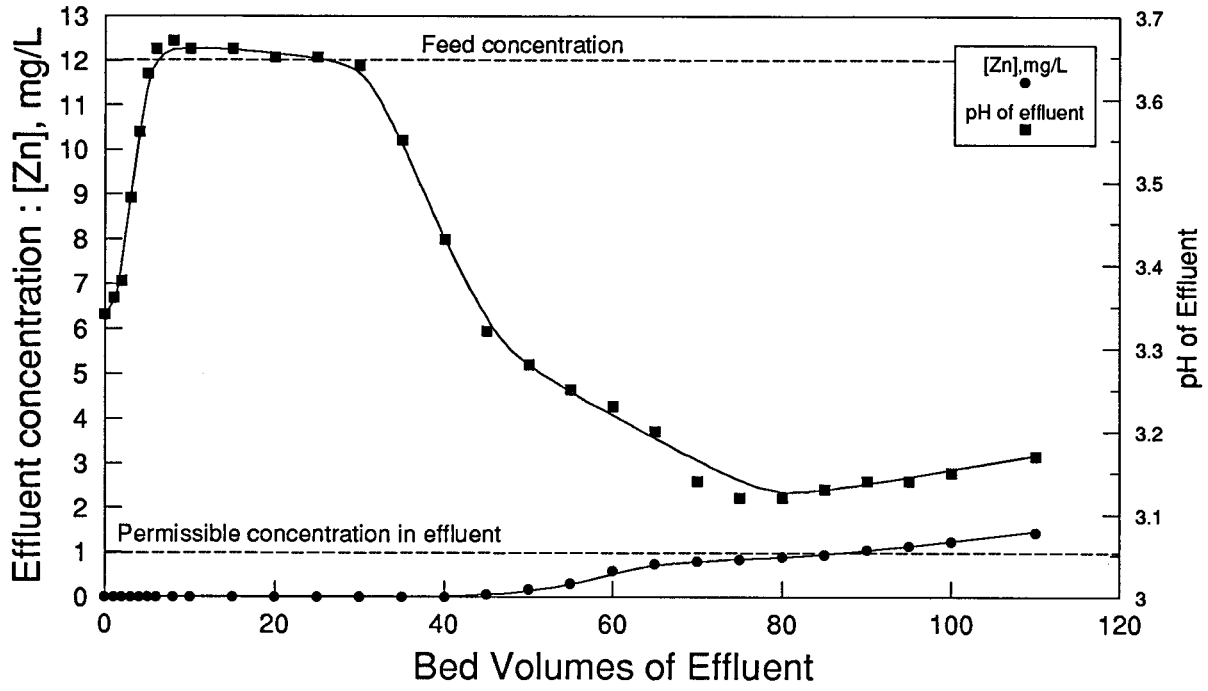

Figure 5.5 : Zinc loading on pre-treated (pH 4) OC 1026 at 25°C. INCO electrolyte feed (pH 3.34 at 25°C, [Zn]=12 mg/L), flow rate=5 BV/hr., OC 1026 bed = 25 ml, resin pre-treatment : $CoSO_4$ **fed at** pH 4 for 12 hours.

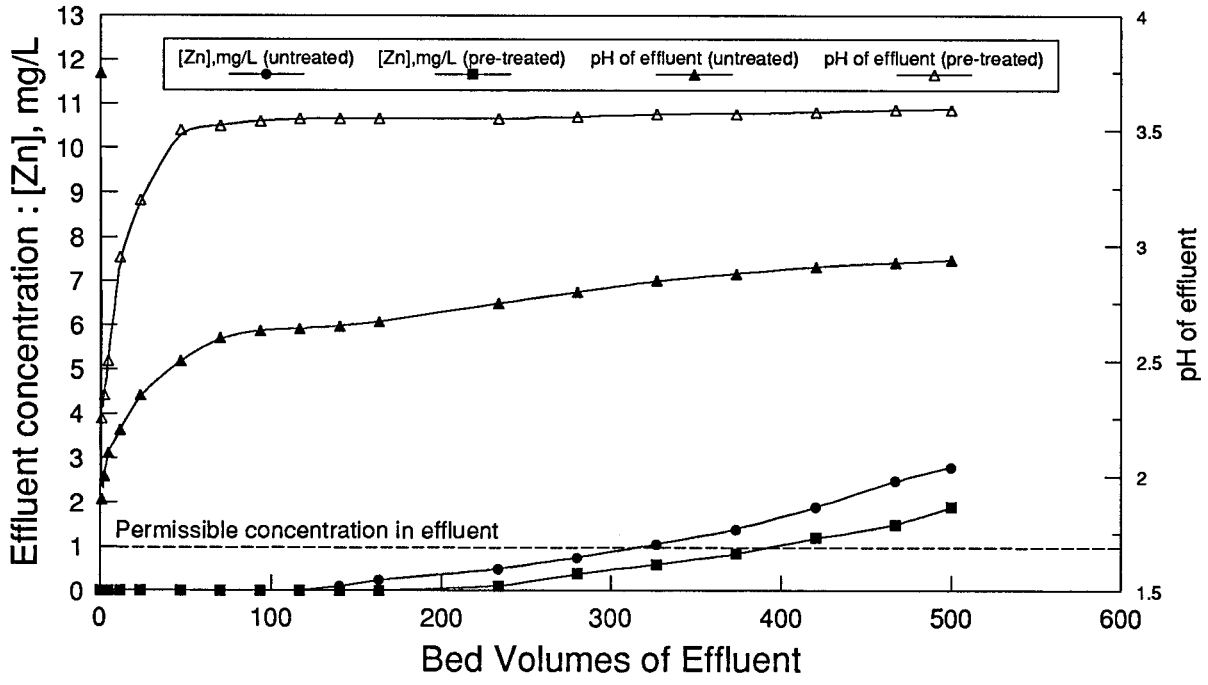

Figure 5.6 : Effect of pre-treatment on pH profile and zinc loading. INCO electrolyte feed (pH 3.75 at 60°C, [Zn]=12 mg/L), flow rate=4.67 BV/hr., OC 1026 bed = 25 ml, resin pre-treatment : INCO electrolyte fed at pH 3 until effluent pH 2.

Table 5.3 : Analysis of INCO electrolyte.

Metal	Co	Ni	Zn	Fe	Cu
conc (g/L)	45	40	0.012	0.008	0.01

As the content of zinc in the electrolyte is low (12 mg/L), its extraction alone by the resin should not result in much of a change in the pH of the effluent. Thus much of the decrease in pH of the effluent observed is due to the extraction of cobalt and so a lower pH may be interpreted as greater cobalt extraction. In the comparison of the pH profiles in Fig. 5.6, it is seen that the pH falls to a lower value of 1.9 for the untreated resin, when compared to a value of 2.35 for the pre-treated resin, thereby indicating that the cobalt extraction is higher initially for the untreated resin. As the loading progresses, the pH profile for the untreated resin rises only gradually up to 2.94 after 500 BV, while for the pre-treated resin the pH rise is extremely rapid and levels off at 3.6 after 500 BV. Thus even as the feeding progresses, the cobalt retention on the untreated resin is higher. Thus pre-treatment has an effect of reducing the initial drop in pH, and maintaining the pH of the column between 3.75 and about 3.6, from 50 BV until the end (500 BV). This levelling of the pH possibly plays a role in delaying the breakthrough of zinc from 320 BV to about 408 BV, and in addition results in a reduction of cobalt retained on the resin as shown in Table 5.4.

Table 5.4 : Effect of pre-treatment on cobalt retained on the resins (25 ml of loaded resin stripped with 10% sulphuric acid).

Treatment	Co (gms.)	Zn (gms.)	Zn/Co selectivity
Untreated resin	0.26	0.17	0.65
Pre-treated resin	0.23	0.20	0.87

5.1.4 Cobalt and zinc retained on pre-treated resin

The loading of the resin pre-treated at pH 3, was carried out till 233.5 BV, 350.25 BV and 500 BV of electrolyte were passed, followed by stripping, to determine the amount of cobalt and zinc retained on the resins after each of these runs. The results in Fig. 5.7 and Table 5.5 show that there is a continuous decrease in the amount of cobalt retained on the resin and a continuous increase in the zinc on the resin with increasing volume treated.

Table 5.5 : Comparison of metal retained on OC 1026 after various effluent bed volumes.

BV of effluent	Co (g)	Zn (g)	Zn/Co selectivity
233.50	0.45	0.059	0.013
350.25	0.37	0.116	0.314
500.00	0.23	0.200	0.870

These data seem to suggest that cobalt was initially loaded on the resin, and then was displaced by the zinc. This is substantiated by the following mass balance:

Between 233.50 BV and 350.25 BV :

Total reduction in cobalt retained on the resin = 0.080 g

Total increase in zinc loaded on the resin = 0.058 g

From the breakthrough curve; amount of zinc loaded from the solution on the resin = 0.060 g

Similarly between 233.5 BV and 500 BV :

Total reduction in cobalt retained on the resin = 0.200 g

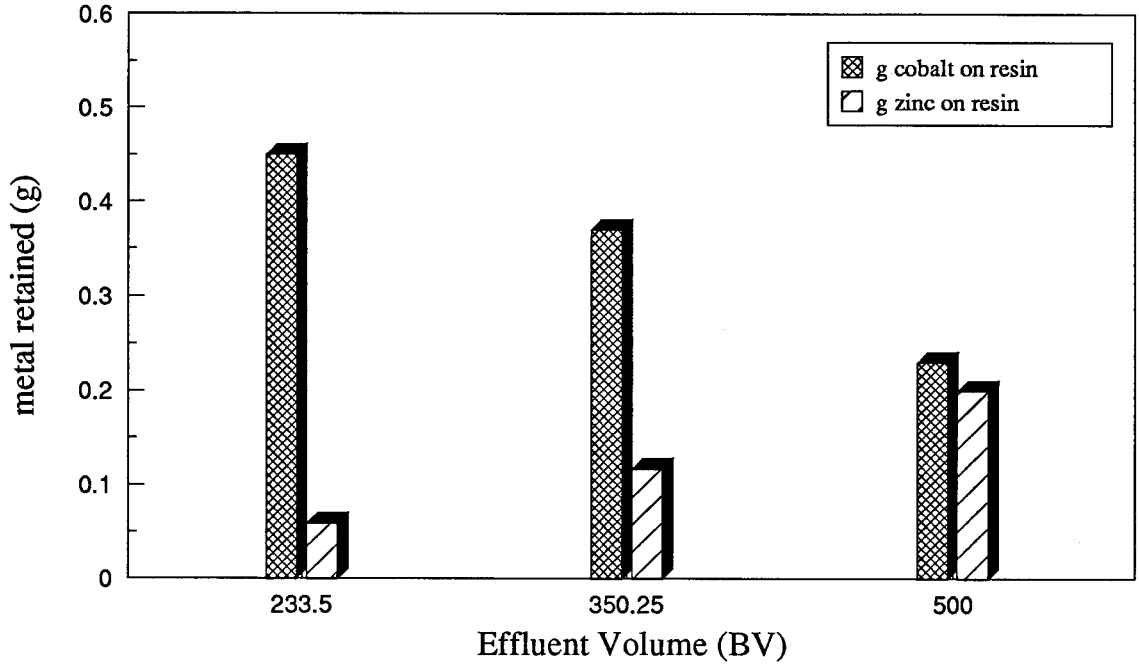

Figure 5.7 : Stripping of zinc and cobalt from OC 1026. Comparison of metal retained in 25 ml of loaded OC 1026; after various effluent bed volumes, determined by stripping the loaded resin by 10% H_2SO_4 at 60°C.

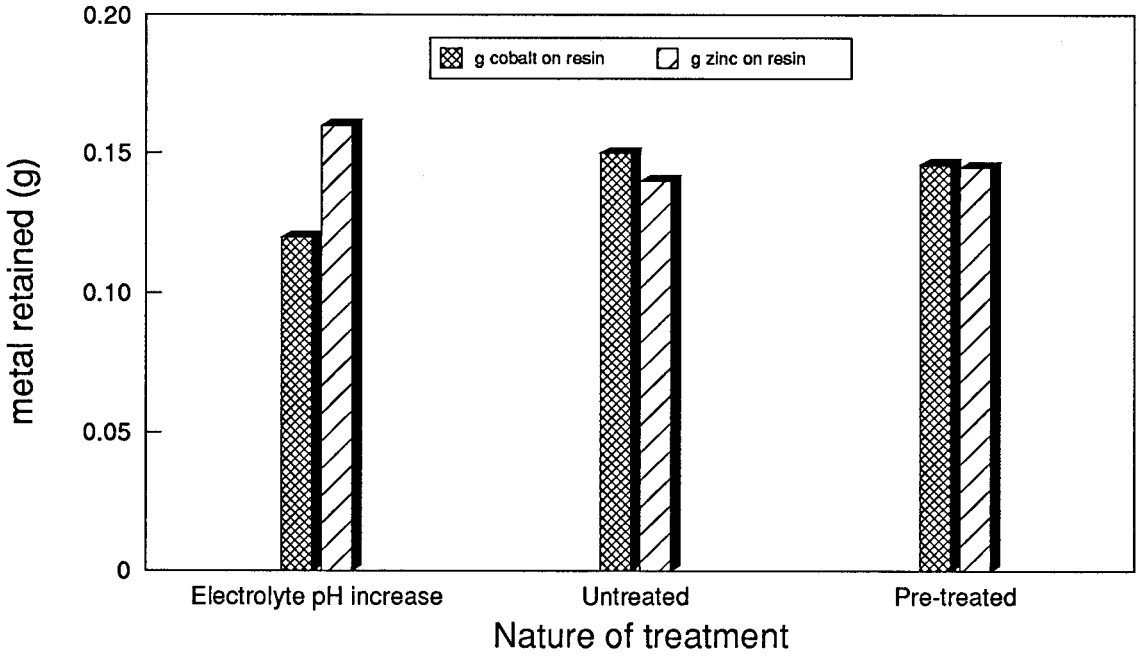

Figure 5.8 : Effects of electrolyte pH increase and pre-treatment on metal retained on the resin. Comparison of metal retained in 25 ml of loaded OC 1026, after resin and electrolyte pre-treatment, determined by stripping the loaded resin by 10% H_2SO_4 at 60°C.

Total increase in zinc loaded on the resin = 0.141 g

From the breakthrough curve; amount of zinc loaded from the solution on the resin = 0.150 g

Thus these data seem to confirm that the resin initially loads cobalt, which is displaced by zinc as the feeding progresses. Correlating this with the observation that the electrolyte pH is low at the early effluent bed volumes, while it increases for the later effluent bed volumes, it may be concluded that cobalt loads on the resin initially at low pH values (between 1.8 - 2.5), while this cobalt is displaced by the zinc at higher pH values (between 3.5 - 3.6). Resin pre-treatment results in the column being maintained between 3.5 and 3.7 for the major part of the loading (after the initial 50 BV of electrolyte have been fed), and thus zinc loading on the pre-treated resin is enhanced as against the untreated resin where the column is at a pH range between 2.6 and 3.

5.1.5 Effect of flow rate on zinc loading and selectivity

Results of tests carried out to determine zinc loading at flow rates of 5 BV/hr. and 10 BV/hr. are summarized below :

Table 5.6 : Effect of flow rate on zinc loading and selectivity: (Loading of untreated resin at 40°C).

Flow rate	Initial pH	pH at 1BV	pH @ 250BV	Break-through	gm. Co on resin	gm. Zn on resin	Zn/Co selectivity
5 BV/hr.	3.7	2.10	2.77	210 BV	0.150	0.140	0.93
10 BV/hr.	3.7	2.25	2.94	190 BV	0.105	0.136	1.30

Thus it is seen that even though zinc loading is enhanced by operating at a lower flow rate, the cobalt retained on the resin is lower when operated at 10 BV/hr. flow rate. This may be because the electrolyte pH is higher than that of the range in which cobalt loads favorably (1.9-2.3), when the column is operated at the higher flow rate.

5.1.6 Effect of temperature on zinc loading and selectivity

The effect of temperature on the loading process was studied at temperatures 60, 40 and 25°C, with the resin pre-treated at a pH of 3, and the results are shown in Fig. 5.9 and Table 5.7.

Table 5.7 : Effect of temperature on zinc loading and selectivity of pre-treated OC 1026.

Temperature	Breakthrough	gm. Co on resin	gm. Zn on resin	Zn/Co selectivity
60°C	408	0.230	0.200	0.870
40°C	250	0.144	0.145	1.007
25°C	140	0.110	0.110	0.909

Lowering the temperature hastens zinc breakthrough, but the amount of cobalt retained on the resin is reduced. Zinc selectivity is highest at 40°C. Hence, operating at 40°C could be considered when it is of the utmost importance to improve selectivity.

5.1.7 Effect of increasing feed electrolyte pH

As a test run, the pH of the feed electrolyte was raised to 5, and this was fed to an untreated bed of OC 1026 at 10 BV/hr. and 40°C. Zinc breakthrough took place only at 250 BV, and this is compared with the performance of the pre-treated and untreated resin (Fig. 5.10) as follows:

Table 5.8 : Effect of increasing feed electrolyte pH on loading (T=40°C).

Treatment	Flow rate	Breakthrough	Co retained	Zn retained	Zn/Co selectivity
Untreated	10 BV/hr.	190.00 BV	0.150	0.14	0.900
Pre-treated	5 BV/hr.	250.00 BV	0.144	0.145	1.007
Elect. pH increase	10 BV/hr.	250.25 BV	0.120	0.16	1.333

Increasing electrolyte pH thus works as well as resin pre-treatment to enhance zinc loading, with significantly higher Zn/Co selectivity.

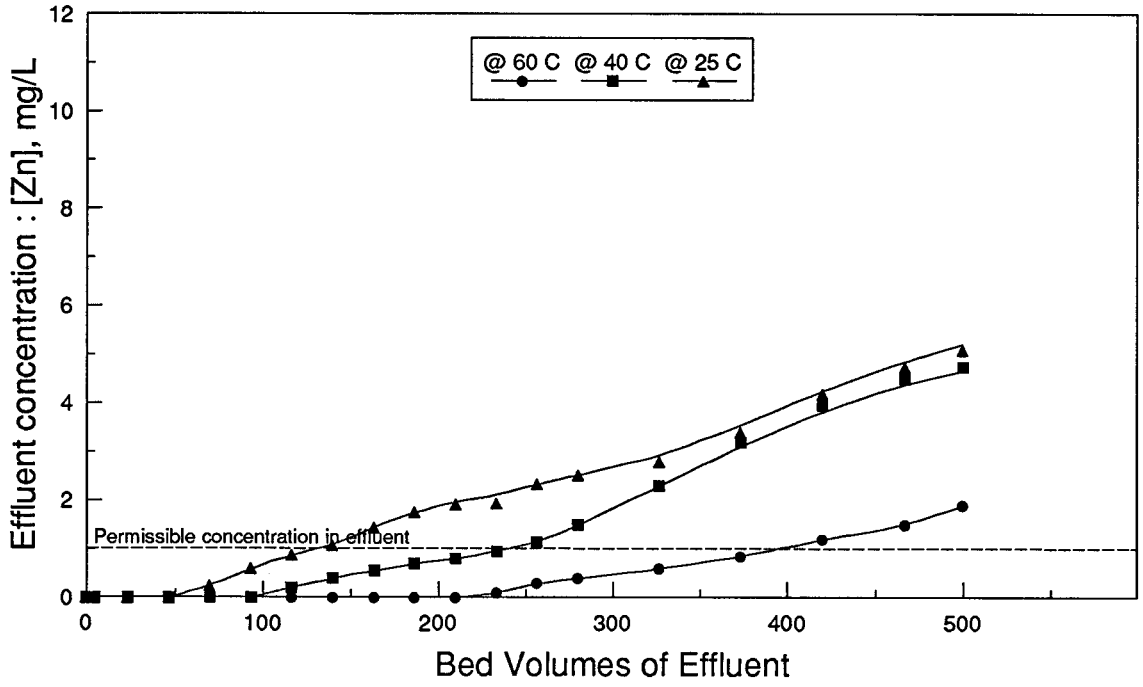

Figure 5.9 : Effect of temperature on zinc breakthrough of OC 1026. INCO electrolyte feed (pH 3.75 at 60°C, [Zn]=12 mg/L), flow rate=4.67 BV/hr., OC 1026 bed = 25 ml, resin pre-treatment : INCO electrolyte fed at pH=3 until effluent pH 2.

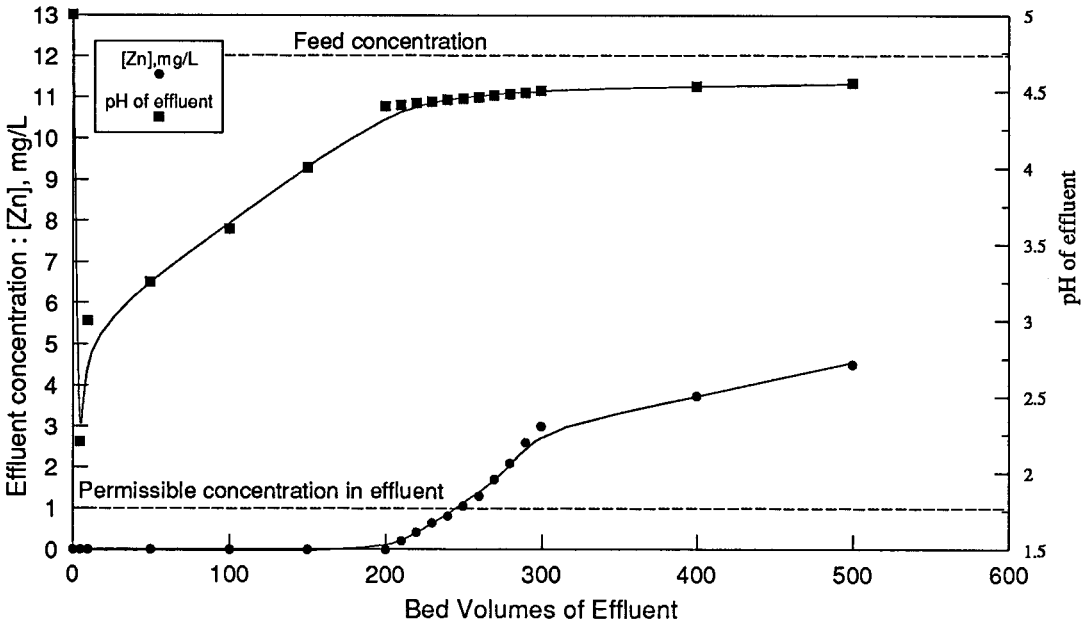

Figure 5.10 : Effect of electrolyte pH increase on zinc breakthrough of untreated OC 1026. INCO electrolyte feed pH raised to 5.0 with NaOH, flow rate=10 BV/hr., temperature=40°C, OC 1026 bed = 25 ml, no resin pre-treatment.

5.1.8 Performance of Cyanex 302 and Cyanex 272

The performance of Cyanex 302 and Cyanex 272 was studied by testing them under conditions similar to those at which tests on OC 1026 were carried out. The resins were pre-treated by feeding INCO electrolyte at a pH of 3, and as the pH reduction for both resins was not as great as that of OC 1026, the effluent pH in both cases was equal to 2.5. For the Cyanex 302 column, zinc breakthrough took place after 175 BV (Fig. 5.11), while for Cyanex 272 breakthrough took place after 160 BV of electrolyte (Fig. 5.13). However for Cyanex 302, the resin was poisoned by the loading of copper and a little iron, which formed a dirty brown band at the top 4 ml of the resin column, and was not stripped off easily even by 10% HCl. The effect of this poisoning on further loading cycles is shown in Fig. 5.12, where the breakthrough took place earlier after each loading cycle, and the poisoned brown band spread slowly but continuously downward through the resin bed.

5.1.9 Comparison of cobalt retained on the resins

Table 5.9 and Fig. 5.16 show a comparison of cobalt retained on the resins after various effluent bed volumes.

Table 5.9 : Comparison of cobalt retained on the resins.

BV of effluent	Co on OC1026(g)	Zn on OC1026(g)	Co on Cy302(g)	Zn on Cy302(g)	Co on Cy272(g)	Zn on Cy272(g)
233.5	0.450	0.059	0.150	0.055	0.185	0.050
350.25	0.370	0.116	0.135	0.067	0.178	0.060
500	0.230	0.200	0.125	0.073	0.170	0.070
Zn/Co selectivity at 500BV	0.870		0.584		0.411	

Thus, it is seen from these data that even though the cobalt retained on the resin after 233.5 BV of electrolyte was much higher for OC 1026 than that for the other resins, after 500 BV of electrolyte,

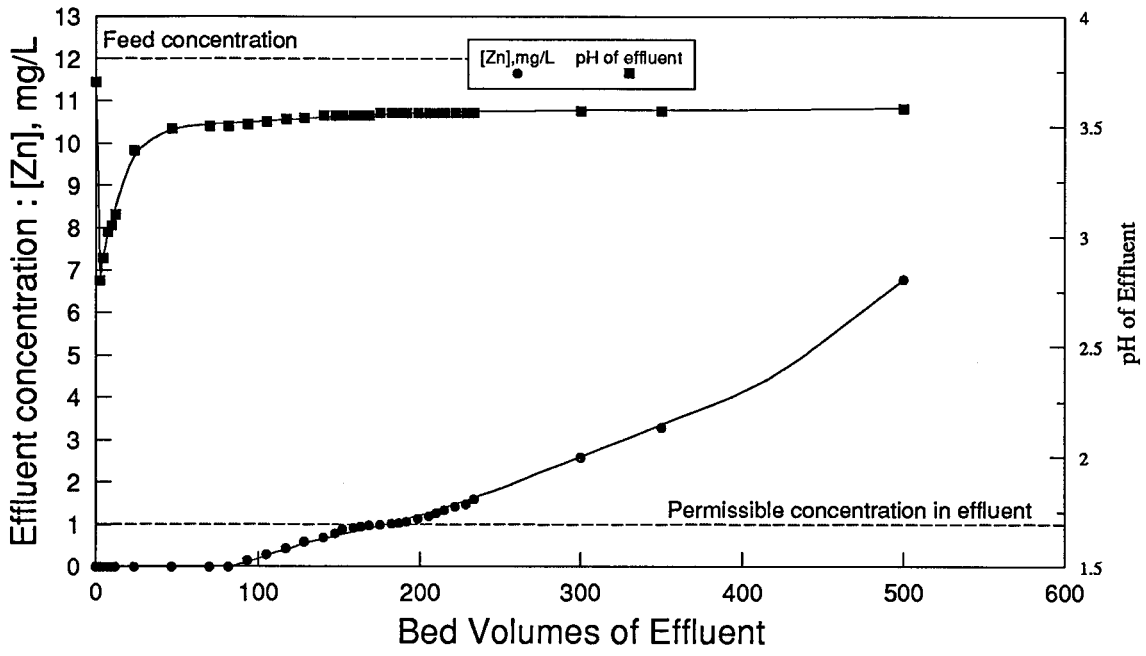

Figure 5.11 : Zinc loading on pre-treated Cyanex 302. INCO electrolyte feed (pH=3.75 at 60°C, [Zn]=12 mg/L), flow rate=4.67 BV/hr., Cyanex 302 bed = 25 ml, resin pre-treatment : INCO electrolyte fed at pH 3 until effluent pH 2.5 .

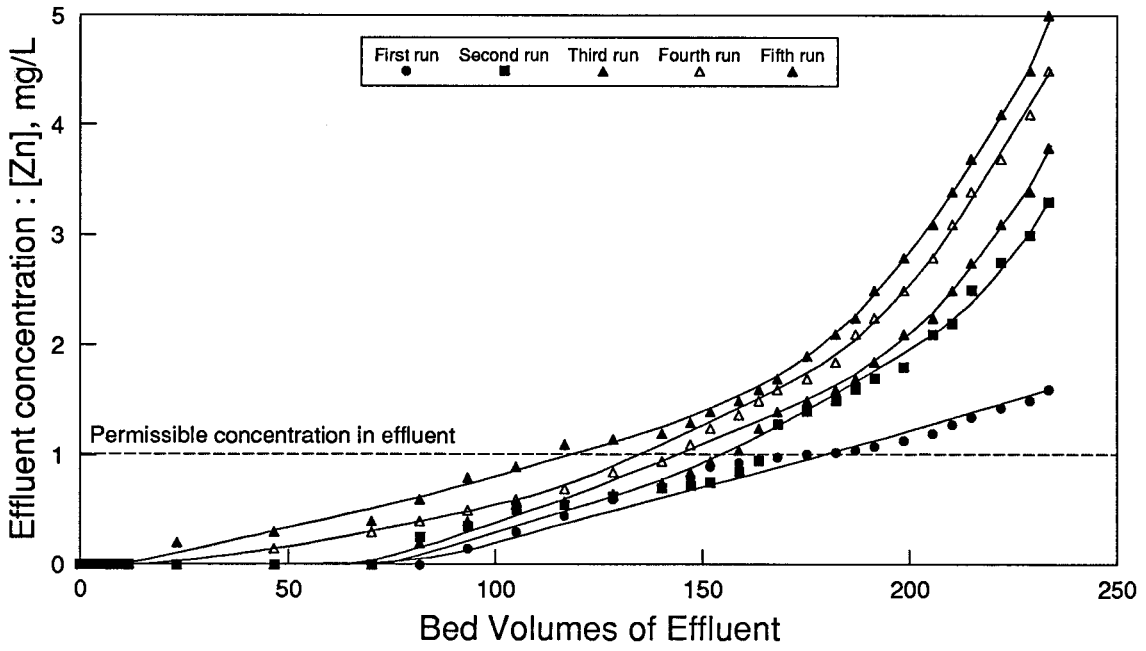

Figure 5.12 : Effect of resin poisoning on zinc breakthrough of Cyanex 302. INCO electrolyte feed (pH 3.75 at 60°C, [Zn]=12 mg/L), flow rate=4.67 BV/hr., Cyanex 302 bed = 25 ml, resin pre-treatment : INCO electrolyte fed at pH 3 until effluent pH 2.5 .

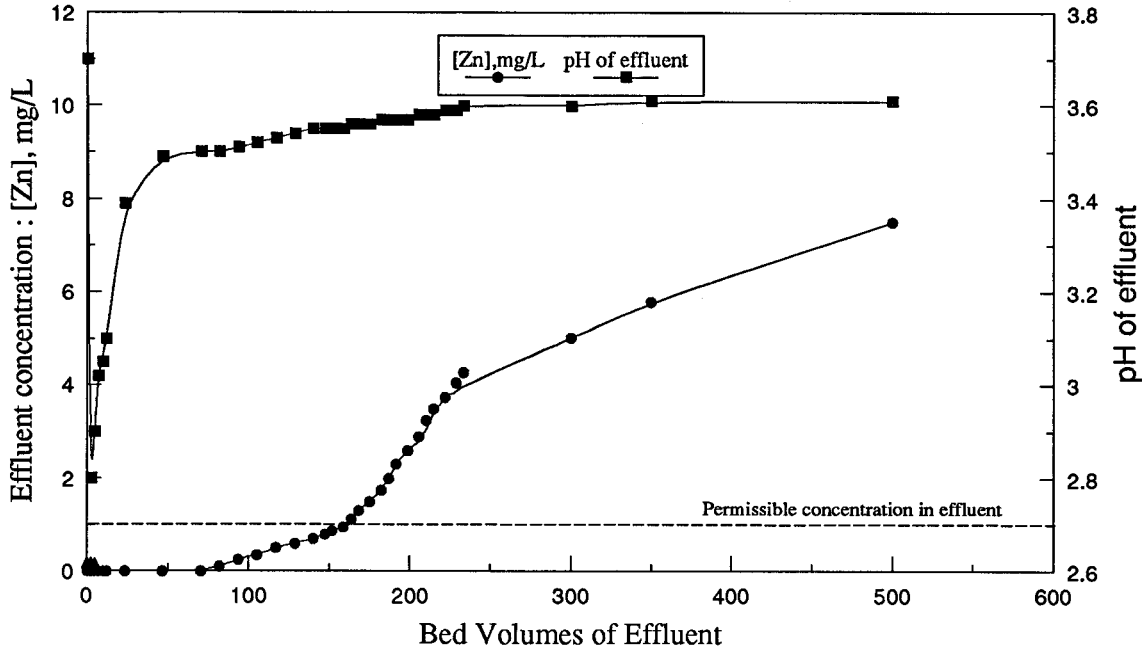

Figure 5.13 : Zinc loading on pre-treated Cyanex 272. INCO electrolyte feed (pH 3.75 at 60°C, [Zn]=12 mg/L), flow rate=4.67 BV/hr., Cyanex 272 bed = 25 ml, resin pre-treatment : INCO electrolyte fed at pH=3 until effluent pH 2.5 .

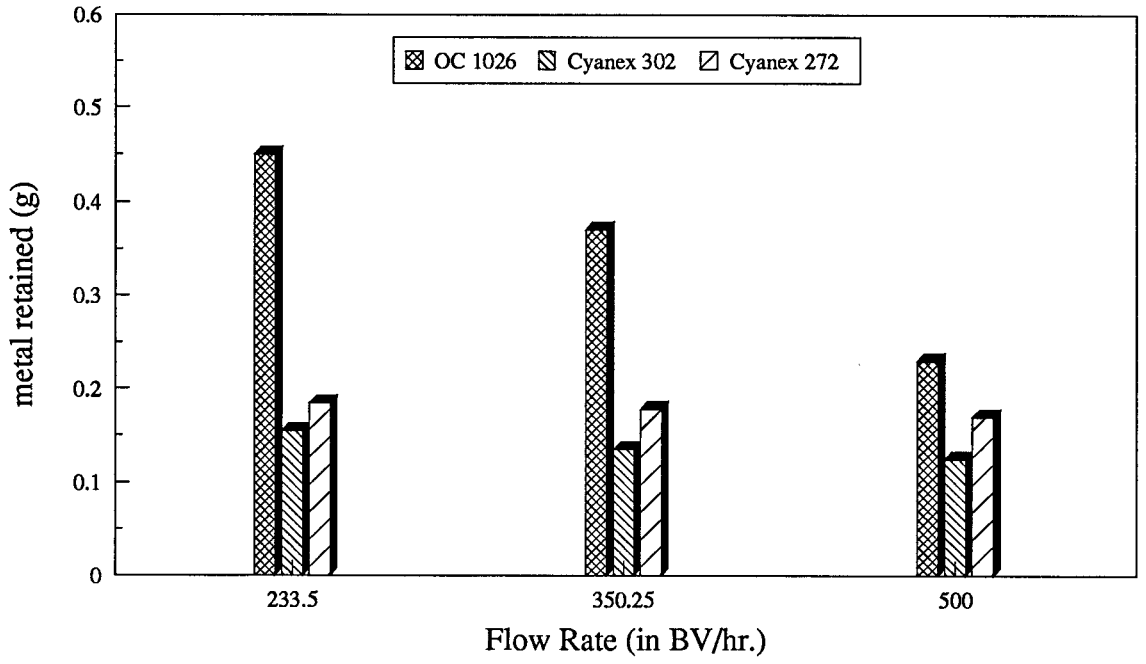

Figure 5.14 : Comparison of cobalt retained in 25 ml of loaded OC 1026, Cyanex 302 and Cyanex 272 (for a similar pre-treatment), determined by stripping the loaded resin by 10% H_2SO_4 at 60°C.

the value of cobalt retained on OC 1026 is comparable to that of the other resins. Yet, in terms of amount of cobalt loaded, Cyanex 302 seems to perform better than OC 1026, even though zinc loading and selectivity are better in the latter. The reason for lower amounts of cobalt loading on pre-treated Cyanex 302 and Cyanex 272, may be that the pH never drops below 2.6 during the loading of these resins, while the pH drops to about 2.3 for loading on pre-treated OC 1026. From the comparison of the pH profiles in Figure 5.6, it was concluded that zinc loads on the resin only as the pH rises, while cobalt continues to load on the resin even at lower pH values, and hence cobalt retention by pre-treated OC 1026 is higher than that by Cyanex 272 and Cyanex 302.

5.2 BATCH RESULTS

5.2.1 Kinetics of zinc loading on OC 1026

The kinetics of zinc loading on OC 1026 was followed in batch loading up to 500 minutes by determining the zinc concentration in the withdrawn aliquots at the particular time intervals. Fig. 5.15 is a plot of fraction of zinc extracted with time. It shows an extremely small incubation time followed by a rapid rise in the first 50 minutes, levelling off gradually. Studies were made on the types of pre-treatment possible, temperature variations and variations in the initial zinc content of electrolyte based on these kinetic results.

5.2.2 Effect of pre-treatment

Fig. 5.16 shows a comparison of the effects of various pre-treatments on the kinetics of zinc loading on OC 1026. All pre-treatments seem to enhance the kinetics of zinc extraction, while pre-treating at pH of 3.5, 3 and 2, provide the maximum improvement; the difference between them being marginal (the curves almost overlap). For the case of Cyanex 302 (Fig. 5.19) pre-treatment at pH 2 was the most favorable pre-treatment. In a comparison of the performance of OC 1026 and Cyanex 302 based on pre-treatments in Figure 5.26,

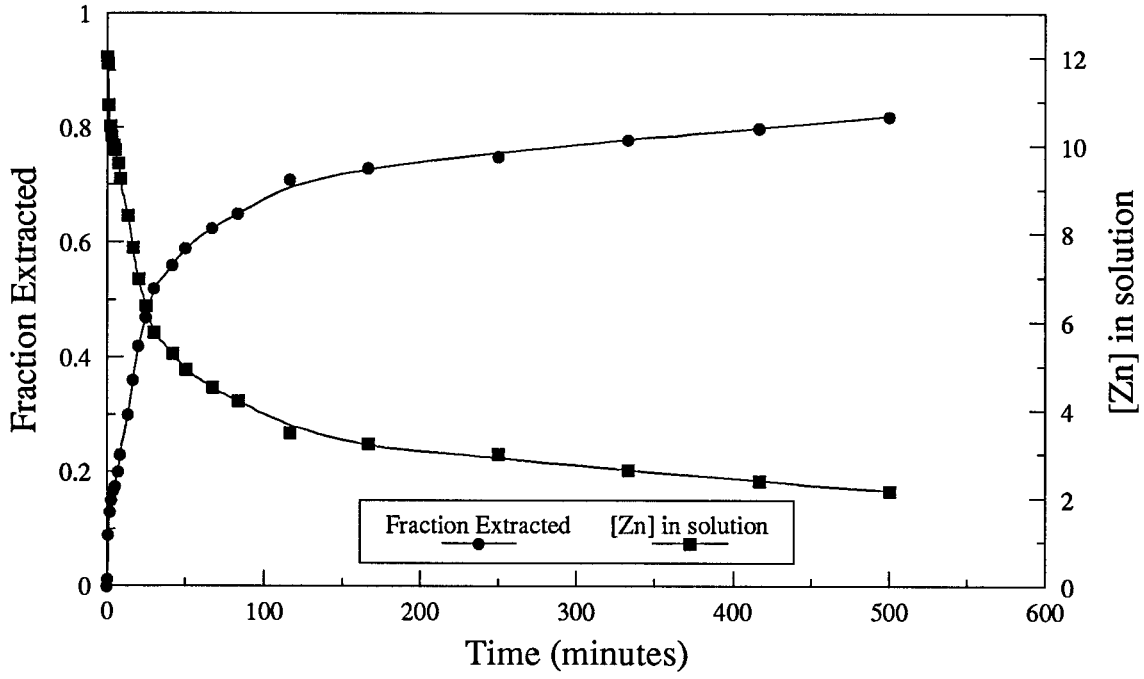

Figure 5.15 : Batch test study of zinc loading kinetics on untreated OC 1026; initial [Zn] = 12 mg/L, pH 3.75, T = 60°C.

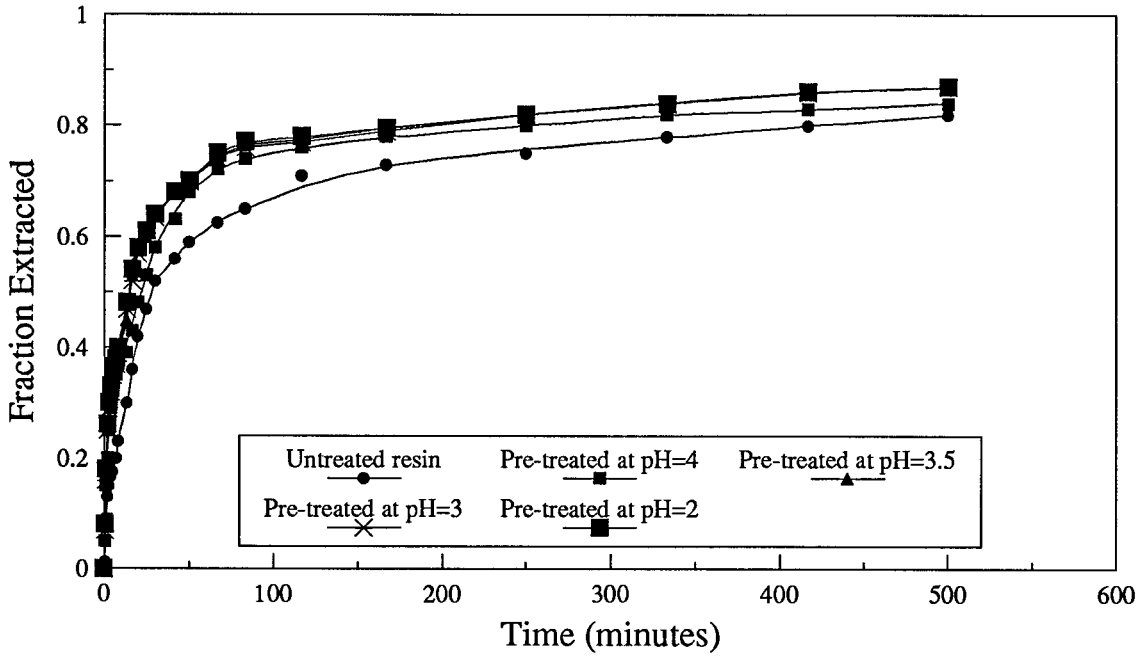

Figure 5.16 : Effect of pre-treatment on the kinetics of zinc uptake. Batch test study of zinc loading on pre-treated OC 1026; initial [Zn] = 12 mg/L, pH 3.0, T = 60°C. Pre-treatment : Equilibrating resin in zinc free INCO electrolyte at pH 3.

it was found that the performance of OC 1026 and Cyanex 302 are almost comparable when pre-treatment was done at pH 3, while for pre-treatment at pH 2, Cyanex 302 performs better than OC 1026.

5.2.3 Effect of initial zinc content

In the study shown in Fig. 5.18, the kinetics of zinc extraction at 40 mg/L zinc is compared to that at 12 mg/L. The increase in zinc content seems to make almost no difference in the zinc loading on OC 1026 in the first 20 minutes, after which time the kinetics of zinc loading are considerably increased at the higher initial zinc content. This seems to suggest that the initial rate limiting step could be particle diffusion (where diffusion rate is independent of concentration), while the dominant mechanism after 20 minutes into the process is film diffusion control (which is dependent on concentration).

5.2.4 Effect of temperature on the kinetics of metal uptake

The kinetics of metal extraction was studied for OC 1026 in Fig. 5.17, for Cyanex 302 in Fig. 5.20 and for Cyanex 272 in Fig. 5.26. In all cases the kinetics are slackened by a lowering of temperature. In an attempt to quantify the influence of temperature and other parameters, and help determine the loading mechanism, the kinetic data was fitted to the models described in Chapter 4.

5.3 Kinetic Model Fit for the Batch Tests

Figures 5.21 and 5.22 show one example of the fitting of the experimental results for the loading of zinc on OC 1026, pre-treated at pH 3. No single model seems to be able to successfully fit the experimental data. From Figure 5.22, it is seen that the data obey the Fickian Particle Diffusion Control (PDC) model, with a resin phase diffusivity $\overline{D} = 9.0x10^{-12}m^2/s$, for the first ten minutes, and then from 20 minutes onwards, obeys the Film Diffusion Control (FDC) model, with a mass transfer coefficient, $k_m = 2.7 \times 10^{-7}$ m/s. Finally after about 150 minutes

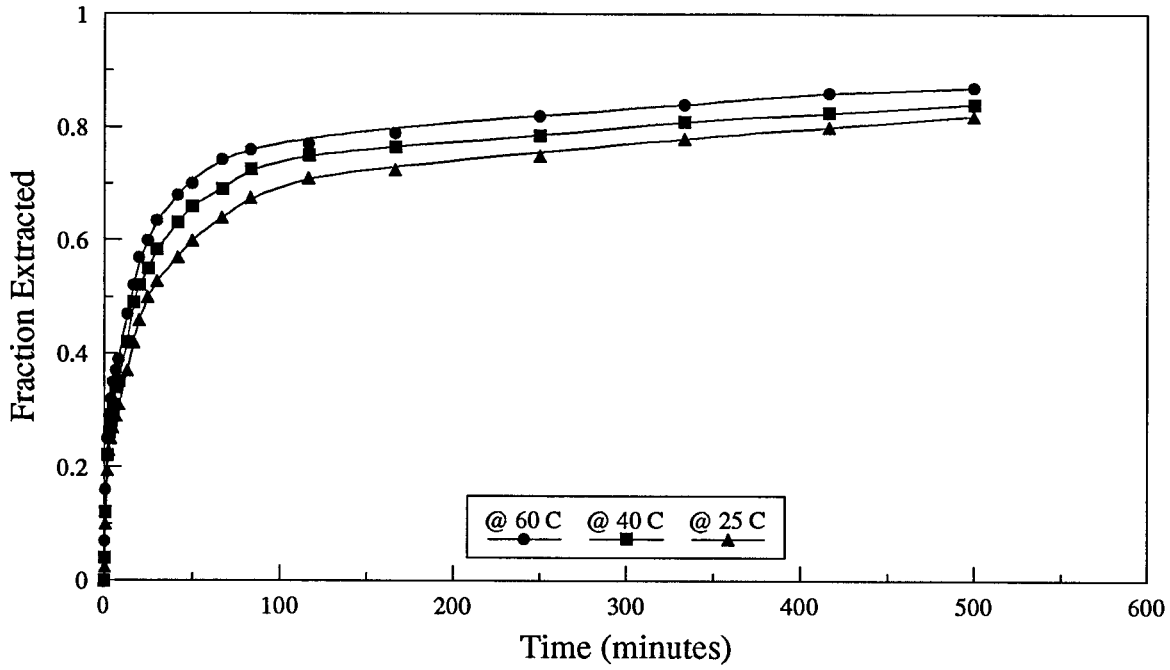

Figure 5.17 : Effect of temperature on the kinetics of zinc uptake. Batch Test Study of zinc loading on pre-treated OC 1026; initial [Zn] = 12 mg/L, pH 3.0. Pre-treatment : Equilibrating resin in zinc free INCO electrolyte at pH=3.

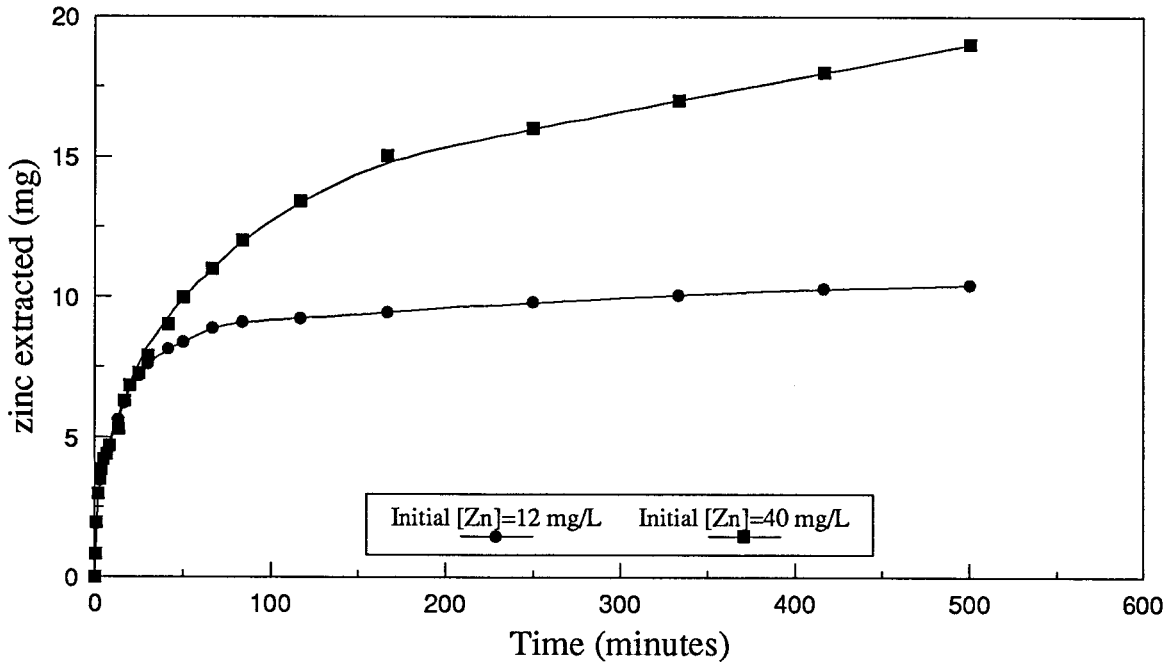

Figure 5.18 : Effect of initial zinc concentration on the kinetics of zinc uptake. Batch Test Study of zinc loading on pre-treated OC 1026, pH 3.0, T = 60°C. Pre-treatment : Equilibrating resin in zinc free INCO electrolyte at pH 3.

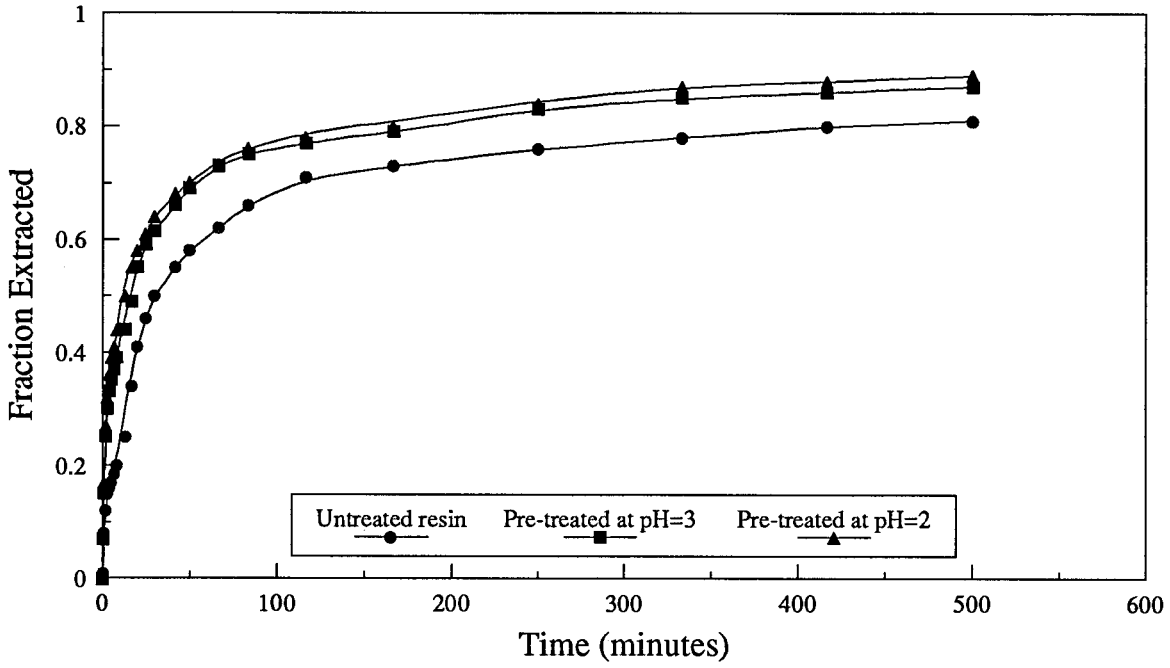

Figure 5.19 : Effect of pre-treatment on kinetics of zinc uptake by Cyanex 302. Batch Test Study of zinc loading on pre-treated Cyanex 302, Initial [Zn] = 12 mg/L, T = 60°C. Pre-treatment : Equilibrating resin in zinc-free INCO electrolyte at particular pH.

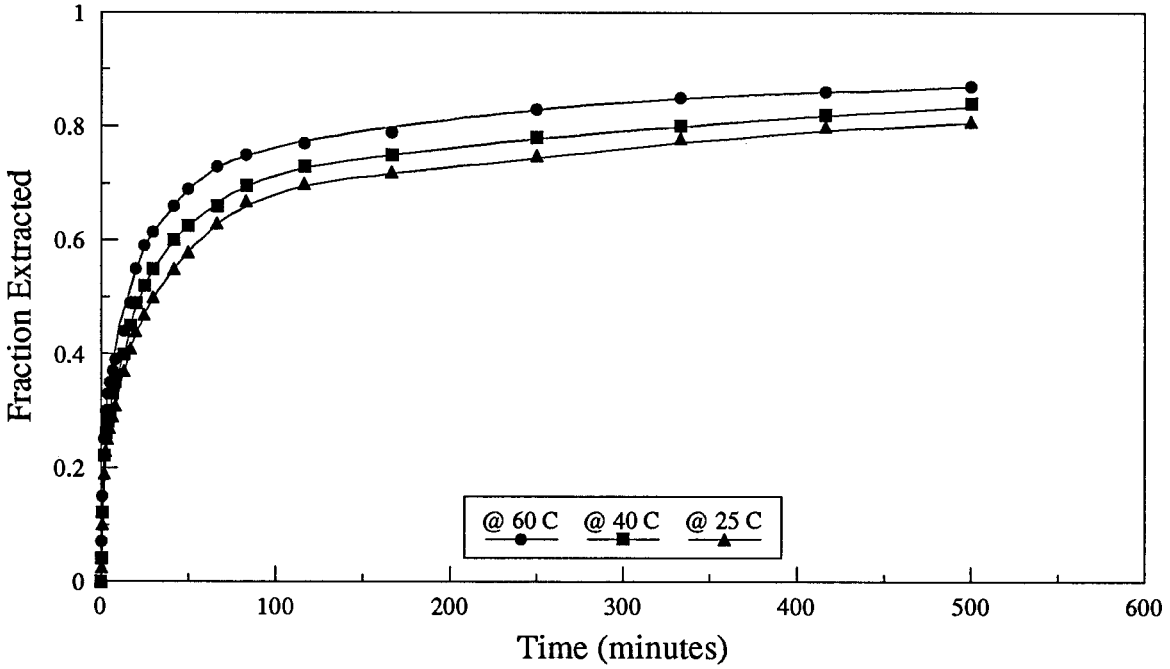

Figure 5.20 : Effect of temperature on kinetics of zinc uptake by Cyanex 302. Batch Test Study of zinc loading on pre-treated resin, Initial [Zn] = 12 mg/L, pH 3.0. Pre-treatment : Equilibrating resin in zinc free INCO electrolyte at pH 3.

(Figure 5.21), the data fall between the Fickian Particle Diffusion Control (PDC) model, with $\overline{D} = 1.5x10^{-11}m^2/s$, and the unreacted core diffusion model with $\overline{D} = 7.3x10^{-12}m^2/s$. Results for other batch tests seemed to almost follow the same trend. It was possible to determine accurately the diffusion and mass transfer coefficients only for the first 150 minutes, as after that the deviations from the models are too large.

Table 5.10 lists the $\overline{D}$ and k_m values obtained for the Fickian PDC and FDC models for the data from the three resins at a given pre-treatment. It is seen that the difference between the $\overline{D}$ and k_m values, of the three resins for a similar pre-treatment is not significant. Hence the kinetic performance of the resins is comparable (also seen in Fig. 5.26).

Table 5.10 : Kinetic model fitted to determine $\overline{D}$ and k_m values.

Resin (Operating temp.=60°C)	$\overline{D}$ (m^2/s)	k_m (m/s)
Untreated OC 1026	1.0×10^{-12}	1.6×10^{-7}
Pre-treated (pH=3) OC 1026	9.0×10^{-12}	2.7×10^{-7}
Untreated Cyanex 302	9.0×10^{-13}	1.0×10^{-7}
Pre-treated (pH=3) Cyanex 302	8.5×10^{-12}	2.1×10^{-7}
Pre-treated (pH=3) Cyanex 272	8.0×10^{-12}	1.8×10^{-7}

Pre-treatment seems to enhance the $\overline{D}$ values of the resins by nearly an order of magnitude, which leads to a slight increase in the k_m values in the aqueous film. The effect of temperature on the $\overline{D}$ and k_m values is shown in Table 5.11. For infinite dilution, the temperature dependence of the liquid diffusivity is usually accounted for by assuming that the term $D_L\eta/T$ is constant (D_L=liquid phase diffusivity, η=viscosity, T=temperature). For more concentrated solutions, the exponential dependence of D_L on T has been suggested [88]:

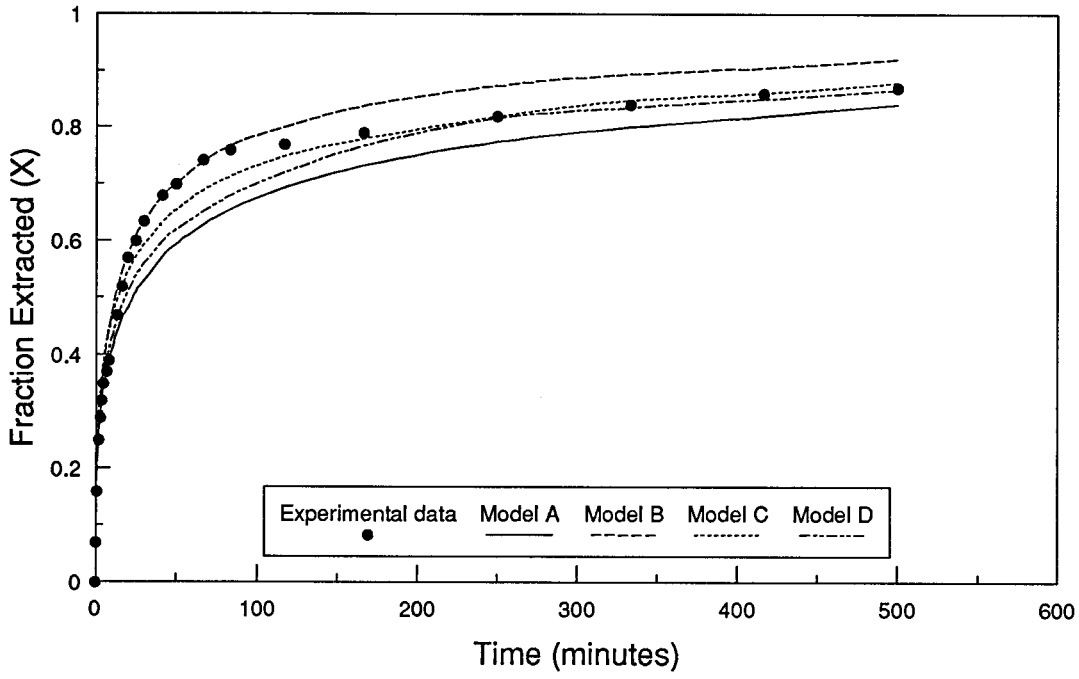

Figure 5.21 : Kinetic model fit of the experimental data for zinc loading on pre-treated (pH=3) OC 1026 at 60°C. Model A=Fickian PDC with $\overline{D}$=9.0 x 10^{-12} m^2/s; Model B=FDC, k_m=**2.7 x 10^{-7} m/s**; Model C=Fickian PDC, $\overline{D}$=1.5 x 10^{-11} m^2/s; Model D=Unreacted Core PDC.

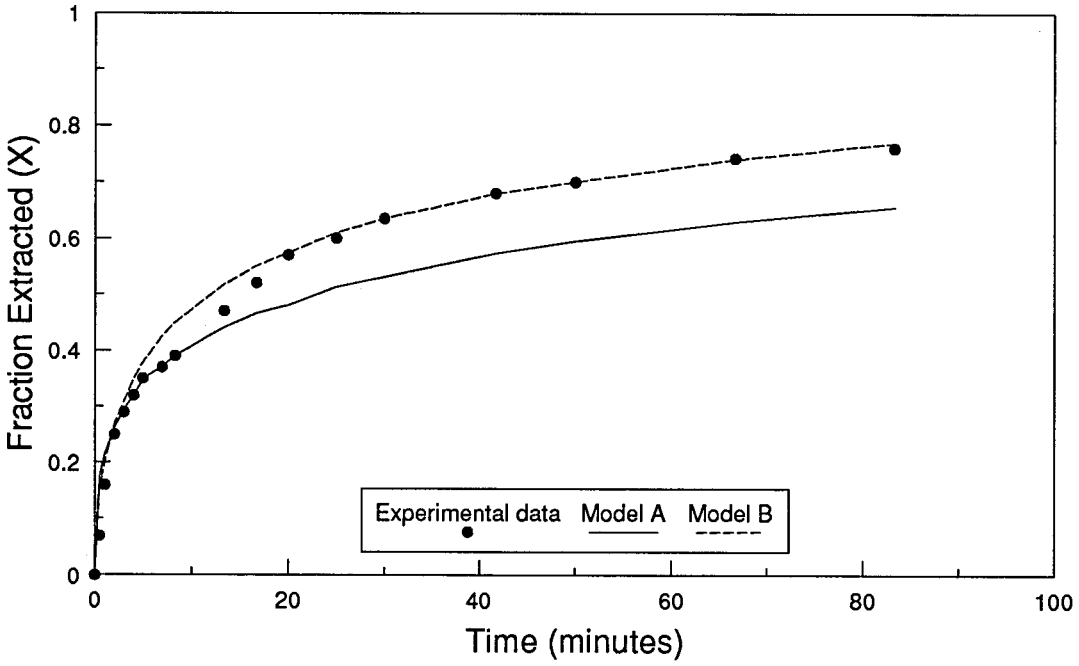

Figure 5.22 : Kinetic model fit of the experimental data for zinc loading on pre-treated (pH=3) OC 1026 at 60°C, for the first 5000 s. Model A=Fickian PDC with $\overline{D}$=9.0 x 10^{-12} m^2/s; Model B=FDC, k_m=2.7 x 10^{-7} m/s.

$$D_i = \frac{RT\lambda_i}{|z_i| F^2} \qquad \text{.....(5.1)}$$

where λ_i = ionic equivalent conductance.

z_i = valency of the i-ion.

F = Faraday's constant.

λ is a function of temperature:

$$\lambda_i(T) = \lambda_i(25°C)\frac{T}{334\eta_w} \qquad \text{.....(5.2)}$$

where : η_w = viscosity of water at T.

As λ_i and η depend on temperature, it was concluded [88,91] that D_i depends exponentially on T. The temperature dependence of the resin phase diffusivity should also follow the same trend [27,88,91]. Arrhenius plots were therefore made of the diffusion coefficients and mass transfer coefficients for the three resins (Figures 5.23 and 5.24). The activation energy for diffusion, E_a, was determined from the slope of the line obtained, and is listed in Table 5.11.

Table 5.11 : Effect of temperature on $\overline{D}$ and k_m values.

Temp.	OC 1026		Cyanex 302		Cyanex 272	
(°K)	$\overline{D}$	k_m	$\overline{D}$	k_m	$\overline{D}$	k_m
333	9.0×10^{-12}	2.7×10^{-7}	8.5×10^{-12}	2.1×10^{-7}	8.0×10^{-12}	1.8×10^{-7}
313	5.9×10^{-12}	1.9×10^{-7}	5.3×10^{-12}	1.5×10^{-7}	4.8×10^{-12}	1.3×10^{-7}
298	4.0×10^{-12}	1.2×10^{-7}	3.5×10^{-12}	1.1×10^{-7}	3.0×10^{-12}	9.5×10^{-8}
E_a (kcal.)	4.6	4.2	4.9	3.7	5.5	3.6

Following the work of Boyd and Saldano [27], the activation energy (E_a) can be used to give a hint as to the nature of the operating mechanism.

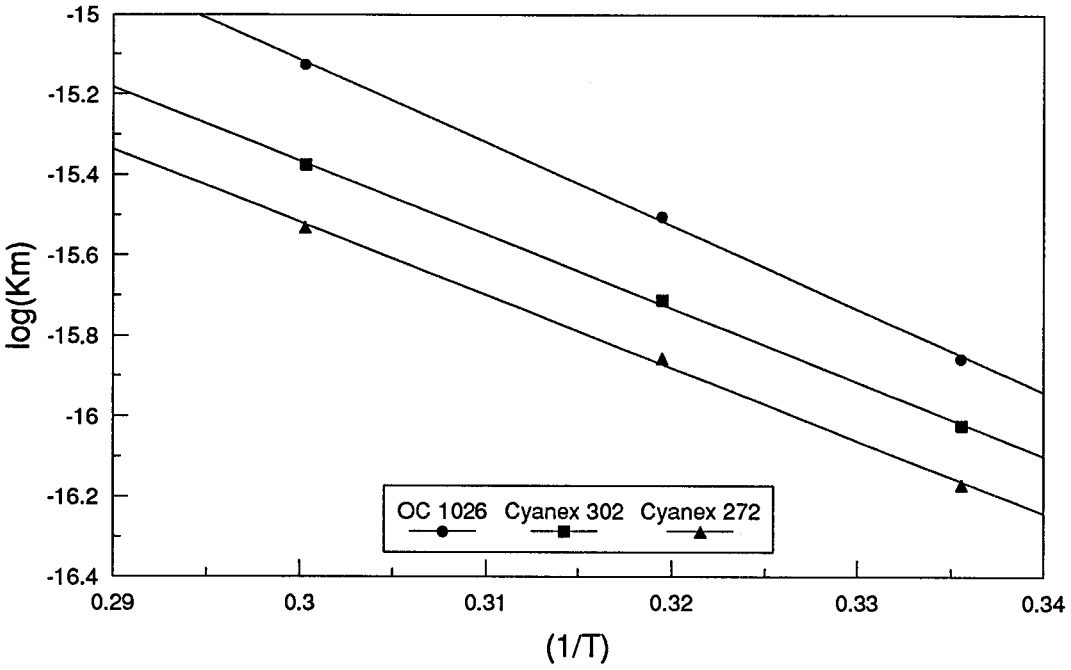

Figure 5.23 : Arrhenius plots for the aqueous phase mass transfer coefficients. Determination of the activation energy for diffusion in the aqueous phase : Slope=-E_a/R, for the resins under a given pre-treatment.

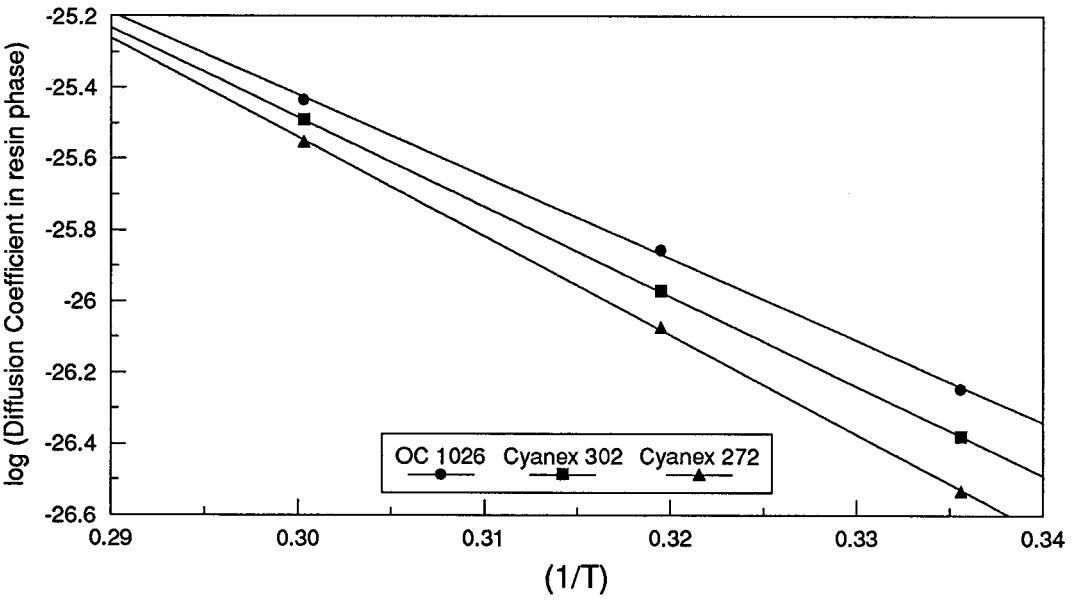

Figure 5.24 : Arrhenius plots for the resin phase diffusion coefficients. Determination of the activation energy for diffusion in resin phase : Slope=-E_a/R, for the resins under a given pre-treatment.

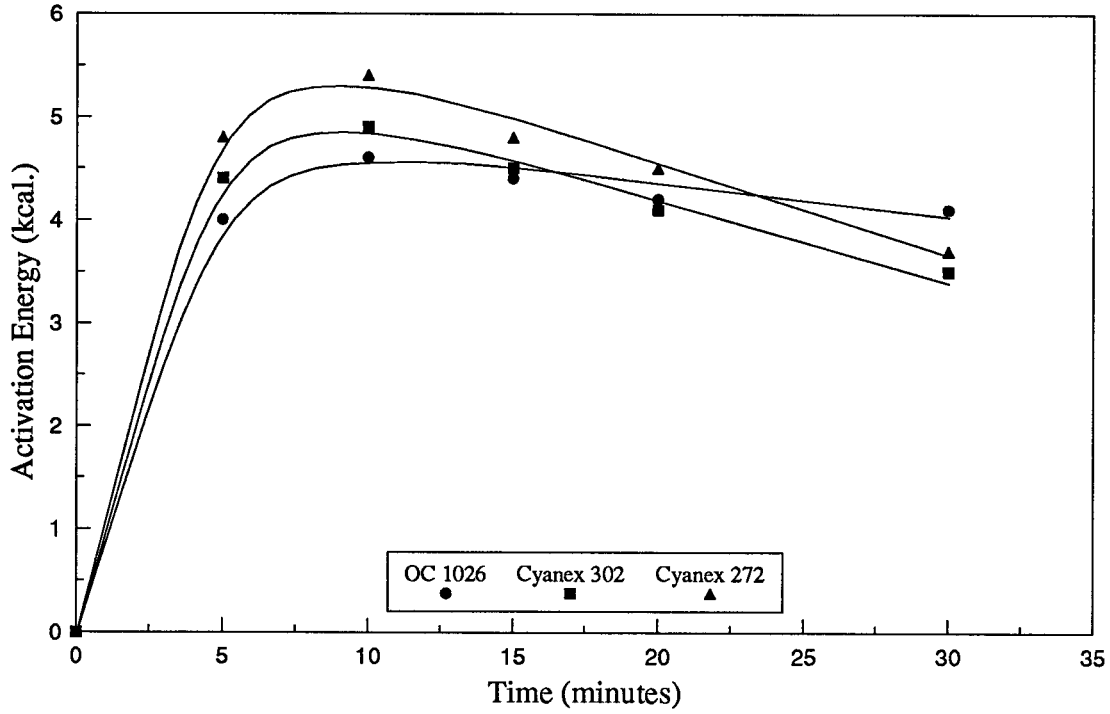

Figure 5.25 : Variation of the activation energy for diffusion with time.

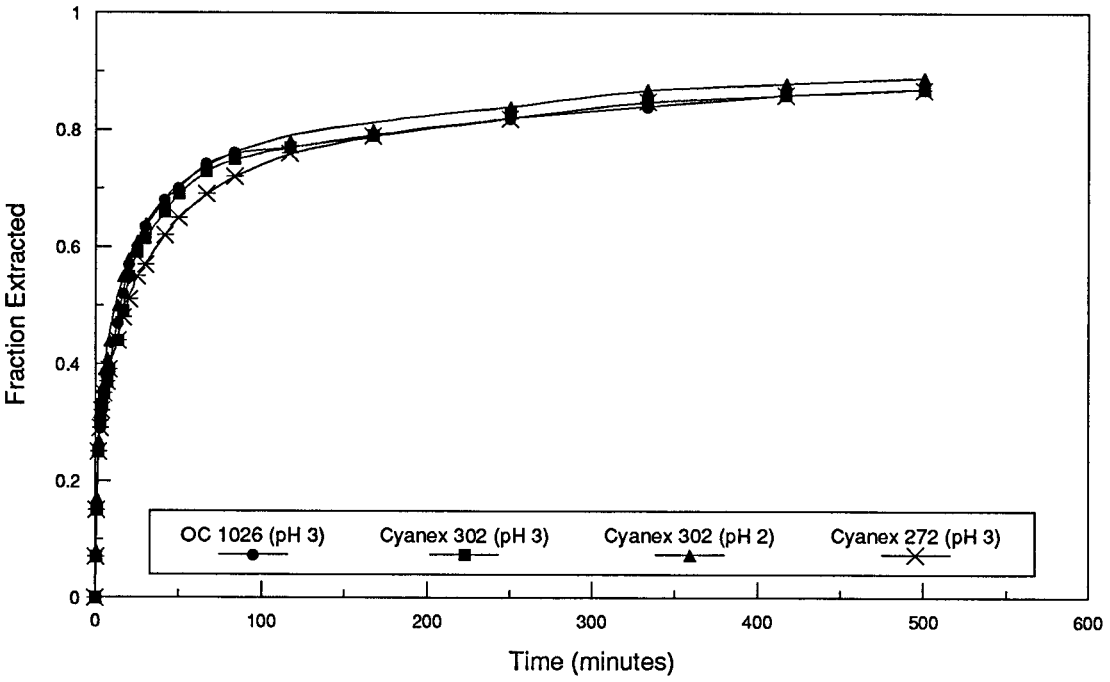

Figure 5.26 : Comparison of the kinetics of zinc uptake by the resins. Batch test study of loading on pre-treated resin; initial [Zn] = 12 mg/L, T=60°C. Pre-treatment : Equilibrating resin in zinc free INCO electrolyte at the particular pH.

Table 5.12 : Determination of the rate controlling mechanism from the Activation Energy.

Activation Energy	Rate Controlling Step
> 12 kcal.	Chemical reaction control
5-9 kcal.	Particle diffusion control
0-4 kcal.	Film diffusion control

From the values reported for the resins in Table 5.11, it seems that the rate controlling step is most certainly a combination of the particle and film diffusion control steps, with PDC prevailing in the initial part of the process (first 15 minutes), while FDC is the dominant mechanism after 20 minutes. This may also be concluded from Figure 5.25, which plots the activation energy for diffusion obtained from $\overline{D}$ and k_m values against time. It shows the activation energy values to be in the particle diffusion regime in the first 15 minutes, while they fall in the film diffusion regime after 20 minutes.

5.4 Kinetic Modelling of the Column Tests

The complete breakthrough curves for zinc loading on OC 1026, Cyanex 302 and Cyanex 272, are presented in Figures 5.27, 5.28 and 5.29 respectively. The value of θ_o (Section 4.5) was fixed at the point where breakthrough was first detected. This was at about 0.9 ppm for OC 1026, 0.95 ppm for Cyanex 302 and 0.6 ppm for Cyanex 272. Based on the method outlined in Section 4.5, a log-log plot is made of $ln(1/(1-c/c_o))$ vs. $(\theta - \theta_o)$, as shown in Figure 5.30 for the resins. This is compared to the analysis of the curve obtained by Strong and Henry [89], and the characteristic parameters were determined as follows:

Table 5.13 : Comparison of characteristic parameters of the breakthrough curve for the resins.

Resin	β	θ_o(hrs.)	θ_m(hrs.)
OC 1026	1.75	87.5	65
Cyanex 302	2.1	37.5	70
Cyanex 272	2.2	25.0	68
Strong et. al	0.9	24.0	40

The breakthrough curve obtained by Strong and Henry (Fig. 5.31) [89] was determined by carrying out the test under conditions in Table 5.14 :

Table 5.14 : Composition of Electrolyte and Operating Conditions of Strong and Henry [89] test (Resin : OC 1026).

Analysis (g/L)					Operating conditions			
Co	Ni	Zn	Fe	Cu	T(°C)	pH	Flow(BV/h)	Volume of resin
40	0.25	0.04	0.004	0.01	40	5.0	10	200 mL

Using these characteristic parameters, the kinetic parameters useful in the design of ion exchange columns, outlined in equations (4.24) - (4.32), were calculated for the respective resins (Table 5.15).

Table 5.15 : Kinetic parameters in the design of ion exchange columns (Resin pre-treated at pH=3, Operating temperature = 60°C, H=27 cm., U_s=1.835 x 10^{-4} m/s).

Resin	θ_s(hrs)	N_z	h_z (cm)	U_z (m/s)	N_{tof}	H_{tof} (m)	D_{bs}	H_{us}
OC 1026	152.5	2.34	11.50	4.91 x 10^{-7}	2.45	26.50	0.574	11.50
Cyanex 302	107.5	1.53	17.65	7.00 x 10^{-7}	2.45	23.78	0.35	17.55
Cyanex 272	93	1.36	19.85	8.10 x 10^{-7}	2.45	23.11	0.27	19.71

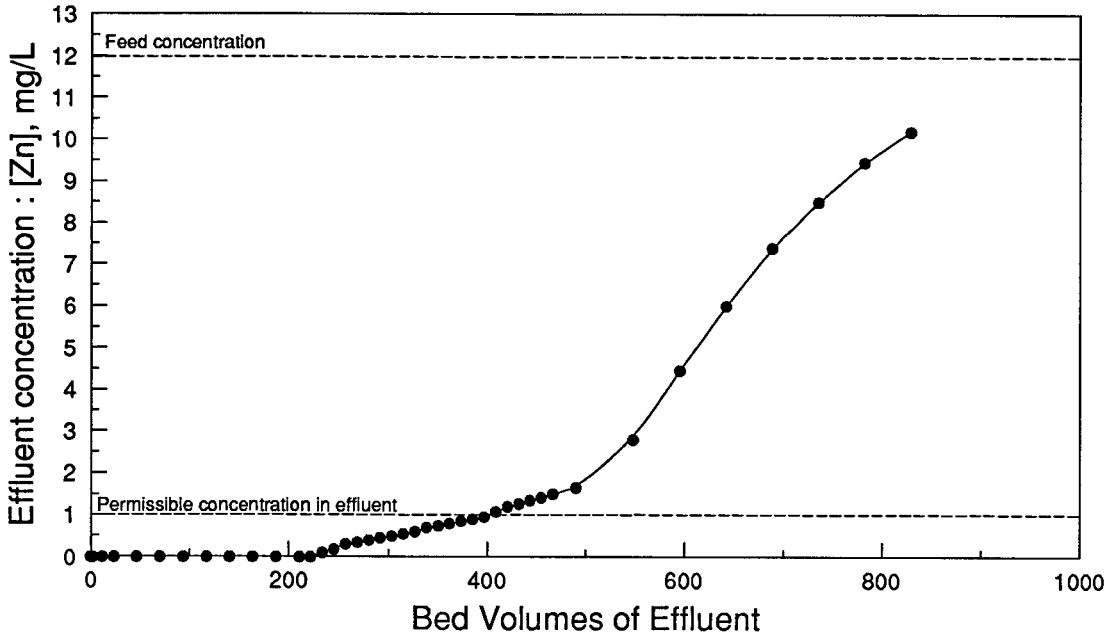

Figure 5.27 : Breakthrough curve for zinc loading on pre-treated OC 1026. INCO electrolyte feed (pH 3.75 at 60°C, [Zn]=12 mg/L), flow rate=4.67 BV/hr., OC 1026 bed = 25 ml, resin pre-treatment : INCO electrolyte fed at pH 3 until effluent pH 2.

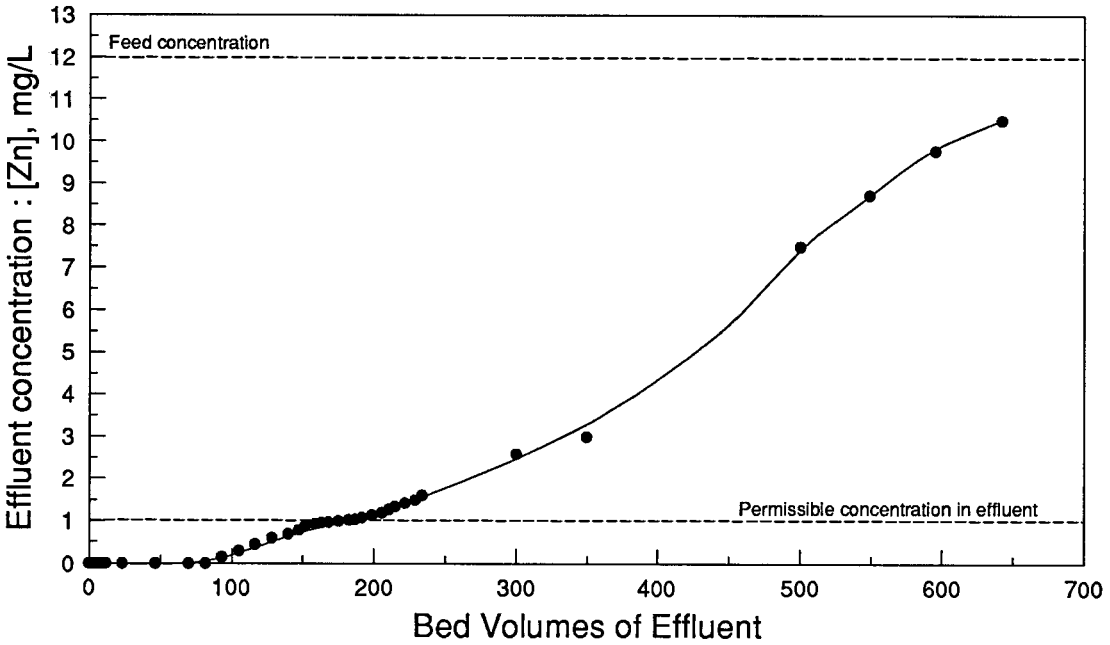

Figure 5.28 : Breakthrough curve for zinc loading on pre-treated Cyanex 302. INCO electrolyte feed (pH 3.75 at 60°C, [Zn]=12 mg/L), flow rate=4.67 BV/hr., Cyanex 302 bed = 25 ml, resin pre-treatment : INCO electrolyte fed at pH 3 until effluent pH 2.5 .

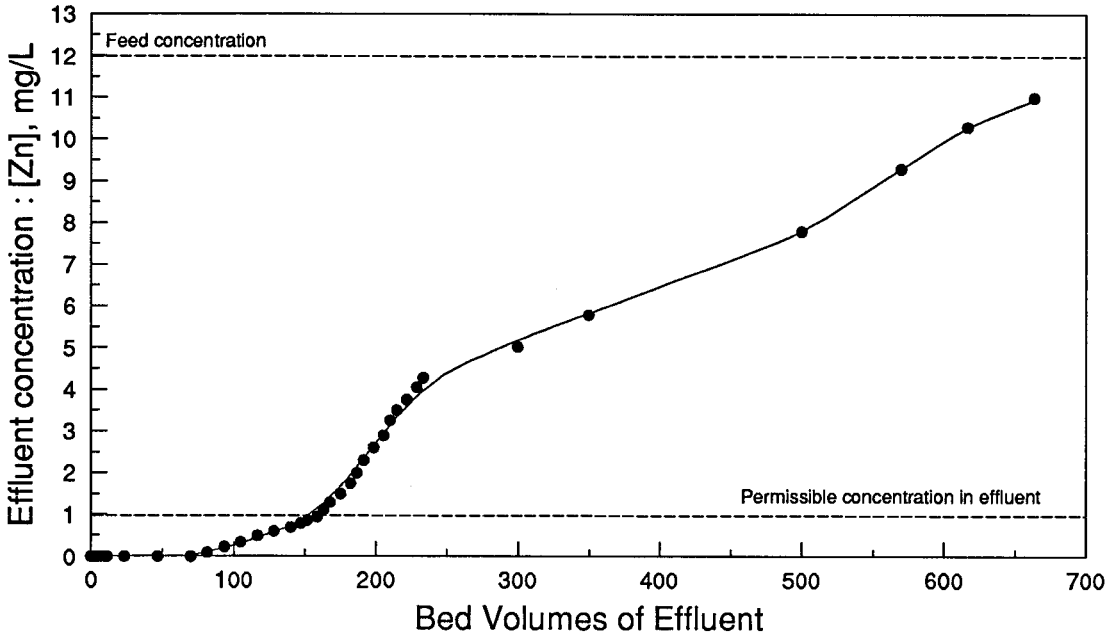

Figure 5.29 : Breakthrough curve for zinc loading on pre-treated Cyanex 272. INCO electrolyte feed (pH 3.75 at 60°C, [Zn]=12 mg/L), flow rate=4.67 BV/hr., Cyanex 272 bed = 25 ml, resin pre-treatment : INCO electrolyte fed at pH 3 until effluent pH 2.

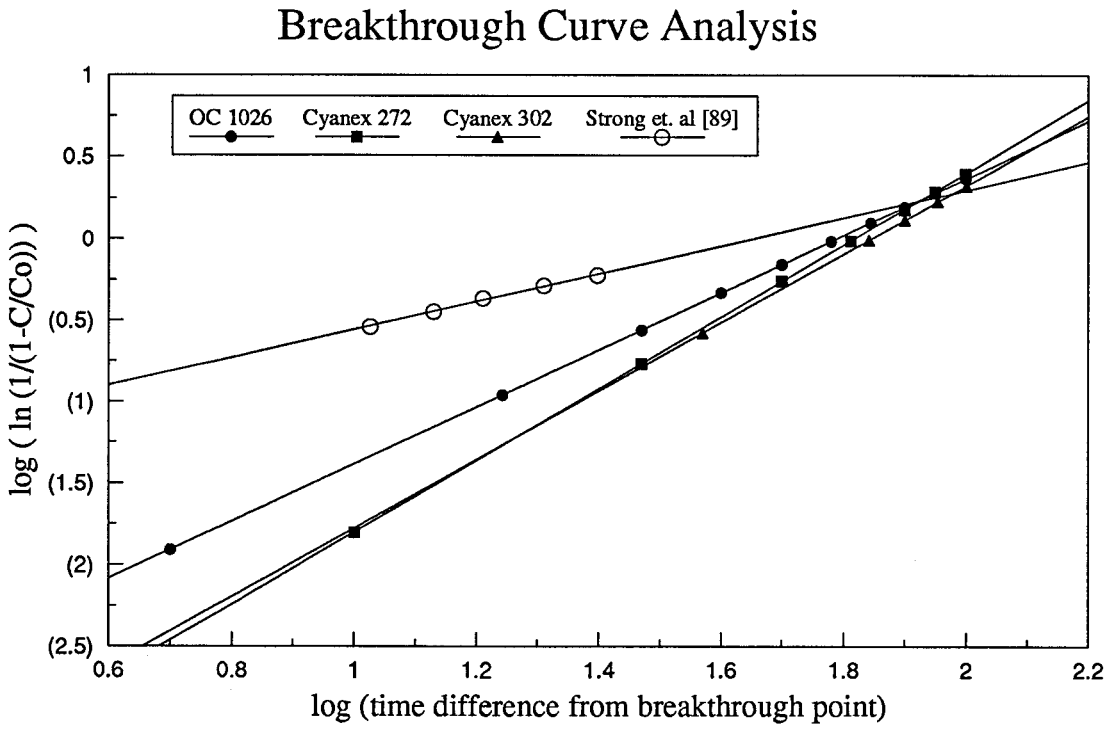

Figure 5.30 : Breakthrough curve analysis. Determination of characteristic parameters of the breakthrough curve. Slope=β; At c/c_o=0.632, mean breakthrough time= time difference.

The minimum superficial velocity of the solution in column processes, in order to be operating in the particle diffusion control regime, as determined from equation (4.36) is in the order of 10^{-7} m/s. As the operating superficial velocity of 1.835×10^{-4} m/s is well above this value, attempt has been made to operate in the particle diffusion control regime. Comparing the breakthrough curve obtained for a column with 25 ml OC 1026 (Fig. 5.27),(operated at 4.67 BV/hr., 60°C), with that obtained by Strong and Henry (Fig. 5.31) [89] using 200 ml of untreated OC 1026 (operated at 10 BV/hr., 40°C), it may be concluded that the curve does not flatten with increasing bed depth, and hence the exchange equilibrium is favorable [15].

Using equation (4.22) the overall mass transfer coefficients for the respective resins in column performance were determined. These values are compared with those determined from the Carberry's correlation (eq. 4.33) [86], and the method in Perry's Chemical Engineering Handbook [88] (equation 4.36), and also with those obtained from the analyses of the batch kinetic data, in Table 5.16.

Table 5.16 : Comparison of the mass transfer coefficients (m/s) obtained by various methods.

Resin	k_f (eq. 4.22)	k_L (eq. 4.33)	k_m (eq. 4.36)	k_m (batch tests)
OC 1026	1.60×10^{-8}	5.5×10^{-7}	6.2×10^{-7}	2.7×10^{-7}
Cyanex 302	1.74×10^{-8}	5.5×10^{-7}	6.2×10^{-7}	2.1×10^{-7}
Cyanex 272	1.87×10^{-8}	5.5×10^{-7}	6.2×10^{-7}	1.8×10^{-7}

From the values of β, it may be concluded that the rate controlling process for the three resins, is possibly in the intermediate region between particle and film diffusion control. This proposition is substantiated by the comparison of the values of mass transfer coefficients; which shows the k_f values to be an order of magnitude smaller than the k_L and k_m values. While, both k_L (from equation (4.33)) and k_m (from equation (4.36)) are obtained by determining the diffusion coefficient from a calculation of the liquid film thickness δ, the value of k_f (from equation (4.22)) is obtained from a more realistic estimate, based on the existing mass transfer conditions of the column. If the rate controlling mechanism were purely film diffusion control, the values of k_f would compare well

with those of k_L and k_m, while if the mechanism was purely particle diffusion control, the variation would be greater [83]. An intermediate regime as is probably the case, with β and mass transfer coefficients in column processes, fairly close to particle diffusion control, while the activation energy for diffusion in batch processes being at the intermediate particle-film diffusion regime, depending on the time range from start of the process, adequately defines the process kinetics.

5.5 Mechanism of the Exchange

Based on the discussion in the preceding sections, a mechanism for the ion exchange separation of zinc from cobalt electrolytes is proposed in this section.

For the case of the untreated resin, (Figure 5.32) the following processes occur during extraction:

- Co^{2+} and Zn^{2+} ions diffuse inside the resin.
- H^+ ions diffuse out as a result of the exchange initiating a large initial pH reduction.

At low metal loadings on OC 1026, the following reactions compete [68,70]:

$$Co^{2+} + 2(HL)_2 \longleftrightarrow CoL_2(HL)_2 + 2H^+ \quad .....(5.3)$$

$$Zn^{2+} + 2(HL)_2 \longleftrightarrow ZnL_2(HL)_2 + 2H^+ \quad .....(5.4)$$

In the case of the pre-treated resin (Figure 5.33), the following steps occur during the pre-treatment and loading cycles:

(a) During pre-treatment, cobalt loads on the resin to displace the H^+ ions from the resin:

$$Co^{2+} + 2(HL)_2 \longleftrightarrow CoL_2(HL)_2 + 2H^+ \quad .....(5.5)$$

Zinc ions present in the solution during column tests, are prevented from loading on to the resins for the following reasons:

-The electrolyte pH is initially reduced to about 3. At this pH Co^{2+} loads more efficiently on the resin than Zn^{2+} (Section 5.1.4).

-As the cobalt loading proceeds, the local pH of the electrolyte reduces to about 2, which further discourages any zinc loading.

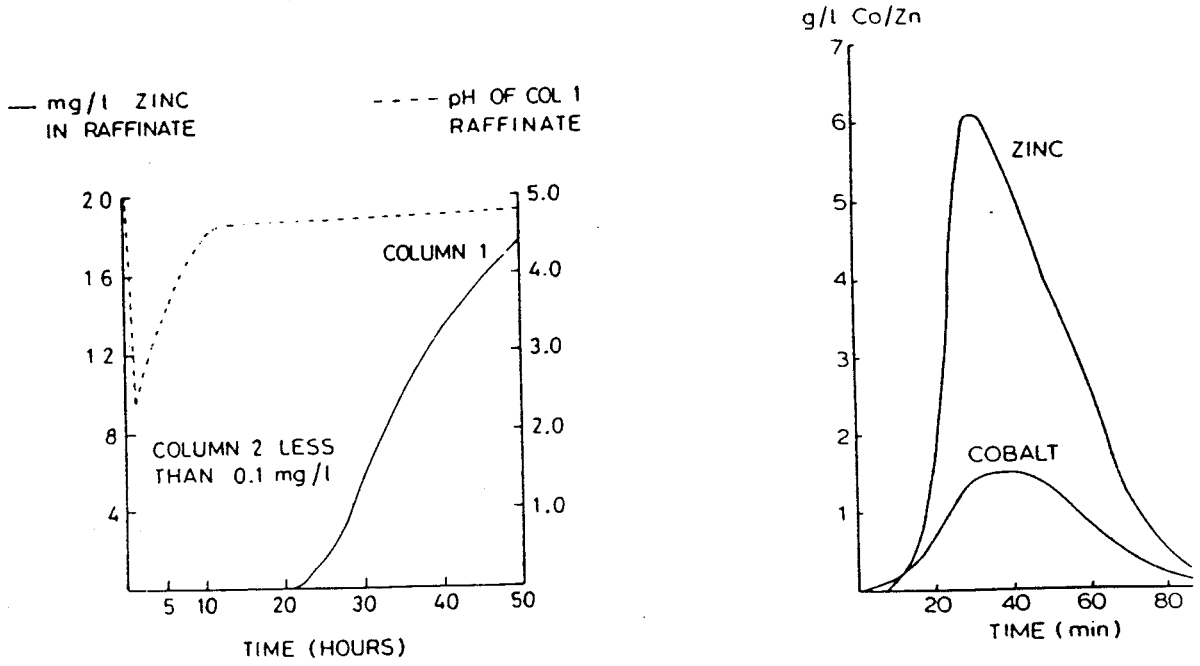

Figure 5.31 : Loading and elution curves for Levextrel zinc removal from cobalt electrolytes. Feed electrolyte : 43 mg/L Zn, pH=5.0; elution with 5% sulphuric acid.

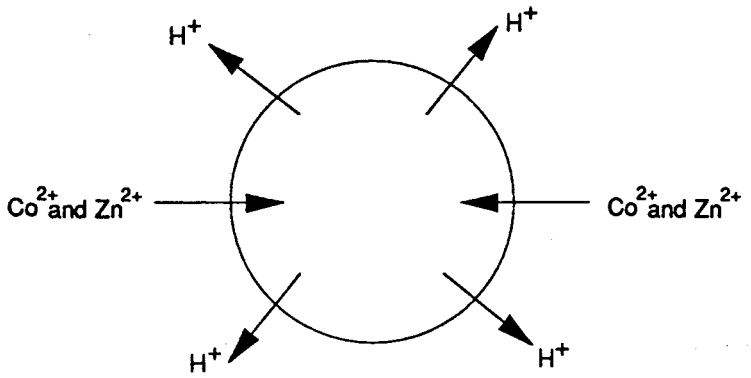

Figure 5.32 : Cobalt and zinc loading on untreated resin from the INCO electrolyte.

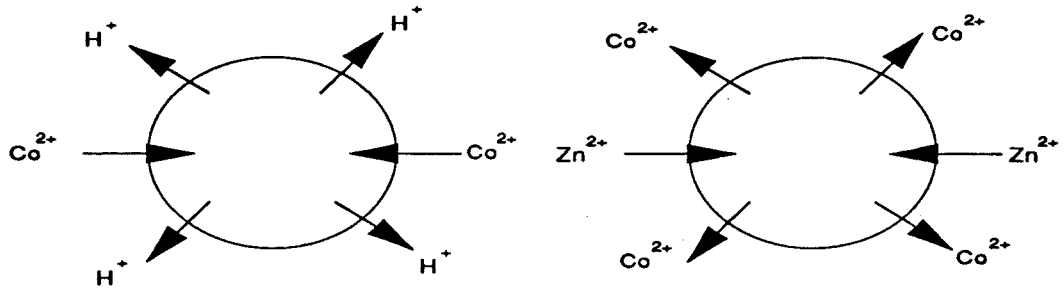

Figure 5.33 : Pre-treatment and loading processes during the ion exchange.

-As cobalt concentration in the electrolyte is 40 g/L, while the zinc concentration is only about 0.012 g/L, the Co^{2+} ions far outnumber the Zn^{2+} ions and thus reduce the competition from the zinc ions.

(b) During the loading cycle, Zn^{2+} ions displace the Co^{2+} ions on the resin by:

$$Zn^{2+} + CoL_2(HL)_2 \longleftrightarrow ZnL_2(HL)_2 + Co^{2+} \quad .....(5.6)$$

This reaction is favoured during the loading cycle, probably due to the following reasons:

-The equilibrium of reaction (5.6) is more favorable and the kinetics are faster than those of reaction (5.4) under the operating conditions of the electrolyte.

-The pH increase that occurs due to the pre-treatment (reaction (5.5)) attaining equilibrium aids reaction (5.6). This was seen in the column runs, where the effluent pH attained a value very close to the feed electrolyte pH within 50 effluent bed volumes, due to resin pre-treatment (Section 5.1.3).

-Reaction (5.6) results in no reduction in pH and hence, Zn^{2+} loading, which occurs at pH values higher than 3.5, is favoured and proceeds continuously.

-The diffusion of Zn^{2+} ions into a resin matrix of $CoL_2(HL)_2$ is faster than the diffusion of Zn^{2+} ions into the $(HL)_2$ matrix. This is supported by the observation that the $\overline{D}$ (diffusion coefficient inside the resin matrix) values are enhanced by nearly an order of magnitude due to pre-treatment (Table 5.10).

Even in the case of the untreated resin, reactions (5.3), (5.4) and (5.6) occur. The function of pre-treatment, however, is to break up these steps and allow cobalt loading (reaction (5.3)) during the pre-treatment cycle and directly begin the loading cycle with zinc displacement of the cobalt complex (reaction (5.6)). The methods used to enhance cobalt loading during pre-treatment and zinc extraction during the loading cycle have been discussed in the previous paragraph. In summary, the pre-treatment step enhances the overall zinc extraction and reduces the net cobalt retained on the resin, due to the following reasons:

(1)Zinc extraction during the loading cycle is greater because of reduced competition from cobalt

ions for the extractant.

(2)The kinetics of exchange of Zn^{2+} for Co^{2+} ions by reaction (5.6) is faster than that of Zn^{2+} for H^{+} ions by reaction (5.4). Pre-treatment initiates reaction (5.5) so that in the loading cycle, reaction (5.5) and (5.6) can occur concurrently to result in better extraction kinetics. The kinetics are improved, not directly due to the improved kinetics of reaction (5.6), but because the diffusion of Zn^{2+} ions into a resin matrix of $CoL_2(HL)_2$ is faster than the diffusion of Zn^{2+} ions into the $(HL)_2$ matrix. This is reflected in the enhanced $\overline{D}$ values due to pre-treatment, and the activation energy for diffusion lies in the region between particle and film diffusion control, rather than chemical reaction control.

(3)The pH reduction during the loading cycle for the pre-treated resin is smaller than in the case of the untreated resin. From the discussion in Sections 5.1.3 and 5.1.4, zinc extraction is favored at pH values between 3.4-3.7 while cobalt extraction is favored at lower values, and hence pre-treatment enhances loading.

6 CONCLUSIONS AND SUGGESTIONS FOR FURTHER WORK

6.1 Summary of the results

The series of column and batch tests on the resins at various operating conditions has yielded some extremely useful results on the performance of the resins, the mechanism of zinc loading and the suitability of their application to the INCO zinc removal process. The following is a critical appraisal of the results.

(1) The loading of zinc onto untreated OC 1026 is extremely efficient as breakthrough does not take place until after 200 BV. However, the cobalt retained on the resin may be in objectionably high amounts.

(2) The resins initially load cobalt at lower pH values, while the zinc loads by displacing cobalt as the pH of the column rises.

(3) Pre-treatment of OC 1026 with INCO electrolyte at pH of 3, improves zinc loading and reduces cobalt retention by maintaining the column at a pH between 3.5-3.7 for a major part of the process, where zinc loads by displacing the cobalt loaded on the resin in the first 50 BV.

(4) Reduction in temperature hastens zinc breakthrough for all of the resins, but reduces the cobalt retained on the resins. At 40°C, the zinc loading is satisfactory, while the cobalt retained is considerably reduced (when compared to the 60°C test).

(5) Increasing the flow rate of the electrolyte through the OC 1026 column, results in a slightly earlier zinc breakthrough, but there is an associated reduction in cobalt retained on the resin, thus improving the selectivity. This reduction in the cobalt retained can be attributed to a smaller pH reduction for the column operating at the faster flow rate.

(6) Increasing the pH of the feed electrolyte enhances zinc loading on OC 1026, resulting in a breakthrough point similar to that of a column pre-treated at pH 3 with INCO electrolyte. However, the selectivity of the former is greater as the cobalt retained is reduced.

(7) The performance of Cyanex 302 and Cyanex 272 is inferior to that of OC 1026 in terms of zinc loading, under the operating conditions of the INCO plant. Yet Cyanex 302 presents the

advantage of lower cobalt retention with a satisfactory zinc loading (breakthrough after 175 BV). However, the resin is poisoned by copper and iron from the electrolyte which hastens zinc breakthrough in further loading cycles. Hence if copper removal was accomplished (by XFS-4195 used for nickel separation) before the use of Cyanex 302 for zinc removal, then this resin could be considered as an alternative because of lower amounts of cobalt retained.

(8) A variety of pre-treatments were tried out in batch tests. For OC 1026 pre-treatment with INCO electrolyte at pH values of 2, 3 and 3.5 enhance kinetics to an equal level when compared to the untreated resin. For Cyanex 302 however, pre-treatment at pH of 2, enhances the kinetics a little more than other pre-treatments. In fact it was found that the kinetics of zinc uptake by Cyanex 302 pre-treated with INCO electrolyte at pH 2, were slightly better than that of OC 1026 pre-treated at pH of 2 or 3. However in column performance, the Cyanex 302 column never reached a pH below 2.7, and hence probably OC 1026 performs better.

(9) Increasing the initial zinc content of the INCO electrolyte makes almost no difference to the zinc loading on OC 1026 in the first 15 minutes, but enhances the kinetics considerably at later time intervals.

(10)Decrease in temperature slackens the kinetics of zinc uptake for all the resins.

(11)The kinetic data could not be fitted to any single model. The data however, obey the Fickian Particle Diffusion Control (PDC) Model for the first 15 minutes, after which they obey the Film Diffusion Control (FDC) Model until 150 minutes. After this, the data lie between models of Particle Diffusion Control (with a $\overline{D}$ value of an order of magnitude higher than the initial PDC $\overline{D}$) and the Unreacted Core Model (where diffusion through the reacted resin layer is rate controlling). The values of $\overline{D}$ and k_m were determined, based on these models for the exchange under different conditions.

(12)Pre-treatment enhances the value of $\overline{D}$ by about an order of magnitude, in the initial PDC region, and this enhances k_m to some extent in the FDC region.

(13)The kinetic performance of the three resins is comparable and the $\overline{D}$ and k_m values are within the same order of magnitude.

(14)The Arrhenius plot ($\log\overline{D}$ vs. T^{-1} and $\log k_m$ vs. T^{-1}) gives values of the activation energy for diffusion to be in the range between particle and film diffusion control regimes, for all the resins.

(15)The column breakthrough curves were used to determine the characteristic parameters β (mean slope of the curve), θ_o (breakthrough time) and θ_m (mean time of the breakthrough function). These were used to determine a range of kinetic parameters useful in the design of ion exchange equipment for the three resins, such as saturation time, height of the ion exchange zone, velocity of the ion exchange zone, degree of bed saturation at breakthrough and height of unused bed at breakthrough.

(16)The characteristic parameters were used to determine the value of the mass transfer coefficient in the column (k_f), which was compared to the values obtained by other methods suggested in the literature. Based on this comparison and the β values, it was concluded that the process kinetics in the column were controlled by a mixture of particle and film diffusion mechanisms for the three resins.

6.2 Conclusions

The major conclusions of this work may be summarized as follows:

(1)The performance of OC 1026 was superior to that of Cyanex 272 and Cyanex 302, under the operating conditions of the INCO zinc removal process plant at Port Colborne.

(2)Column operating conditions such as resin pre-treatment, electrolyte pre-treatment, temperature and flow rate have a significant influence on the zinc loading and the selectivity characteristics of the resins. For OC 1026, it was found that a resin pre-treatment at a pH of 3, or an electrolyte pH increase to 5, along with operation at a temperature of 40°C and a flow rate of 10 BV/hr., provided the maximum improvement to zinc loading and selectivity.

(3)The kinetics of zinc loading on pre-treated OC 1026, Cyanex 302 and Cyanex 272 are comparable at similar operating conditions.

(4)In batch tests, the loading process operated in the area between particle and film diffusion

control, with PDC being rate controlling in the first 15 minutes, while FDC becomes important later. The column process is also a mixed particle-film diffusion controlled process, with the characteristic parameters being a little closer to particle diffusion control.

6.3 Suggestions for further work

This work leaves a number of unexplained results and further work in the following directions could shed light on the process mechanism and help in process optimization:

(1)Studies need to be made on various other possible pre-treatments for the resins, to improve their zinc loading and selectivity characteristics. For Cyanex 302 studies need to be made for specific pre-treatments or process changes in order to avoid the resin poisoning by copper.

(2)The results of the column and batch studies from this work, need to be substantiated by SEM-WDX studies (X-ray microprobe analyses) of the resin cross-section, to gain an insight into the process mechanism, and understand why cobalt loads on the resin initially, while zinc loads by displacing the cobalt from the complex. This analysis may also aid in understanding how resin pre-treatment exactly influences the process, and why it enhances the resin phase diffusivity by an order of magnitude. Similar studies can be done in column processes, on resin samples taken from the top, middle and bottom portion of the bed, to explain the effect that local pH has on zinc loading and selectivity.

(3)The accuracy of batch studies should be greatly enhanced by using zinc selective electrodes and monitoring the E_h values, rather than the technique of determining zinc concentration at various time intervals, as done in this project. Work is thus needed in this direction, to accurately determine the values of diffusion and mass transfer coefficients.

REFERENCES

1. *Exodus* 15: 23-25.

2. Aristotle, *Works*, (Clarendon Press, London, 1927), Vol. 7, p.933b.

3. Thompson, H.S.; *J. Roy. Agr. Soc. Engl.*, Vol. 11 (1850), p.68.

4. Way, J.T.; *J. Roy. Agr. Soc. Engl.*, Vol. 11 (1850), p.313; Vol. 13 (1852), p.123.

5. Harm, F. and A. Rumpler; *5th Intern. Congr. Pure Appl. Chem.* (1903), p.59.

6. Adams, B.A. and E.L.Holmes; *J. Soc. Chem. Ind. (London)*, Vol.54, (1935), p.16.

7. Tompkins, E.R.; J.X. Khym, and W.E. Cohn; *J. Am. Chem. Soc.*, Vol. 69 (1947), p2769.

8. Ketelle, B.H. and G.E. Boyd, *J. Am. Chem. Soc.*, Vol. 69 (1947), p.2800.

9. Spedding, F.H.; E.I. Fulmer, T.A. Butler, E.M. Gladrow, M. Gobush, P.E. Porter, J.E. Powell, and J.M. Wright, *J. Am. Chem. Soc.*, Vol. 69 (1947), p.2812.

10. D'Alelio, G.F. (General Electric Co.); US Patent 2,366,007 (1944).

11. Wheaton, R.M. and W.C. Bauman; *I&EC*, Vol. 43 (1951), p1088.

12. Breck, D.W.; "Zeolite Molecular Sieves : Structure, Chemistry, and Use" (Wiley, New York, 1974), p.95.

13. Christensen, J.J. and R.M. Izzat, "Handbook of Metal-Ligand Heats and Related Thermodynamic Quantities", 3rd. Ed. (New York, Wiley & Sons 1980).

14. Warshawsky, A.; Modern Research in Ion Exchange, in "Ion Exchange Science and Technology", Edited by Rodrigues, A.; NATO ASI Series, Martinus Nijhoff Publ. 1986.

15. Helfferich, F.;"Ion Exchange", McGraw-Hill, N.Y. (1962).

16. Vermeulen, T.; G. Klein and N.K. Hiester; "Adsorption and Ion Exchange", in Perry's Chem. Eng. Handbook, 5-th Edition, Sec. 16, Mc-Graw Hill Book Co., NY (1973).

17. Paterson, R.; "An introduction to ion exchange", Heyden & Sons Ltd., London (1970).

18. Marinsky, J.A.; Ed. of "Ion Exchange, Vol. I", Marcel Dekker Inc., NY (1966).

19. Hudson, M.J.; Co-ordination chemistry of selective ion exchange resins, in "Ion Exchange : Science and Technology", Edited by : Aliro Rodrigues, NATO ASI Series 1985.

20. Liberti Lorenzo; "Planning and interpreting kinetic investigations", in "Ion Exchange : Science

and Technology", Edited by : Aliro Rodrigues, NATO ASI Series 1985.

21.Boyd, G.E.; A.W. Adamson and L.S. Myers Jr.; *J. Am. Chem. Soc.*, Vol. 69 (1947), p.2836.

22.Wen, C.Y.; *Ind. Eng. Chem.*, Vol. 60 (1968), p.34.

23.Kunii, P. and O. Levenspeil; "Fluidization Enginnering", Wiley, New York, NY, 1969.

24.Yagi, S. and P. Kunii; *Chem. Eng. (Tokyo)*, 19 (1955), 500.

25.Wheeler, A.; "Advances in Catalysis", 3, 249, (1951).

26.Mackie, J.S. and P.Meares, *Proc. Roy. Soc. (London)*, A232 (1955) 498.

27.Boyd, G.E. and B.A. Saldano, *J. Am. Chem. Soc.*, 75 (1953) 6091-9.

28.Sillen, L.G. and A.E. Martell; "Stability of metal-ion complexes", The Chemical Society, Burlington House, London, Spec. Publ. no. 17 and no.25.

29.Gluckauf, E. and J.I. Coates; *J. Chem. Soc.*, (1947) 1315-21.

30.Vermeulen, T.; *Ind. Eng. Chem.*, 45, (1953) 1664-70.

31.Crank, J.; "The Mathematics of Diffusion", (Clarendon Press, Oxford, 1975).

32.Thomas, H.C.; Heterogenous Ion Exchange in a Flowing System, *J. Am. Chem. Soc.*, 66 (1944) 1664.

33.Thomas, H.C.; The Kinetics of Fixed-Bed Ion Exchange, in "ION EXCHANGE", ed. F.C. Nachod, p.29 (Academic Press, NY 1964).

34.Gilliland, E.R. and R.F. Baddour; The Rate of Ion Exchange, *Ind. Eng. Chem.* 45 (1953) 330.

35.Helfferich, F.; *J. Phys. Chem.*, 69 (1965) 1178-87.

36.Dana, P.R. and T.D. Wheelock; *Ind. Eng. Chem. Fundam.*, 13 (1974) 20-6.

37.Holl, W. and H. Sontheimer; *Chem. Eng. Sci.*, 32, (1977) 755-62.

38.Helfferich, F.; Ion exchange kinetics - evolution of a theory, in "Mass Transfer and Kinetics of Ion Exchange", NATO ASI Series, Martinus Nijhoff Pub. (1982).

39.Helfferich, F. and M.S. Plesset; *J. Chem. Phys.* 28 (1958) 418.

40.Barrer, R.M.; R.F.Bartholomew and L.C.V. Rees; *J. Phys. Chem. Solids*, 24 (1963) 309.

41.Brooke, N.M., and L.C.V. Rees; *Trans. Faraday Soc.* 12 (1968) 3383.

42.Schlogl. R.; *Stofftransport durch Membranen* (Steinkopff, Dermstadt, 1964).

43.Baypai, R.K.; A.K. Gupta and M. Gopala Rao; *AIChE J.* 20 (1974) 989.

44.Helfferich, F.; *J. Phys. Chem.* 69 (1965) 1178.

45.Shewnon, P.G.; "Diffusion in Solids" (McGraw Hill, New York, 1963).

46.De Groot, S.R. and P. Mazur; Thermodynamics of Irreversible Processes, (North Holland, Amaterdam, 1962).

47.Lightfoot, E.N. and E.M. Scattergood; *AIChE J.*, 11 (1965) 175.

48.Graham, E.E., and J.S. Dranoff; Applications of the Stafan-Maxwell equations to diffusion in ion exchangers; *IEC Fundamentals* (1982).

49.Kressman, T.R.E., and J.A. Kitchener; *Discussions Faraday Soc.*, 7 (1949), 90.

50.Tetenbaum, M., and H.P. Gregor; *J. Phys. Chem.*, 58 (1954), 1156-63.

51.Hale, D.K., and D. Reichenberg; *Disc. Faraday Soc.*, 7 (1949) 79-85.

52.Reichenberg, D.; *J. Am. Chem. Soc.*, 75 (1953), 589-97.

53.Semenovskaya, T.D.; V.T. Avgul, A.Ya. Pronin and K.V. Chmutav, *Zhur. Fiz. Khim.*, 53 (1979) 1850-2.

54.Smith, M.; "Chemical Engineering Kinetics", 2-nd Edition, Mc-Graw Hill, New York, N.Y. (1970).

55.Wilke, J. and O.A. Hougen; *Trans. Am. Inst. Chem. Eng.*, 41 (1945) 445.

56.Bahu, R.E.; M.J. Craske and M. Streat, *Proc. Int. Conf. on Theory and Practice of Ion Exchange*, SCI Cambridge, (1976).

57.Boghetich, G., and D. Petruzelli; *ICP, XI*, 10 (1981).

58.Hoell, W., and G. Geiselhart; *Desalination*, 25 (1978) 217.

59.Kauczor, H.W., and A. Mayer; *Hydrometallurgy*, 3 (1978), 65.

60.Warshawsky, A.; Extraction with solvent impreganated resins, in "Ion Exchange and Solvent Extraction", Eds.: Marinsky J.A., and Y. Marcus, Vol. 8, Marcel Dekker, 1981.

61.Agnew, R.; P. Garritsen and D. MacVicar; Production of electrolytic cobalt rounds at INCO's cobalt refinery in Port Colborne, Ontario, Canada, in "Extractive Metallurgy of Nickel and Cobalt", Edited by G.P. Tyroler and C.A. Landolt, The Metallurgical Society Inc. Publication, 1988.

62.Agnew, R.G.; L.D. Kowal and D. Young; Process optimisation at INCO's cobalt refinery, in "Electrometallurgical Plant Practice", Pergamon Press 1990.

63.Ettel, V.A.; "Process for recovering cobalt electrolytically", US Patent no. 4274930. 1980.

64.Renzoni, L.S. and Barker, W.W.; Production of electrolytic cobalt rounds at INCO's Cobalt Refinery in Port Colborne, in "Extractive Metallurgy of Copper, Nickel and Cobalt", Queneau, P. (Ed.), AIME p.537 (1961).

65.Kerfoot, D.G.E., and D.R. Wier; The hydro and electrometallurgy of nickel and cobalt, in "Extractive Metallurgy of Nickel and Cobalt", Edited by G.P. Tyroler and C.A. Landolt, The Metallurgical Society Inc. Publication, 1988.

66."Developments in Solvent Extraction", S. Algret ed., Ellis Horwood Ltd., Chichester, England (1988).

67.Ajawin, L.A.; E.S. Perez de Ortiz and H. Sawistowski, *Chem. Eng. Res.* Des., 61 (1983) 62.

68.Cianetti, C., and P.R. Danesi; *Solv. Ext. Ion Ex.*, 1, (1983) 9.

69.Sastre, A.M., and M. Muhammed; *Hydrometallurgy*, 12, (1983), 177.

70.Komasawa, I.; T. Otake and Y. Hagaki, *J. Inorg. Nucl. Chem.*, 43(12), (1981) 3351.

71.Ritcey, G.; A. Ashbrook and L. Lucas; Development of solvent extraction process for the separation of cobalt from nickel, *CIM Bull.*, 68(753)111, 1975.

72.Nogueira, E.D.; J.M. Regife and P.M. Blythe; Zincex - the development of a secondary zinc process, *Chem. Ind.*,(2) (1980), p.63-67.

73.Ajawin. L.A.; E.S. Perez de Ortiz and H. Sawistowski, Kinetics of extraction of zinc by di (2-ethylhexyl) phosphoric acid in n-heptane, *Proceedings of ISEC'80*, Paper 80-112, (1980).

74.Rice, N.M., and M.R. Smith; *J. Appl. Chem. Biotechnol.*, 25 (1975) p.379-402.

75.Flett, D.S.; *J. Chem. Biotechnol.*, 29 (1979) p.258-272.

76.Rickleton, W.A.; D.S. Flett, and D.W. West, *Hydrometallurgy*, 9, (1982) 115.

77.Sastre, A.M.; N. Miralles and E. Figuerola, *Solvent Extr. Ion Exch.*, 8 (1990) p.597-614.

78.Sole, K.C. and J.B. Hiskey; *Hydrometallurgy*, 30 (1992) p.345-365.

79.Caravaca, C., and F.J. Alguocil; *Hydrometallurgy*, 27 (1991), p.327-338.

80.Levenspeil, O.; "Chemical Reaction Engineering", John Wiley & Sons, Inc., NY (1972).

81.Ishida, M., and C.Y. Wen; *Chem. Eng. Sci.*, 26, 1031-41 (1971).

82.Smith, J.M.; "Chemical Engineering Kinetics", Mc-Graw Hill Book Company, NY (1970).

83.Doulah, M.S.; and S.A. Jafer; A method for the prediction of mass transfer parameters in an ion exchange process, in "Ion Exchange for Industry", editor: Streat, M., Ellis Horwood Pub., (1988).

84.Micheals, A.S.; *Ind. Eng. Chem.*, 44(8), 1922-30 (1952).

85.Rodrigues, A.; and C. Costa; Fixed bed processes : a strategy for modelling, in "Ion Exchange : Science and Technology", Edited by : Aliro E. Rodrigues, NATO ASI Series, Martinos Nijhoff Pub. (1986).

86.Carberry, J.J.; *A.I.Ch.E.J.*, 6 (3), 460-63 (1960).

87.Glueckauf, E.; in "Ion exchange and its applications", edited by the Society of Chemical Industry, p. 34 (1955).

88.Perry, R.; and D. Green; "Chemical Engineering Handbook", 50-th edition, Mc-Graw Hill Pub. (1991).

89.Strong, B.; and R.P. Henry; *Hydrometallurgy*, 1, 311-317 (1976).

90.Cussler, E.L.; "Diffusion, Mass transfer in fluid systems", Cambridge Univ. Press, Cambridge, 1984.

91.Babjak, G.; "A study of ion exchange kinetics involving chelating resin" Ph.D. thesis, Univ. of Waterloo (1982).

92.Kauczor, H.W.; and Meyer, A.; *Hydrometallurgy* 3 (1978) 65-73.

93.Simon, G.P.; "Ion Exchange Training Manual", Van Nostrand Reinhold, New York (1991).

94.Lewatit OC 1026 brochure, Bayer AG. Leverkusen; Order no. OC/I 20208.

Appendix A : Raw Experimental Data from Column Tests

Table A-1 : Zinc loading on untreated OC 1026

Resin : 25 ml OC 1026
Pre-treatment : None
Operating Temperature : 40°C
Feed Flow rate : 5 BV/hr. and 10 BV/hr.
Feed Electrolyte Composition : Co=40 g/L, Ni=35 g/L, Zn=0.012 g/L, Fe=0.001 g/L, Cu=0.01 g/L.
Feed Electrolyte pH : 3.7

Flow rate :	5 BV/hr.		10 BV/hr.	
Effluent Volume(BV)	[Zn] (mg/L)	pH	[Zn] (mg/L)	pH
0	0.00	3.70	0.00	3.70
2	0.00	2.10	0.00	2.25
5	0.00	2.20	0.00	2.40
10	0.00	2.25	0.00	2.45
15	0.00	2.30	0.00	2.50
20	0.00	2.35	0.00	2.55
25	0.00	2.40	0.00	2.60
30	0.00	2.45	0.00	2.65
40	0.00	2.52	0.00	2.72
50	0.00	2.55	0.00	2.75
60	0.00	2.57	0.00	2.77
70	0.00	2.60	0.00	2.80
80	0.00	2.62	0.05	2.81
90	0.10	2.63	0.12	2.82
100	0.15	2.64	0.18	2.83
120	0.25	2.65	0.27	2.84
140	0.40	2.66	0.45	2.85
150	0.45	2.67	0.50	2.86
160	0.50	2.68	0.60	2.87
170	0.60	2.69	0.70	2.88
180	0.80	2.70	0.90	2.89
190	0.85	2.71	1.10	2.90
200	0.92	2.72	1.35	2.91
210	1.10	2.73	1.65	2.92
220	1.50	2.74	1.90	2.93
230	1.75	2.75	2.25	2.93
240	1.90	2.76	2.50	2.94
250	2.00	2.77	2.70	2.94

Table A-2 : Effect of temperature on zinc loading of untreated OC 1026

Resin : 25 ml OC 1026
Pre-treatment : None
Operating Temperature : 60°C
Feed Flow rate : 4.67 BV/hr.
Feed Electrolyte Composition : Co=40 g/L, Ni=35 g/L, Zn=0.012 g/L, Fe=0.001 g/L, Cu=0.01 g/L.
Feed Electrolyte pH : 3.75

Effluent Volume(BV)	[Zn] (mg/L)	pH
0.000	0.00	3.75
1.000	0.00	1.90
2.335	0.00	2.00
4.670	0.00	2.10
11.675	0.00	2.20
23.350	0.00	2.35
46.700	0.00	2.50
70.050	0.00	2.60
93.400	0.00	2.63
116.750	0.00	2.64
140.100	0.10	2.65
163.450	0.25	2.67
233.500	0.50	2.75
280.200	0.76	2.80
326.900	1.06	2.85
373.600	1.40	2.88
420.300	1.90	2.91
467.000	2.50	2.93
500.000	2.80	2.94

Table A-3 : Zinc loading on pre-treated OC 1026

Resin : 25 ml OC 1026.
Pre-treatment : INCO electrolyte fed at pH=3 until effluent
Operating Temperature : pH=2.
Feed Flow rate : 60°C.
Feed Electrolyte Composition : 4.67 BV/hr.
Co=40 g/L, Ni=35 g/L, Zn=0.012 g/L,
Feed Electrolyte pH : Fe=0.001 g/L, Cu=0.01 g/L.
3.75.

Effluent Volume(BV)	[Zn] (mg/L)	pH
0.000	0.00	3.70
2.335	0.00	2.35
11.675	0.00	2.95
23.350	0.00	3.20
46.670	0.00	3.50
70.050	0.00	3.52
93.400	0.00	3.54
116.750	0.00	3.55
140.100	0.00	3.55
163.450	0.00	3.55
186.800	0.00	3.55
210.150	0.00	3.55
221.825	0.00	3.55
233.500	0.10	3.55
245.175	0.18	3.55
256.850	0.30	3.56
268.525	0.35	3.56
280.200	0.40	3.56
291.875	0.45	3.56
303.550	0.50	3.56
315.225	0.55	3.56
326.900	0.60	3.57
338.575	0.70	3.57
350.250	0.75	3.57
361.925	0.80	3.57
373.600	0.85	3.57
385.275	0.90	3.57
396.950	0.95	3.58
408.625	1.07	3.58
420.300	1.20	3.58
431.975	1.27	3.58
443.650	1.35	3.59
455.325	1.42	3.59
467.000	1.50	3.59

Table A-4 : Effect of temperature on zinc loading on pre-treated OC 1026

Resin : 25 ml OC 1026.
Pre-treatment : INCO electrolyte fed at pH=3 until effluent
Operating Temperature : pH=2.
Feed Flow rate : 40°C, 25°C.
Feed Electrolyte Composition : 4.67 BV/hr.
Co=40 g/L, Ni=35 g/L, Zn=0.012 g/L,
Feed Electrolyte pH : Fe=0.001 g/L, Cu=0.01 g/L.
3.7.

Temperature	40°C		25°C	
Effluent Volume(BV)	[Zn] (mg/L)	pH	[Zn] (mg/L)	pH
0.000	0.00	3.70	0.00	3.34
2.335	0.00	2.40	0.00	2.25
4.670	0.00	2.80	0.00	2.80
23.350	0.00	3.30	0.00	3.20
46.700	0.00	3.50	0.00	3.21
70.050	0.00	3.53	0.25	3.22
93.400	0.00	3.55	0.60	3.23
116.750	0.20	3.55	0.88	3.24
140.100	0.40	3.55	1.07	3.24
163.450	0.55	3.55	1.46	3.25
186.800	0.70	3.55	1.76	3.25
210.150	0.80	3.55	1.91	3.25
233.500	0.95	3.55	1.95	3.25
256.850	1.15	3.55	2.34	3.25
280.200	1.50	3.55	2.53	3.25
326.900	2.30	3.55	2.80	3.25
373.600	3.20	3.55	3.40	3.25
420.300	3.95	3.55	4.20	3.25
467.000	4.50	3.55	4.75	3.25
500.000	4.75	3.55	5.10	3.25

Table A-5 :Zinc loading on untreated OC 1026 with increased feed electrolyte pH

Resin :. 25 ml OC 1026
Pre-treatment : None.
Operating Temperature : 40°C.
Feed Flow rate : 10 BV/hr.
Feed Electrolyte Composition : Co=40 g/L, Ni=35 g/L, Zn=0.012 g/L, Fe=0.001 g/L, Cu=0.01 g/L.
Feed Electrolyte pH : 5.0.

Effluent Volume(BV)	[Zn] (mg/L)	pH
0	0.00	5.00
5	0.00	2.20
10	0.00	3.00
50	0.00	3.25
100	0.00	3.60
150	0.00	4.00
200	0.00	4.40
210	0.21	4.41
220	0.42	4.42
230	0.65	4.43
240	0.81	4.44
250	1.05	4.45
260	1.30	4.46
270	1.70	4.47
280	2.10	4.48
290	2.60	4.49
300	3.00	4.50
400	3.75	4.53
500	4.50	4.55

Table A-6 : Zinc loading on pre-treated Cyanex 272

Resin : 25 ml Cyanex 272
Pre-treatment : INCO electrolyte fed at pH=3 until effluent pH=2.5
Operating Temperature : 60°C
Feed Flow rate : 4.67 BV/hr.
Feed Electrolyte Composition : Co=40 g/L, Ni=35 g/L, Zn=0.012 g/L, Fe=0.001 g/L, Cu=0.01 g/L.
Feed Electrolyte pH : 3.75

Effluent Volume(BV)	[Zn] (mg/L)	pH
0.000	0.00	3.70
2.335	0.00	2.80
4.670	0.00	2.90
7.005	0.00	3.02
9.340	0.00	3.05
11.675	0.00	3.10
23.350	0.00	3.39
46.700	0.00	3.49
70.050	0.00	3.50
81.725	0.10	3.50
93.400	0.24	3.51
105.075	0.35	3.52
116.750	0.50	3.53
128.425	0.60	3.54
140.100	0.70	3.55
147.105	0.80	3.55
151.775	0.87	3.55
158.780	0.95	3.55
163.450	1.12	3.56
168.120	1.30	3.56
175.125	1.50	3.56
182.130	1.75	3.57
186.800	2.00	3.57
191.470	2.30	3.57
198.475	2.60	3.57
205.480	2.90	3.58
210.150	3.25	3.58
214.820	3.50	3.58
221.825	3.75	3.59
228.830	4.06	3.59
233.500	4.28	3.60
300.000	5.02	3.60
350.000	5.80	3.61
500.000	7.50	3.61

Table A-7 : Zinc loading on pre-treated Cyanex 302.

Resin : 25 ml Cyanex 302
Pre-treatment : INCO electrolyte fed at pH=3 until effluent
Operating Temperature : pH=2.5
Feed Flow rate : 60°C
Feed Electrolyte Composition : 4.67 BV/hr.
Co=40 g/L, Ni=35 g/L, Zn=0.012 g/L, Fe=0.001 g/L, Cu=0.01 g/L.
Feed Electrolyte pH : 3.75

	Cycle 1		Cycle 2	Cycle 3	Cycle 4	Cycle 5
Effluent Volume(BV)	[Zn],mg/L	pH	[Zn],mg/L	[Zn],mg/L	[Zn],mg/L	[Zn],mg/L
0.000	0.00	3.70	0.00	0.00	0.00	0.00
2.335	0.00	2.80	0.00	0.00	0.00	0.00
4.670	0.00	2.90	0.00	0.00	0.00	0.00
7.005	0.00	3.02	0.00	0.00	0.00	0.00
9.340	0.00	3.05	0.00	0.00	0.00	0.00
11.675	0.00	3.10	0.00	0.00	0.00	0.00
23.350	0.00	3.39	0.00	0.00	0.00	0.20
46.700	0.00	3.49	0.00	0.00	0.15	0.30
70.050	0.00	3.50	0.00	0.00	0.30	0.40
81.725	0.00	3.50	0.25	0.20	0.40	0.60
93.400	0.15	3.51	0.35	0.40	0.50	0.80
105.075	0.30	3.52	0.50	0.55	0.60	0.90
116.750	0.45	3.53	0.55	0.58	0.70	1.10
128.425	0.60	3.54	0.62	0.65	0.85	1.15
140.100	0.70	3.55	0.70	0.75	0.95	1.20
147.105	0.80	3.55	0.72	0.85	1.10	1.30
151.775	0.90	3.55	0.75	0.95	1.25	1.40
158.780	0.93	3.55	0.85	1.05	1.37	1.50
163.450	0.96	3.55	0.95	1.25	1.50	1.60
168.120	0.98	3.55	1.28	1.40	1.60	1.70
175.125	1.01	3.56	1.40	1.50	1.70	1.90
182.130	1.03	3.56	1.50	1.60	1.85	2.10
186.800	1.05	3.56	1.60	1.70	2.10	2.25
191.470	1.08	3.56	1.70	1.85	2.25	2.50
198.475	1.14	3.56	1.80	2.10	2.50	2.80
205.480	1.20	3.56	2.10	2.25	2.80	3.10
210.150	1.28	3.56	2.19	2.50	3.10	3.40
214.820	1.35	3.56	2.50	2.75	3.40	3.70
221.825	1.43	3.56	2.75	3.10	3.70	4.10
228.830	1.50	3.56	3.00	3.40	4.10	4.50
233.500	1.60	3.56	3.30	3.80	4.50	5.00

Appendix B : Raw Experimental Data from Batch Tests

Table B-1 : Effect of pre-treatment on zinc loading of OC 1026

Resin : 1.000 g OC 1026.
Pre-treatment : Resin equilibrated in Zn-free electrolyte at a particular pH value.
Operating Temperature : 60°C.
Feed Electrolyte Composition : Co=40 g/L, Ni=35 g/L, Zn=0.012 g/L, Fe=0.001 g/L, Cu=0.01 g/L.
Feed Electrolyte Volume : 500 ml.
Fraction Extracted : X

Pre-treatment	Untreated	at pH=3	at pH=2	at pH=3.5	at pH=4
Time (minutes)	X	X	X	X	X
0.000	0.000	0.000	0.000	0.000	0.000
0.500	0.012	0.070	0.080	0.080	0.050
1.000	0.090	0.160	0.180	0.170	0.150
2.000	0.130	0.250	0.260	0.250	0.200
3.000	0.150	0.290	0.300	0.300	0.250
4.000	0.167	0.320	0.330	0.320	0.290
5.000	0.175	0.350	0.365	0.350	0.320
7.000	0.200	0.370	0.380	0.375	0.350
8.330	0.230	0.390	0.400	0.395	0.370
13.330	0.300	0.470	0.480	0.450	0.390
16.670	0.360	0.520	0.540	0.530	0.430
20.000	0.420	0.570	0.580	0.575	0.480
25.000	0.470	0.600	0.610	0.600	0.530
30.000	0.520	0.635	0.640	0.640	0.580
41.670	0.560	0.680	0.680	0.680	0.630
50.000	0.590	0.700	0.700	0.700	0.680
66.670	0.625	0.742	0.750	0.745	0.720
83.330	0.650	0.760	0.770	0.765	0.740
116.670	0.710	0.770	0.780	0.775	0.760
166.670	0.730	0.790	0.795	0.795	0.780
250.000	0.750	0.820	0.820	0.820	0.800
333.330	0.780	0.840	0.840	0.840	0.820
416.670	0.800	0.860	0.860	0.860	0.830
500.000	0.820	0.870	0.870	0.870	0.840

Table B-2 : Effect of temperature on zinc loading of OC 1026

Resin : 1.000 g OC 1026.
Pre-treatment : Resin equilibrated in Zn-free electrolyte at pH=3.0.
Operating Temperature : 60°C,40°C or 25°C.
Feed Electrolyte Composition : Co=40 g/L, Ni=35 g/L, Zn=0.012 g/L, Fe=0.001 g/L, Cu=0.01 g/L.
Feed Electrolyte Volume : 500 ml.
Electrolyte pH : 3.00.
Fraction Extracted: X

Operating temperature	60°C	40°C	25°C
Time (minutes)	X	X	X
0.000	0.000	0.000	0.000
0.500	0.070	0.040	0.025
1.000	0.160	0.120	0.100
2.000	0.250	0.220	0.195
3.000	0.290	0.260	0.230
4.000	0.320	0.280	0.250
5.000	0.350	0.300	0.270
7.000	0.370	0.340	0.290
8.330	0.390	0.350	0.310
13.330	0.470	0.420	0.370
16.670	0.520	0.490	0.420
20.000	0.570	0.520	0.460
25.000	0.600	0.550	0.500
30.000	0.635	0.584	0.528
41.670	0.680	0.631	0.570
50.000	0.700	0.660	0.600
66.670	0.742	0.690	0.640
83.330	0.760	0.725	0.675
116.670	0.770	0.750	0.710
166.670	0.790	0.765	0.725
250.000	0.820	0.785	0.750
333.330	0.840	0.810	0.780
416.670	0.860	0.825	0.800
500.000	0.870	0.840	0.820

Table B-3 : Effect of initial [Zn] on loading of pre-treated OC 1026

Resin : 1.000 g OC 1026.
Pre-treatment : Resin equilibrated in Zn-free electrolyte at pH=3.0.
Operating Temperature : 60°C.
Feed Electrolyte Composition : Co=40 g/L, Ni=35 g/L, Zn=0.040 g/L, Fe=0.001 g/L, Cu=0.01 g/L.
Feed Electrolyte Volume : 500 ml.
Electrolyte pH : 3.00.
Fraction Extracted: X.

Time(minutes)	mg extracted
0.00	0.00
0.50	0.84
1.00	1.94
2.00	3.00
3.00	3.50
4.00	3.85
5.00	4.20
7.00	4.40
8.33	4.70
13.33	5.30
16.67	6.30
20.00	6.85
25.00	7.30
30.00	7.90
41.67	9.00
50.00	10.00
66.67	11.00
83.33	12.00
116.67	13.40
166.67	15.00
250.00	16.00
333.33	17.00
416.67	18.00
500.00	19.00

Table B-4 : Effect of pre-treatment and temperature on loading of Cyanex 302

Resin : 1.000 g Cyanex 302.
Pre-treatment : Resin equilibrated at a particular pH.
Operating Temperature : 60°C, 40°C or 25°C.
Feed Electrolyte Composition : Co=40 g/L, Ni=35 g/L, Zn=0.012 g/L, Fe=0.001 g/L, Cu=0.01 g/L.
Feed Electrolyte Volume : 500 ml
Fraction Extracted: X

Temperature	60°C	60°C	60°C	40°C	25°C
Pre-treatment	Untreated	at pH=3	at pH=2	at pH=3	at pH=3
Time	X	X	X	X	X
0.000	0.000	0.000	0.000	0.000	0.000
0.500	0.010	0.070	0.080	0.040	0.025
1.000	0.080	0.150	0.170	0.120	0.100
2.000	0.120	0.250	0.270	0.220	0.190
3.000	0.150	0.300	0.320	0.260	0.230
4.000	0.160	0.330	0.360	0.280	0.250
5.000	0.170	0.350	0.390	0.300	0.270
7.000	0.185	0.370	0.410	0.330	0.290
8.330	0.200	0.390	0.440	0.350	0.310
13.330	0.250	0.440	0.500	0.400	0.370
16.670	0.340	0.490	0.550	0.450	0.410
20.000	0.410	0.550	0.580	0.490	0.440
25.000	0.460	0.590	0.610	0.520	0.470
30.000	0.500	0.614	0.640	0.550	0.500
41.670	0.550	0.660	0.680	0.600	0.550
50.000	0.580	0.690	0.700	0.625	0.580
66.670	0.620	0.730	0.730	0.660	0.630
83.330	0.660	0.750	0.760	0.695	0.670
116.670	0.710	0.770	0.780	0.730	0.700
166.670	0.730	0.790	0.800	0.750	0.720
250.000	0.760	0.830	0.840	0.780	0.750
333.330	0.780	0.850	0.870	0.800	0.780
416.670	0.800	0.860	0.880	0.820	0.800
500.000	0.810	0.870	0.890	0.840	0.810

Table B-5 : Effect of temperature on loading of Cyanex 272

Resin : 1.000 g Cyanex 272.
Pre-treatment : Resin equilibrated at pH=3.
Operating Temperature : 60°C, 40°C or 25°C.
Feed Electrolyte Composition : Co=40 g/L, Ni=35 g/L, Zn=0.012 g/L, Fe=0.001 g/L, Cu=0.01 g/L.
Feed Electrolyte Volume : 500 ml.
Electrolyte pH : 3.0.
Fraction Extracted: X.

Temperature	60°C	40°C	25°C
Time	X	X	X
0.000	0.000	0.000	0.000
0.500	0.070	0.040	0.025
1.000	0.150	0.120	0.100
2.000	0.250	0.220	0.190
3.000	0.290	0.250	0.220
4.000	0.320	0.270	0.240
5.000	0.350	0.290	0.260
7.000	0.370	0.330	0.280
8.330	0.390	0.350	0.300
13.330	0.440	0.390	0.350
16.670	0.480	0.430	0.390
20.000	0.510	0.460	0.425
25.000	0.550	0.500	0.450
30.000	0.570	0.530	0.480
41.670	0.620	0.570	0.530
50.000	0.650	0.600	0.560
66.670	0.690	0.640	0.600
83.330	0.720	0.675	0.630
116.670	0.760	0.720	0.680
166.670	0.790	0.750	0.710
250.000	0.820	0.780	0.750
333.330	0.850	0.800	0.780
416.670	0.860	0.820	0.800
500.000	0.870	0.830	0.810